Journal of Photochemistry and Photobiology C: Photochemistry Reviews 25 (2015) 1–29

Contents lists available at ScienceDirect

Journal of Photochemistry and Photobiology C: Photochemistry Reviews

journal homepage: www.elsevier.com/locate/jphotochemrev

Review

Visible-light activation of TiO_2 photocatalysts: Advances in theory and experiments

Vinodkumar Etacheri[a,b], Cristiana Di Valentin[c], Jenny Schneider[d], Detlef Bahnemann[d,e], Suresh C. Pillai[f,g,*]

[a] School of Chemical Engineering, Purdue University, 480 Stadium Mall Drive, West Lafayette, IN 47907, United States
[b] Centre for Research in Engineering Surface Technology (CREST), FOCAS Institute, Dublin Institute of Technology, Kevin Street, Dublin 8, Ireland
[c] Dipartimento di Scienza dei Materiali, Università di Milano Bicocca, via Cozzi 55, 20125 Milano, Italy
[d] Institut fuer Technische Chemie, Gottfried Wilhelm Leibniz Universitaet Hannover, Callinstrasse 3, D-30167 Hannover, Germany
[e] Laboratory for Nanocomposite Materials, Department of Photonics, Faculty of Physics, Saint-Petersburg State University, Ulianovskaia str. 3, Peterhof, Saint-Petersburg 198504, Russia
[f] Nanotechnology Research Group, Department of Environmental Science, Institute of Technology Sligo, Sligo, Ireland
[g] Centre for Precision Engineering, Materials and Manufacturing Research (PEM), Institute of Technology, Sligo, Sligo, Ireland

ARTICLE INFO

Article history:
Received 25 April 2015
Received in revised form 17 August 2015
Accepted 24 August 2015
Available online 28 August 2015

Keywords:
Photo-induced reactions
Solar energy
Mechanism
Fundamentals
Doping
Graphene
Energy and environmental
Air pollution
Sustainable
Photovoltaic
Hydrogen production
Tutorial review

ABSTRACT

The remarkable achievement by Fujishima and Honda (1972) in the photo-electrochemical water splitting results in the extensive use of TiO_2 nanomaterials for environmental purification and energy storage/conversion applications. Though there are many advantages for the TiO_2 compared to other semiconductor photocatalysts, its band gap of 3.2 eV restrains application to the UV-region of the electromagnetic spectrum ($\lambda \leq 387.5$ nm). As a result, development of visible-light active titanium dioxide is one of the key challenges in the field of semiconductor photocatalysis. In this review, advances in the strategies for the visible light activation, origin of visible-light activity, and electronic structure of various visible-light active TiO_2 photocatalysts are discussed in detail. It has also been shown that if appropriate models are used, the theoretical insights can successfully be employed to develop novel catalysts to enhance the photocatalytic performance in the visible region. Recent developments in theory and experiments in visible-light induced water splitting, degradation of environmental pollutants, water and air purification and antibacterial applications are also reviewed. Various strategies to identify appropriate dopants for improved visible-light absorption and electron–hole separation to enhance the photocatalytic activity are discussed in detail, and a number of recommendations are also presented.

Contents

* Corresponding author at: Nanotechnology Research Group, Department of Environmental Science, Institute of Technology Sligo, Sligo, Ireland.
E-mail address: pillai.suresh@itsligo.ie (S.C. Pillai).

http://dx.doi.org/10.1016/j.jphotochemrev.2015.08.003
1389-5567/

Dr. Vinodkumar Etacheri obtained his PhD in Materials Chemistry from Dublin Institute of Technology (DIT), Ireland in 2011. This work under the guidance of Prof. Suresh C. Pillai involved the development of new generation visible-light active TiO_2 nanomaterials. He then completed postdoctoral research at Bar Ilan University, Israel, and University of Michigan, USA in the area of Li-ion and Li-O_2 batteries. Currently he is working as a research associate at Purdue University, USA, developing nanomaterials for a wide range of electrochemical energy storage systems. His research areas extent from semiconductor photocatalysis for environmental remediation, antibacterial applications, and water oxidation, to engineering of carbon and metal oxide based electrodes for rechargeable batteries and supercapacitors.

Prof. Cristiana Di Valentin was born in Maniago (PN), Italy on 29/07/1973. She graduated in Chemistry in 1997 at the University of Pavia where she also received her Ph.D. degree in 2000 in collaboration with the Technische Universität München. She was appointed by the University of Milano-Bicocca as Assistant Professor in 2002 and as Associate Professor in 2012. She has been visiting scientist at the Technische Universität München, Universitat de Barcelona, Ecole Nationale Superieure de Paris and Princeton University. Her research activity spans from *ab initio* computational study of reaction mechanisms in organic chemistry and homogeneous catalysis to heterogeneous catalysis, photocatalysis, doped and defective semiconducting oxides, graphene and carbon based materials for fuel cells.

Jenny Schneider received her M.Sc. degree in Material- and Nanochemistry in 2011 from the Gottfried Wilhelm Leibniz University Hannover. She is currently a Ph.D. student with Prof. Bahnemann at the Gottfried Wilhelm Leibniz University Hannover, investigating the reaction dynamics of photogenerated charge carriers in different photocatalysts by means of laser flash photolysis spectroscopy. Her research interests include the mechanism(s) of photocatalysis, the detailed understanding of photocatalytically induced chemical conversions as well as theoretical simulations of photocatalytic processes.

Prof. Dr. rer. nat. habil. Detlef Bahnemann has received his PhD in Chemistry from the Technical University Berlin in 1981 and his Habilitation in the area of Technical Chemistry from the Leibniz University Hannover in 2012. He is currently the Head of the Research Unit "Photocatalysis and Nanotechnology" at the Institute of Technical Chemistry of the Leibniz University Hannover in Germany and also the Director of the Research Institute on Nanocomposite Materials for Photonic Applications at Saint Petersburg State University in Russia. His main research topics include photocatalysis, photoelectrochemistry, solar chemistry and photochemistry focussed on the synthesis and the detailed investigation of the physical–chemical properties of semiconductor and metal nanoparticles. He holds an Honorary Professorship at the Robert Gordon University in Aberdeen/Scotland (United Kingdom), an Honorary Professorship at the Xinjiang Technical Institute of Physics and Chemistry (Chinese Academy of Sciences) in Urumqi (China), the Erudite Professorship at the Mahatma Gandhi University in Kottayam (India), a Guest Professorship of Tianjin University (China), a Visiting Professorship under the Academic Icon Programme at the University of Malaya (Malaysia), and is DeTao Master of Photocatalysis, Nanomaterials and Energy Applications (China). Prof. Bahnemann is the lead author of more than 290 publications in peer reviewed journals that have been cited more than 24,000 times (h-index: 60 according to ISI, 68 according to Google Scholar Citations) and has edited 4 scientific books.

Prof. Suresh C. Pillai was born in Karukachal, Kottayam, Kerala, India. He has completed his BSc and MSc (with first rank) from Mahatma Gandhi University, Kottayam. Suresh has obtained his PhD in the area of Nanotechnology from Trinity College (TCD), The University of Dublin, Ireland and then performed a postdoctoral research at California Institute of Technology (Caltech), USA. He has then worked at CREST in DIT as a senior scientist responsible for nanotechnology research before moving to Institute of Technology Sligo as a senior lecturer in environmental nanotechnology. He is an elected fellow of the Royal Microscopical Society (FRMS) and the Institute of Materials, Minerals and Mining (FIMMM). He is responsible for acquiring more than €3 million direct R&D funding. Prof. Pillai is a recipient of a number of awards for research accomplishments including the 'Industrial Technologies Award 2011' from Enterprise Ireland for commercialising nanomaterials for industrial applications. He was also the recipient of the 'Hothouse Commercialisation Award 2009' from the Minister of Science, Technology and Innovation and also the recipient of the 'Enterprise Ireland Research Commercialization Award 2009'. He has also been nominated for the 'One to Watch' award 2009 for commercialising R&D work (Enterprise Ireland). One of the nanomaterials based environmental technologies developed by his research team was selected to demonstrate as one of the fifty 'innovative technologies' (selected after screening over 450 nominations from EU) at the first Innovation Convention organised by the European Commission on 5–6th December 2011. He is the national delegate and technical expert for ISO standardization committee and European standardization (CEN) committee on photocatalytic materials.

1. Introduction

Photocatalysis refers to the acceleration of a chemical reaction in the presence of substances called photocatalysts, which can absorb light quanta of appropriate wavelengths depending on the band structure [1–4]. Usually semiconductors including TiO_2, Fe_2O_3, WO_3, ZnO, CeO_2, CdS, Fe_2O_3, ZnS, MoO_3, ZrO_2, and SnO_2 are selected as photocatalysts due to their narrow band gap and distinct electronic structure (unoccupied conduction band and occupied valence band) [5–24]. In semiconductor photocatalysis, electrons from the valence band of a semiconductor are excited to the conduction band by light of higher energy than the respective band gap, resulting in the formation of e^-_{CB}/h^+_{VB} pairs (Fig. 1). Conduction band electrons are good reducing agents (+0.5 to −1.5 V vs. NHE) whereas the valence band holes (h^+_{VB}) are strong oxidizing

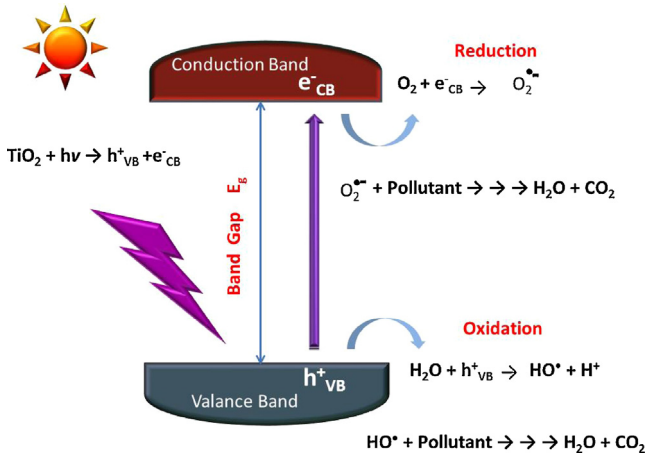

Fig. 1. Mechanism of semiconductor photocatalysis.
Reproduced with permission from Ref. [4]. Copyright 2015 Elsevier Science.

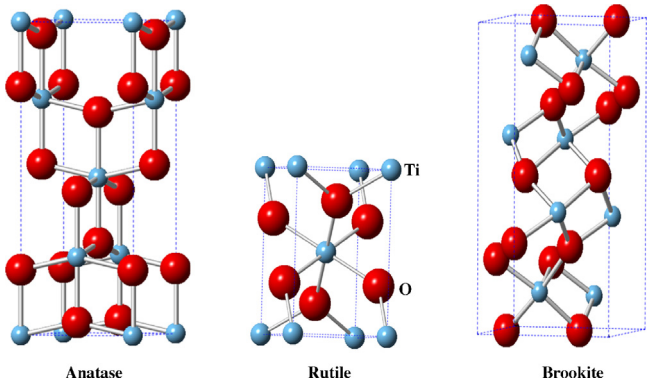

Fig. 2. Crystal structure of anatase, rutile and brookite.

agents (+1.0 to +3.5 V vs. NHE) [25]. The lack of a continuum of interband states in semiconductors assures an adequately extended lifetime for photogenerated e^-_{CB}/h^+_{VB} pairs to initiate redox reactions on the catalyst surface. Electrons in the conduction band can reduce O_2 to form superoxide radicals ($O_2^{\bullet-}$). Additional reaction of $O_2^{\bullet-}$ with holes on the valence band produce singlet oxygen ($^1O_2$) [26,27]. Subsequent reactions of valence band holes with surface adsorbed H_2O or HO^- result in the formation of hydroxyl radicals ($HO^\bullet$), hydrogen peroxide (H_2O_2), and protonated superoxide radicals ($HOO^\bullet$). H_2O_2 is furthermore reported to be resulting from the coupling of two $HOO^\bullet$ [28,29]. Further reaction of H_2O_2 with $HO^\bullet$ results in the formation of protonated superoxide radicals ($HOO^\bullet$) [4,30].

During the photocatalytic process, free electrons/holes, and reactive oxidizing species (ROS) such as $HO_2^\bullet$, $HO^\bullet$ and $O_2^{\bullet-}$ react with the surface adsorbed impurities including inorganic, organic compounds, and biological species (bacteria, virus, etc.) leading to their decomposition. The efficiency of a photocatalytic reaction mainly depends on the capability of the photocatalyst to generate longer-lived electrons and holes that result in the formation of reactive free radicals. Usually, the crucial aspect is the creation and efficient utilization of the reactive oxidizing species (ROS). Semiconductor nanomaterials, especially TiO_2 find a wide range of applications in the area of photocatalysis, pigments, dye sensitized solar cells, air/water sanitization, initiation of chemical reactions, optoelectronics, cancer therapy, cathodic protection of metals from corrosion, electrochromic displays, and light-activated antibacterial surfaces [6–8,10,11,13,17,19,31–46]. Currently, researchers all over the world are trying to improve the efficiency and selectivity of TiO_2 photocatalysts for various applications. Although a number of review papers and feature articles published recently on the advances of TiO_2 photocatalysis [1–4,7,47–50], theoretical and experimental strategies for visible light activation have not been described comprehensively. To gain further insights into the development of next generation photocatalysts, it is highly desirable to condense the advances in experimental as well as theoretical approaches. The aim of this review is to summarize the progress in experimental methods, theoretical approaches, and electronic structure modelling of TiO_2 for the visible-light activation. Several recommendations are also presented for improving the visible-light absorption and the electron–hole separation of the current generation of TiO_2 photocatalysts.

2. Basic principles and mechanism of photocatalysis

2.1. Structural and electronic properties

The initial work of water decomposition using electrodes composed of TiO_2 was done by Fujishima and Honda [5]. They found that the photolysis of water into their its individual constituents (H_2 and O_2) is greatly affected by the nature of surface defects. However, the quantum efficiencies of TiO_2 in solar energy conversions are rather poor due to the usually faster recombination of electron–hole pairs [13,51]. Since its invention in 1972, the light-induced decomposition of organic species is the most vigorously investigated application of TiO_2 photocatalysis. For the first time, the photocatalytic reduction of CN^- in aqueous solution was reported in 1977 by Frank and Bard [52,53]. This investigation triggered the use of TiO_2 photocatalysis for water purification by exploiting solar irradiations [18,54,55]. Other noteworthy advances include the invention of dye sensitized solar cells by Grätzel et al., which are composed of titanium dioxide anodes and the discovery of anti-fogging abilities of TiO_2 surfaces by Wang et al. [33,56]. The extensive use of titanium dioxide for a wide range of applications as compared with other photocatalysts results from its non-toxicity, abundance (inexpensiveness), thermal/chemical stability, and high redox potential [18,57,58]. Anatase (tetragonal), rutile (tetragonal), and brookite (orthorhombic) are three polymorphs of TiO_2. Band gaps of anatase, rutile and brookite phases are 3.2, 3.0 and 3.4 eV respectively [59–61]. Wider band gaps are common for poorly crystallized nanoparticles and thin films, and a band gap narrowing up to 0.2 eV was observed for TiO_2 nanomaterials having 5–10 nm particle size. Anatase and brookite are meta-stable phases, whereas rutile is thermodynamically stable. Anatase and brookite TiO_2 irreversibly and exothermically converts to rutile at temperatures exceeding 600 °C [8,10,62,63]. Due to superior mobility of electron–hole pairs, and improved surface hydroxyl density, anatase TiO_2 exists as the photocatalytically most active polymorph of TiO_2 [54,64,65]. In contrast, the photocatalytic performance of rutile TiO_2 is not promising, and the activity of the brookite phase has not been systematically investigated [19,66]. A number of factors, such as surface area, particle size, ratio of polymorphs, type of dopants, defect concentration, synthesis method, and phase purity, strongly affect the photocatalytic activity of TiO_2 [67–69].

The crystal structure of TiO_2 polymorphs can be explained by the different spatial arrangements of TiO_6 octahedra (Ti^{4+} ions bordered by six O^{2-} ions). The differences between the three crystal structures are the various degrees of distortion and 3-D assembly of the TiO_6 octahedra (Fig. 2). In the anatase tetragonal crystal structure ($a = b = 3.78$ Å, $c = 9.50$ Å) each octahedron shares corners to form (0 0 1) planes. The tetragonal structure of rutile ($a = b = 4.58$ Å,

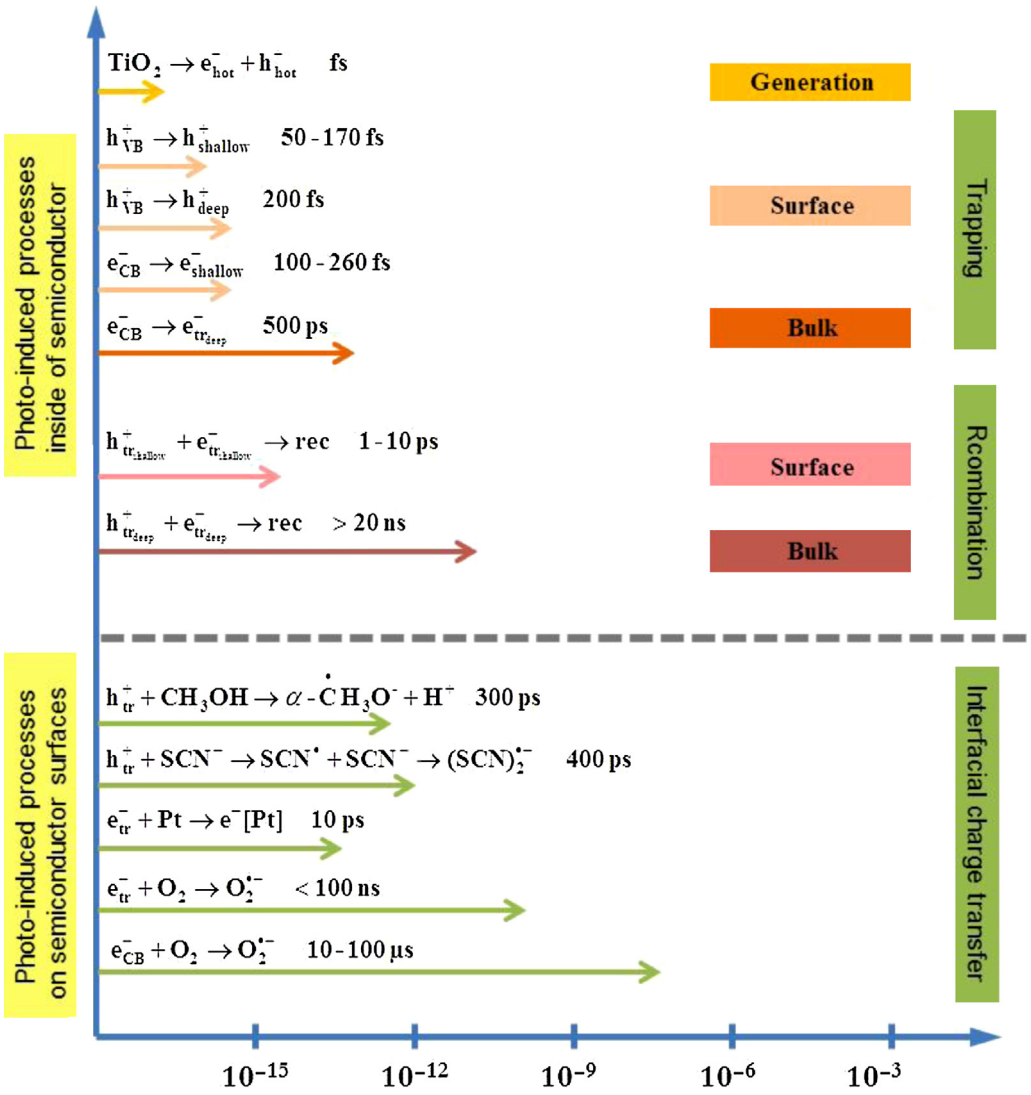

Scheme 1. Various steps involved in TiO_2 photocatalysis.
Reproduced with permission from Ref. [3]. Copyright 2014 American Chemical Society.

c = 2.95 Å), on the other hand consists of edge sharing octahedrons forming the (0 0 1) planes. The orthorhombic structure of brookite phase (a = 5.43 Å, b = 9.16 Å, c = 5.13 Å) is made up of both corner and edge sharing octahedra. These different crystal structures result in various densities and electronic structures of the three TiO_2 polymorphs. Titanium dioxide usually exists as an n-type type semiconductor due to the presence of oxygen vacancies [70]. The photocatalytic activity of amorphous TiO_2 is negligible compared to that of crystalline TiO_2 [71,72]. This is because the crystalline structure minimizes the photo excited electron hole recombination.

2.2. Mechanism of photocatalysis

As described in the introduction part, illumination of TiO_2 with light waves of energy greater than its band gap results in the formation of electron–hole pairs. Hoffmann et al. proposed a general mechanism for TiO_2 photocatalysis based on the laser flash photolysis measurements [18]. Various steps in the mechanism with corresponding reaction times are presented in Scheme 1. According to this mechanism, in the picosecond to nanosecond time domain a competition exists between the trapping and recombination of the photogenerated electron–hole pairs.

A second type of competition during the millisecond to microsecond exists between the interfacial charge transfer and recombination of the trapped species. The overall quantum efficiency of the photocatalytic process depends on the net effect of these competitions. The quantum efficiency of a photocatalytic reaction is expected to increase by increasing the lifetime of electron–hole pairs and the rate of the interfacial charge transfer process. This mechanism does not consider the direct transfer of photogenerated holes to adsorbed electron donors.

However, it was assumed that the hole-transfer occurs only through a surface trapped hole species or through the hydroxyl radical. This hypothesis was proved by the identification of hydroxylated compounds during the photocatalytic decomposition of halogenated aromatic compounds. Additionally, this study has provided evidence for the fact that hydroxyl radicals are the primary oxidizing species in photo-activated TiO_2 [73–75]. Electron paramagnetic resonance (EPR) spectroscopy also confirmed the formation of hydroperoxy ($^{\bullet}O_2H$) and hydroxyl radicals ($^{\bullet}OH$) during the illumination of aqueous TiO_2 suspensions [76–80]. Mao et al. investigated the kinetics of the hydroxyl radical mediated oxidation of chlorinated hydrocarbons. The strong dependence between the C—H bond strengths and the rate of oxidation confirmed the abstraction of an H atom by $^{\bullet}OH$ as the rate-determining step [81].

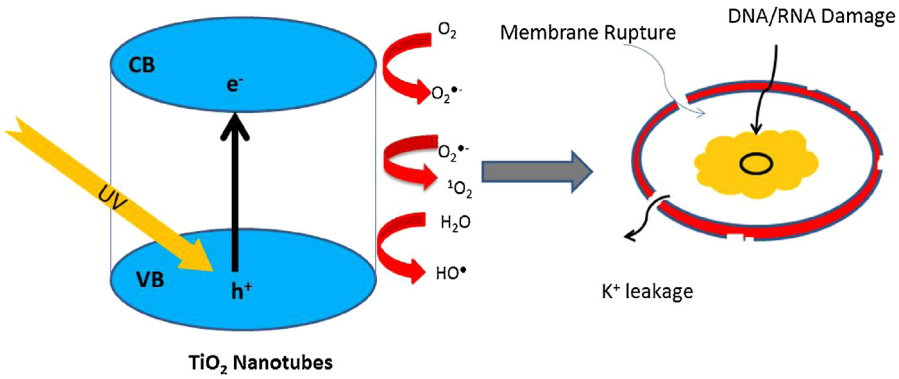

Fig. 3. Schematic representation of the bacterial photokilling using TiO_2.
Reproduced with permission from Ref. [93]. Copyright 2015 Elsevier Science.

The rate of the decomposition of pollutants was found to be highly dependent on its adsorbed concentration, which also implies that the hydroxyl radical concentration on the catalyst surface determines the reaction kinetics [82,83]. On the other hand, the direct oxidation mechanism using valence band holes prior to their trapping is also reported in the literature. Mao et al. reported the photo-Kolbe type oxidation of oxalic acid and trichloroacetic acid using TiO_2 valence band holes [81]. During the TiO_2 sensitized decomposition of potassium iodide, 2,4,5-trichlorophenol and thianthrene, products of the direct electron transfer oxidation reaction were observed, while the authors were unable to find evidence for hydroxyl radical reaction [84]. In addition, experimental evidence for the hole-mediated decomposition of organic moieties such as acetate, glyoxylate, and formate on the TiO_2 surface has also been reported [85]. However, OH radicals and holes exhibited different regioselectivities in the photocatalytic oxidation of 4-hydroxybenzyl alcohol (HBA) on ZnO and on TiO_2 [86]. In addition to hole's and hydroxyl radical's, involvement of H_2O_2 in the photocatalytic decomposition of various inorganic and organic compounds was also found [87]. In this mechanism, highly reactive $^{\bullet}OH$ species are generated as a result of the homolytic scission of hydrogen peroxide, or H_2O_2 act as an electron acceptor. In most of the photocatalytic reactions, two-electron reduction of oxygen results in the formation of H_2O_2.

Similarly, Gerischer et al. identified oxygen reduction as the rate-determining step in semiconductor photocatalysis [88,89]. Through ^{18}O isotopic studies, Hoffman et al. showed that all hydrogen peroxide arises from dioxygen reduction using conduction band electrons while in the absence of oxygen, no H_2O_2 was detected [90]. They also proposed that hydroxyl radicals bound on TiO_2 surface ($TiOH^{\bullet+}$) acts as the principal oxidizing agents in the absence of O_2. Because of the more negative conduction band level of TiO_2 as compared to the hydrogen production level (E_{H_2/H_2O}), photo-excited electrons can result in the water splitting to generate hydrogen. Photo-excited electron–hole pairs in TiO_2 can also destroy bacteria and other micro-organisms. This happens due to strong redox reactions of the electron–hole pairs with proteins and amino acids, which are the building blocks of micro-organisms. Hashimoto and co-workers explained the mechanism of photokilling of *Escherichia coli* bacteria on nanocrystalline TiO_2 coatings [91]. They observed the photodecomposition of bacterial cell wall due to the decay of lipopolysaccharide (LPS), which is the major constituent of the cell wall [92]. Recently, Pillai and co-workers reported the photocatalytic antimicrobial properties of partially crystalline nanotube TiO_2 bundles [93]. These nanotube materials were found to be highly effective in disinfecting both *E. coli* (97.53%) and *Staphylococcus aureus* (99.94%). The high-aspect ratios of the nanotubes (Fig. 3) employed and the presence of a large number of surface hydroxyl groups were reported as the reasons for high antibacterial activity.

It is thus clear that the antibacterial effect of TiO_2 is a bactericidal action (which involves decomposition of the cell wall), and not a simple bacteriostatic action. Photo-induced bacterial-killing mechanism on titanium dioxide surface has also been demonstrated by other studies [94–96]. In the first step, electron–hole pairs are created by the irradiation of light on the semiconductor surface. The reactive oxygen species (ROS), such as $O_2^{\bullet-}$, $^1O_2$, $HO^{\bullet}$, H_2O_2, and $HO_2^{\bullet}$ formed by the reaction between electron–hole pairs and surface adsorbed H_2O, HO^- and O_2. Further reaction of these species results in the bacterial decomposition. Initially the reactive oxygen species attack the weak points of bacterial cell wall resulting in a leakage of the internal components, followed by the total decomposition of the damaged cells [93,94,96]. The observed rate of photokilling was low for micro-organisms having a cell wall. Those without a cell wall undergo fast photo-degradation due to direct attack of electron hole pairs on cytoplasmic membrane. Thus, photocatalysis can be used as a powerful tool for the destruction of micro-organisms [91,92,97].

Zhang et al. studied the mechanism of the OH radical production in anatase and rutile photocatalysts by employing two different probe molecules such as coumarin and coumarin-3-carboxylic acid [98]. Rutile TiO_2 was found to produce smaller amount of OH radicals compared to anatase crystals (Fig. 4). Hydroxyl radical formation on anatase TiO_2 surface was explained by the conversion of trapped holes. Whereas on rutile TiO_2 surface, Ti-peroxo (Ti-OO-Ti) formed by the combination of two trapped holes act as a catalyst to generate OH radicals from water. The authors furthermore concluded that conduction band reduction of H_2O_2 does not contribute towards OH radical generation [98]. These findings are very significant towards optimizing the photocatalytic activity of TiO_2 polymorphs for various applications.

2.3. Limitations of TiO_2 photocatalyst

One of the main shortcomings of TiO_2 photocatalyst is the recombination of photo-generated charge carriers, which decreases the quantum efficiency of the overall reaction [40]. The photo-excited electrons return back to the valence band radiatively or non-radiatively during the recombination processes [99–101]. These events can occur either in the bulk or on the surface and is normally induced by defects, impurities and other crystal bulk/surface imperfections [40,102]. Trapping of the photo-generated electrons by the reduction of surface Ti^{4+} ions to Ti^{3+} species happens in ~30 ps, while the recombination occurs within 10 ns [102]. Many methods including heterojunction formation, doping with ions, and nanosized crystals have been demonstrated

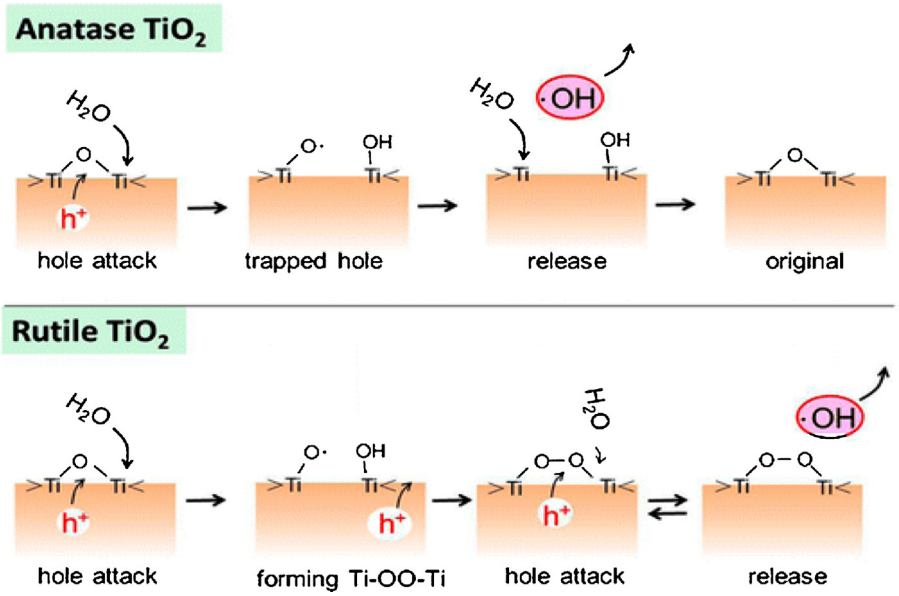

Fig. 4. Scheme showing the mechanism of OH radical production with anatase and rutile.
Reproduced with permission from Ref. [98]. Copyright 2014 American Chemical Society.

to reduce photo-excited charge carrier recombination [103–110]. For example, TiO_2 partially loaded with Ag and Au noble metal nanoparticles exhibited superior photocatalytic activities [63,111]. This was due to the fact that the metal nanoparticles act as electron traps during the photocatalytic reaction, and thereby decreasing the rate of electron–hole recombination. Additionally, the industrial TiO_2 Evonik Degussa P-25 being a mixture of 30% rutile and 70% anatase, is often found to exhibit notably higher photocatalytic activities compared to other phase-pure TiO_2 samples [112]. Superior photocatalytic activities of these biphasic TiO_2 resulted from the efficient transfer of electron from the conduction band of anatase to those of rutile TiO_2. Notably, higher visible-light induced photocatalytic activities of N-doped, and S, N-codoped anatase–rutile nanoheterojunctions have been reported by Etacheri et al. [11,17]. They explained details of the electronic structure of these heterostructure photocatalysts, and attributed the observed superior photocatalytic activities to the efficient transfer of photogenerated electrons from the conduction band of anatase to that of rutile. In conclusion, any factor increasing the life-time of electron–hole pairs can substantially increase the photocatalytic performance and thus the quantum efficiency of TiO_2 photocatalysts.

The poor thermal stability of the photocatalytically most active anatase phase is another main disadvantage of TiO_2 photocatalyst. Anatase TiO_2, the most photocatalytically active polymorph, is thermally less stable and undergoes irreversible transformation to the less active rutile phase above 600 °C [10,113]. This confines the high temperature (≥700 °C) applications including ceramic materials. The anatase to rutile transformation (ART) is slow below 600 °C and extremely rapid above 700 °C. The transformation involves co-operative movement of the individual O^{2-} and Ti^{4+} ions. During ART, two Ti—O bonds of the anatase crystal structure (edge-shared) are broken to form the corner shared rutile structure (Fig. 5) [113–116]. As mentioned in the introduction part (Section 1), both rutile and anatase have tetragonal crystal structure and previous reports proved that the kinetic stability of anatase is higher than that of rutile under ambient conditions.

A thermodynamic phase stability calculation by Banfield and co-workers demonstrated that a critical particle-size of around 14 nm is required to initiate anatase to rutile transformation [117,118].

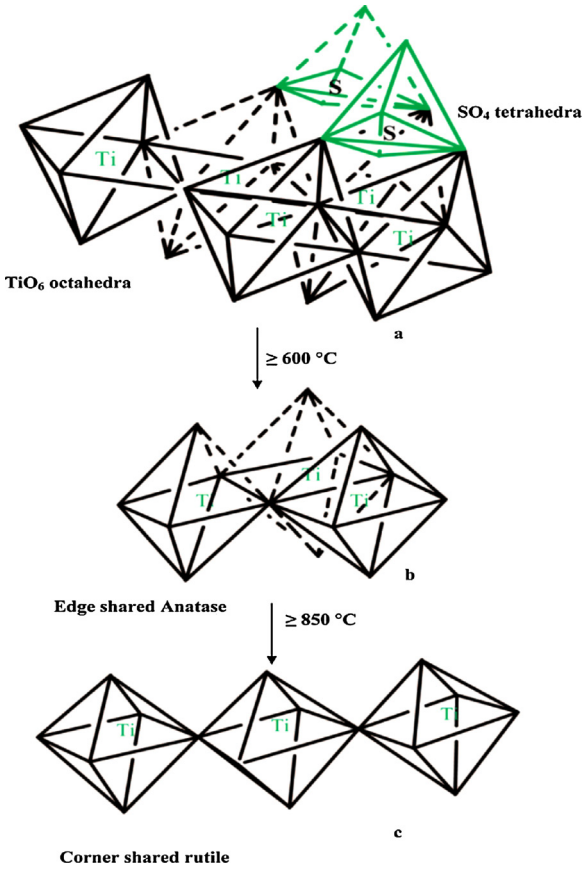

Fig. 5. The schematic representation of the transformation of edge shared anatase photocatalysts to corner shared rutile from a titanyl oxysulfate precursor.
Reproduced with permission from Ref. [113]. Copyright 2008 American Chemical Society.

The anatase phase is more stable below this critical size [10]. An activation energy of 90 kcal/mol is required for the transformation, which follows first order kinetics. Creation of lattice vacancies through removal of oxygen ions accelerates the ART. The

transformation temperature depends on several factors such as (a) impurity content (b) reaction atmosphere (c) particle size and its morphology (d) degree of agglomeration and (e) synthesis method of anatase TiO_2. Another serious drawback of the TiO_2 photocatalyst is the wide band gap of anatase TiO_2 ($E_{bg} \sim 3.2$ eV), which restrains its use to UV light ($\lambda \leq 390$ nm) [8]. Because of this, TiO_2 displays a high photocatalytic activity only when it is irradiated by UV light. Even though the absorption onset of the high temperature stable rutile phase ($E_{bg} \sim 3.0$ eV) occurs around 413 nm, its performance is restricted due to the less negative reduction potential of the conduction band electrons, and faster recombination of the electron–hole pairs [66]. This means that only ~5% of the solar radiations can be utilized by the conventional TiO_2 photocatalysis, which adversely affect the commercialization of TiO_2 based photocatalysts [17,119]. It is therefore crucial to develop visible-light active TiO_2 to effectively exploit solar-radiations or other artificial lights. Studies began in the 1980s to synthesize narrow band-gap titanium dioxide that can absorb and efficiently utilize both UV (290–400 nm) and visible (400–700 nm) light. Various techniques employed for the visible light activation are explained in detail in the following sections.

3. Advances in the theoretical approaches to model photocatalysts and their photoactivity

Theory can be applied to investigate various aspects of the photocatalytic cycle; in particular, the light absorption process, the electron/hole transport in the bulk and their migration to the surface, the band edge alignments of semiconductors, and surface photo-redox chemistry, just to cite the most relevant ones. If accurate methods and models are used, the theoretical insights can be fruitfully used to improve the photocatalytic performance, especially in the range of visible-light.

3.1. Photocatalysts electronic structure

Density functional theory (DFT) has gained a prominent position in the general scenario of computational materials science thanks to its rather high accuracy at a relatively low cost. This applies also to the case of materials for photocatalysis (e.g. TiO_2), where the accurate description of the electronic structure is crucial in order to correctly understand and foresee their interaction with light and the photo-response. However, standard DFT approaches, such as LDA and GGA methods, suffer of the residual electron self-interaction and an improper description of electron correlations causing the well-known underestimation of the band gap and excessive delocalization of the dopant induced states. Two pragmatic approaches for the correction of self-interaction are the hybrid density functional methods, which include a fraction of exact (Hartree–Fock type) exchange, and the DFT + U methods, where an on-site Hubbard U electron repulsion is added on selected localized orbitals. These methods presented a better explanation of the fundamental gap but also of the location of the impurity-states induced by the presence of dopants in the band-gap of TiO_2, which is critical for the visible light absorption process.

Hybrid density functionals, with a typical 20–25% contribution of exact exchange, overestimate the TiO_2 band gap. A reduction of this contribution to 12–15% makes the Kohn-Sham gap match the experimental fundamental gap. With the DFT + U method, very large and unphysical U values ($U = 6$ eV) for the on-site correction on Ti 3d states are required to reproduce the experimental band gap, whereas the use of the self-consistent linear response derived U values ($U = 3.23$ eV for anatase and $U = 3.25$ for rutile) only slightly improves the GGA band gap [120]. The latter are anyhow better suitable for the correct description of the electronic modifications induced by the dopants.

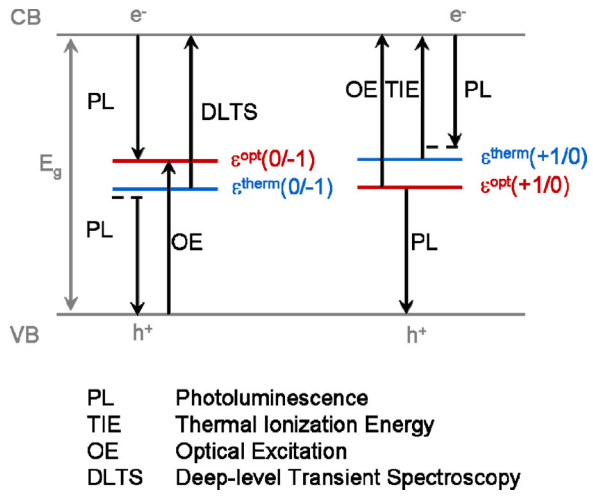

Fig. 6. Schematic representation of electronic transitions in doped or defective semiconductors in relation with the spectroscopic techniques which can probe them. The ↑ arrows indicate an electron excitation, the ↓ arrows indicate an electron decay. ε^{therm} and ε^{opt} are defined with respect to the valence band maximum for (0,−1) and (+1,0) charge state transitions.

Reproduced with permission from Ref. [121]. Copyright 2014 American Chemical Society.

3.2. Doped and defective photocatalysts

The visible light activation of photocatalysts is often the result of electronic structure engineering of materials through doping or defectivity. These approaches cause the modification of the band structure or the introduction of new defect states in the photocatalyst band gap, whose correct position and description are not easily obtained by the ground state DFT calculations. It is common practice to estimate the semiconductor band gap and the energy levels introduced in the gap by defect centres using single-particle Kohn–Sham eigenvalues. This approach, however, is not well justified and can be used only for qualitative comparisons with optical or photoemission experimental data. The problem of the position of defect states in the gap can be partly solved by the calculation of the "transition energy levels" between different charge states of the (intrinsic or extrinsic) defect under investigation. These quantities (commonly referred to as ε^{opt} or ε^{therm}, for optical and adiabatic transitions, respectively) are obtained from total energies calculation and converted into formation energy of the defect in a specific charge state. This approach is analogous to the delta-self-consistent-field method which allows to compute electronic excitations in finite systems from total energy differences. The transition energy levels (Fig. 6) formalism provides a rigorous framework for computing then excitation and emission energies in doped or defective semiconductors that can be directly compared with experiments [121,122]. Many successful examples of the use of transition energy levels to rationalize optical and photocatalytic properties of materials already exist in the literature [123–131].

3.3. Photocatalysts light-induced excitation

To compute excitation energies, one should go beyond DFT, either through many-body perturbation theory (MBPT), in the GW approximation and the Bethe–Salpeter equation, or the time-dependent DFT (TD-DFT) method. A number of studies on bulk TiO_2 have recently appeared in the literature [123,124,132–134].

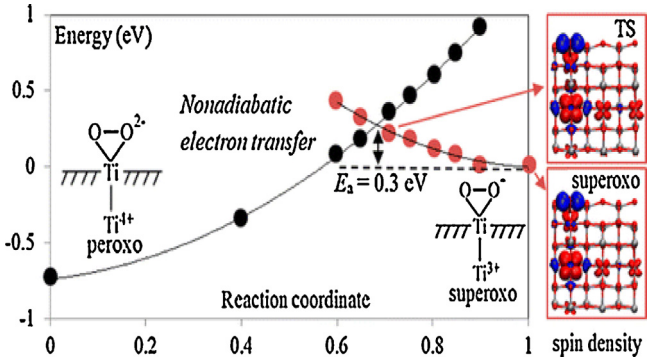

Fig. 7. Schematic diagram showing the transfer of an electron from a reduced TiO_2 surface to oxygen molecule.

Reproduced with permission from Ref. [137]. Copyright 2013 American Chemical Society.

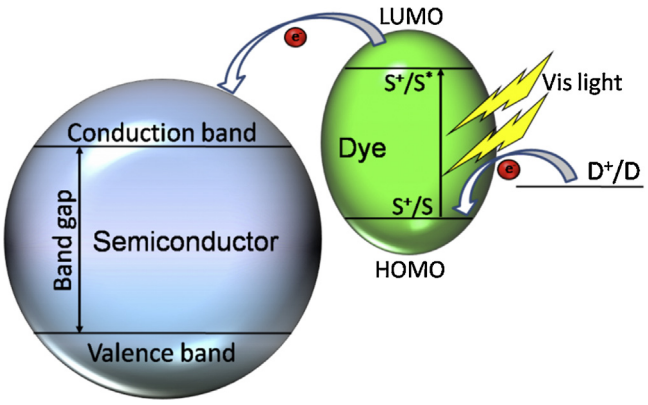

Fig. 8. Mechanism of dye sensitized semiconductor photocatalysis.

However, these approaches are still either too costly or not sufficiently accurate for extended systems, particularly if exposing surfaces. A more simplified approach to simulate the photoexcited TiO_2 is based on spin-constrained DFT, where the first excited state is obtained by imposing a triplet spin state configuration to the model system [135]. Structural relaxation in the excited state is then achievable (not possible with any other more sophisticated method), which allows one to compute the emission energy from a self-trapped exciton. Comparison of the computed with the experimental luminescence values is excellent (2.6 vs. 2.3 eV), especially considering the inherent approximations [136]. The same approach can be used to describe separated electron/hole pairs, travelling from the bulk to the surface where they become self-trapped. Self-trapping energies are interesting quantities since they define how surface traps are competitive with respect to electron or hole transfers to chemical adsorbates, which are the first chemical step of any redox process in the photocatalytic cycle.

3.4. Redox processes at the photocatalysts surface

Photoinduced electrons and holes are generally considered to travel from the bulk to the surface. Recently, the driving force for this migration has been determined to be the larger trapping energy at a surface rather than at a bulk regular site [135]. Chemical species adsorbed on the surface are excellent scavengers for electrons and holes. Calculations show that the O_2 molecule is capable of very easily removing the electron from the catalyst to form first superoxo and then peroxo species (Fig. 7) [137].

Organic acids and alcohols were also computed to be excellent hole scavengers, which is a hint that the direct oxidation mechanisms is a viable path for certain chemical species [138]. Hydroxyl species are found to facilitate photo-oxidation reaction of methyl chloride on rutile (1 1 0) surface [139].

4. Historical developments of visible-light active TiO_2 photocatalysts

As discussed earlier, one of the major drawbacks of pure TiO_2 is the large band gap implying that this material can only be activated using an irradiation with photons in the UV region ($\lambda \leq 387$ nm). In order to obtain activity in the visible region, it is essential to modify the semiconductor materials by using dye sensitization, noble metal loading, transition metal addition and non-metal doping. Modification with transition metal ions was the first method reported for their visible-light activation of TiO_2 [140]. The main drawback of these catalysts is the formation of recombination sites for photogenerated charge carriers and thus lowering the quantum efficiency. Transition metals also block the active surface reaction sites. In 1986 Sato discovered that modification of TiO_2 with NH_4OH resulted in their visible light absorption [141]. Later Asahi et al. for the first time investigated the photocatalytic activity of N-doped TiO_2 [142]. After this report, significant efforts have been devoted for the development of various anion doped TiO_2 photocatalysts [143,144].

4.1. Dye-sensitization

This is one of the widely used techniques for the utilization of visible-light in photocatalytic and photovoltaic systems [145–148]. During visible-light irradiation, excited electrons are transferred from the dyes to the conduction band of the semiconductor (Fig. 8). Some dyes are even capable of producing electrons by absorbing visible-light in the absence of semiconductors. Nevertheless, in the absence of semiconductor charge separators, photocatalytic activities of these dyes are too low. Visible-light absorption and electron transfer to the conduction band of TiO_2 often resulted in a superior photocatalytic activity. Degradation of the dye itself is one of the main issues in the dye-sensitization of semiconductors. This was usually overcome by dye regeneration by using sacrificial agents, or redox systems like EDTA and I_3^-/I^- pair [149]. Optimum conditions to obtain higher photocatalytic efficiencies are fast electron transfer to the semiconductor and slow recombination. In the case of dye-sensitization, electron injections occur in a femtosecond scale compared to the recombination of electron–hole pairs in nanoseconds to milliseconds scale [150–154]. Advantages of the dye-sensitized photocatalytic reactions are the fast injection of electrons to the semiconductor and slow backward reaction. Visible-light induced hydrogen generation through dye-sensitized water splitting was reported by previous researchers [155,156]. These studies illustrated that the electron injection occurs only from the dye molecules adsorbed on the surface of the photocatalyst. Dye-sensitization was also identified as highly effective for the degradation of a number of pollutants under visible irradiation [157,158].

4.2. Noble metal loading

Noble metals for instance Au, Ag, Pt, Pd, and Rh have been reported as very efficient dopants for the visible-light activation and thereby improving the performance of TiO_2 photocatalysts [159–164]. Fermi levels of these noble metals are lower than that of TiO_2, which results in the effective transfer of the photogenerated electrons from the conduction band of TiO_2 to metal particles (Fig. 9) [165]. This electron trapping process significantly reduces the electron–hole recombination rate, which results in stronger photocatalytic reactions. Electron spin resonance (ESR)

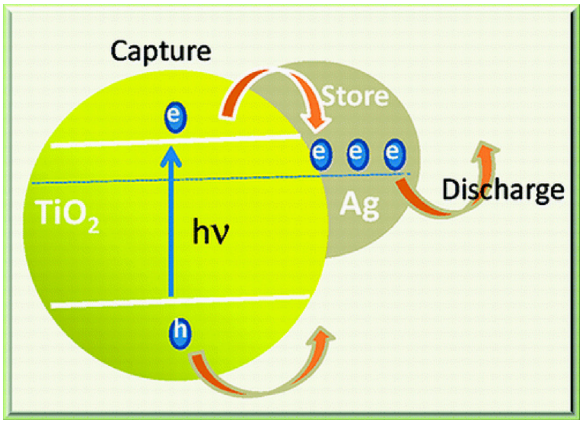

Fig. 9. Electron transfer mechanism in silver loaded TiO_2. Reproduced with permission from Ref. [165] Copyright 2011 American Chemical Society.

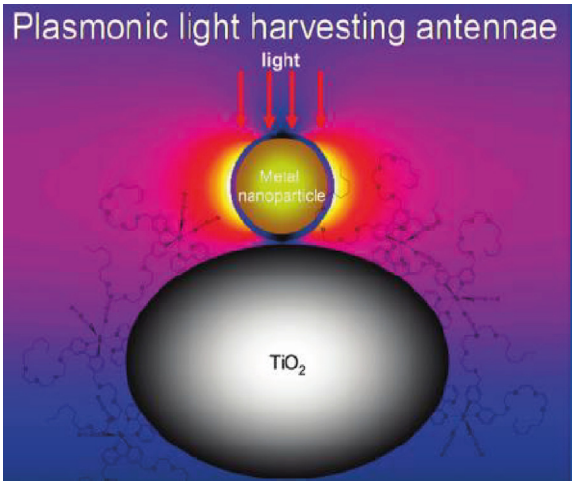

Fig. 10. Plasmonic light harvesting using core-shell metal-insulator nanoparticles. Reproduced with permission from Ref. [180]. Copyright 2011 American Chemical Society.

spectroscopy was used by previous researchers to investigate the charge transfer mechanism in these metals doped TiO_2 [166]. Anpo and Takeuchi employed electron paramagnetic resonance (EPR) spectroscopy to establish electron transfer between Pt nanoparticles and TiO_2 [167]. Bamwenda et al. investigated the effect of Au and Pt nanoparticles on the photocatalytic activity of TiO_2 materials through the photocatalytic splitting of water-ethanol mixture [160]. Seery et al. improved the visible-light photocatalytic activity of TiO_2 by silver doping. They observed superior UV, and Vis-light absorption due to silver plasmon resonance [168].

A number of synthetic methods including sol–gel process, hydrothermal method, impregnation, and photo-deposition were reported for the fabrication of noble metal modified TiO_2 [168–170]. Photocatalytic activities of these modified samples were highly dependent on both the synthesis method and work function of the noble metal. Among the various noble metal modified TiO_2 samples, Pt and Au loaded were found to be most effective and less sensitive to the synthesis methods. The higher effectiveness resulted from the higher work-functions and optimum electron-affinity associated with Pt and Au. Sakthivel et al. studied the photocatalytic activities of Au, Pt, and Pd modified TiO_2 through photo-oxidation of acid green-16 and determined the optimum loading for each metal [161]. A reduced photocatalytic performance was identified above an optimum metal content, which was proven to be resulting from a reduced photon absorption by TiO_2 and from the action of excess metal as electron–hole recombination centres. The noble metal loaded TiO_2 photocatalysts show also different photocatalytic activities for hydrogen production depending on the noble metal and on the sacrificial reagent.

Recently, TiO_2 loaded with metallic nanoparticles possessing unique properties, such as localized surface plasmon resonance (LSPR), are widely used for photocatalytic reactions in visible wavelengths [165,171]. Modification of semiconductor nanostructures with plasmonic metal-nanoparticles improved the efficiency of water splitting, decomposition of organic compounds, and photovoltaic devices (by 10–15%) [171–175]. For instance, Tian et al. reported superior visible-light photocatalytic decomposition of methanol and ethanol on Au-nanoparticles loaded TiO_2 films [176,177]. Furube et al. used transient absorption spectroscopy for the investigation of charge separation/recombination dynamics in Au-nanoparticles loaded TiO_2 [178]. Their results proved plasmon induced electron transfer to TiO_2. Efficient utilization of the near IR radiations and photoelectric conversion by Au-nanorod arrays modified TiO_2 single crystals were reported by Nishijima et al. [179]. It was found that a thin coating of silica on Au nanoparticles (Fig. 10) significantly improved the photocatalytic rate by reducing the carrier recombination [180].

Plasmon sensitization was also used in combination with dye sensitization. For instance, addition of Ag nanoparticles increased the absorption coefficient and efficiency of dye-sensitized solar cells [180,181]. Similarly, Rand et al. modified the tandem solar cells with Ag-nanoparticles and observed an unexpected improvement in the charge generation and visible-light absorption [182]. They attributed the surface plasmon modes of Ag-nanoparticles to the increased photocurrent generation. In addition, a number of studies demonstrated the superior plasmon-sensitized visible-light photocatalytic activities of TiO_2 loaded with Au and Ag nanoparticles [183–185]. Several methods for silver nanoparticle deposition on TiO_2 such as thermal evaporation, magnetron sputtering, electrochemical deposition, hydrothermal treatment and photocatalytic reduction have been demonstrated by previous researchers [186–191]. In addition to Au and Ag nanoparticles, TiO_2 nanotube arrays sensitized with Pd nanoparticles were highly efficient towards the visible-light induced photoelectrocatalytic water splitting [192].

LSPR improves the photocatalytic activity in three different ways by; (1) extending light absorption of semiconductor to longer wavelengths, (2) increasing the scattering of visible-light, and (3) creating electron–hole pairs by transferring the electrons from the metal nanoparticles to the conduction band of semiconductors. When the semiconductor and plasmonic metal nanoparticles are in direct contact, direct electron transfer (DET) results from the metal to the conduction band of the semiconductor [183,193,194]. The critical factor deciding the feasibility of DET is the arrangement of the plasmonic metal Fermi level and semiconductor band levels. Consequently, if the electronic energy levels match, metal to semiconductor transfer of holes or electrons can occur even at energies below the band gap. Previous researchers confirmed LSPR mediated transfer of electrons from gold nanoparticles to the conduction band of TiO_2 [185]. Recent studies proved that the photocatalytic activity improvement was unchanged even after an insulating layer was added between the semiconductor and plasmonic metal [183]. As a result, it was concluded that electron–hole pairs are created on the semiconductor by a radiative contribution of the LSPR-mediated local electromagnetic field (LEMF) [172,174,195].

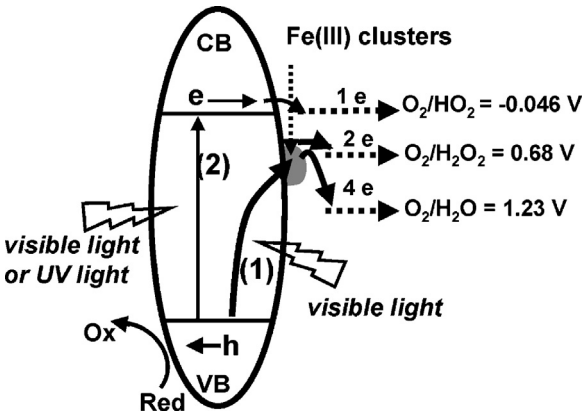

Fig. 11. Schematic diagram illustrating the possible photocatalytic mechanism of Fe(III)/TiO_2 involving interfacial electron transfer and multielectron oxygen reduction.

Reproduced with permission from Ref. [205]. Copyright 2010 American Chemical Society.

4.3. Transition metal doping

Improved visible-light photocatalytic activities of various transition metal doped TiO_2 has been comprehensively investigated [196–202]. These studies proved that doping results in the increased visible-light absorption. As a result of transition metal doping, impurity energy levels are created in the band gap, which results in visible-light absorption. Photocatalytic activities are also improved by electron transfer between TiO_2 and transition metal ions [203]. Choi et al. doped TiO_2 with 21 transition metal ions and investigated their photocatalytic activities [196]. Visible-light photo-responses were observed for TiO_2 photocatalyst as a result of most of these metal ion doping. Extensive research on the enhancement of TiO_2 photocatalytic activities has been performed through doping of transition and rare earth metal ions, especially for air and water sanitization applications [196–198]. Among the various metal ions studied by Choi et al., increased photocatalytic activity was identified for Mo, V, Re, Ru, Fe, Rh, and Os ions doped TiO_2 [196]. Whereas Al and Co ions reduced the activity. Fe and Cu ions create additional energy levels near the valence band as well as conduction band of TiO_2, which result in the trapping of both electrons and holes. Consequently, it is highly recommended to dope TiO_2 with either Fe or Cu ions to obtain superior photocatalytic activity [196,197].

Hashimoto et al. designed and fabricated Cu(II) and Fe(III) grafted TiO_2 photocatalysts for efficient visible-light induced decomposition of 2-propanol to CO_2 via acetone [204,205]. In this case, visible-light activation was caused by the interfacial charge transfer from the valence band holes to Cu(II) ions. Cu(I) ions formed by the reduction of Cu(II) also act as a multi-electron oxygen reduction catalyst. Reaction rates of Cu(II)/TiO_2 catalyst was 2.1 fold higher than those of N-doped TiO_2 under similar experimental conditions [204]. Fe(III)-grafted rutile TiO_2 displayed optical absorption in the visible region above 400 nm, which resulted from the interfacial charge transfer from the valence band of TiO_2 to the surface Fe(III) species [205]. Superior quantum efficiency of 22% was observed for Fe(III)/TiO_2 in the visible-light region (400–530 nm), and photocatalytic activity can be maintained up to 580 nm with a quantum efficiency of 10%. High performance of Fe(III)/TiO_2 was attributed to the accumulation of photogenerated holes in the valence band of TiO_2 and the catalytic reduction of oxygen by photoreduced Fe(II) species on TiO_2 surface (Fig. 11). Morikawa et al. loaded N-doped TiO_2 with Fe, Cu and Pt to improve the visible-light response [206]. It was found that Pt, Fe and Cu loading resulted in similar rate enhancement towards acetaldehyde oxidation, while Pt, and Cu gave the highest rate for toluene and acetic acid oxidation. Rate of formic acid oxidation was enhanced by factors of 5 and 22 on loading Fe and Pt respectively. Extremely high rate enhancement of formic acid oxidation was attributed to the combined effect of photocatalysis and thermal catalysis. Such transition metal loading of N-doped TiO_2 was also reported by other researchers for the improved visible-light activation of TiO_2 [207].

Peng et al. investigated the photocatalytic activity of Be doped TiO_2 [208]. They found that metal ion doping close to the surface improves charge carrier separation, whereas deep doping accelerates carrier recombination. These findings were in good agreement with the results of Choi et al. [196]. Wu et al. investigated the effects of transitional metal ions (Cr, Mn, Fe, Co, Ni and Cu) doping on the photocatalytic activity of TiO_2 through the photocatalytic oxidation of acetic acid [201]. Enhanced photocatalytic activities were observed for Cu, Mn and Fe ions doped TiO_2 as they can trap electrons as well as holes, whereas Cr, Co and Ni ions doped samples were not much active as they can trap only one charge carrier. Dhanalakshmi et al. investigated the dye sensitized hydrogen production efficiency of Cu-modified TiO_2 and compared with that of Pt-doped compositions and the enhancing effect was found to be comparable [146]. Hydrogen production efficiency of Cu-modified TiO_2 particles from methanol solution was also investigated by Wu and Lee [209]. A ten-fold enhancement in the hydrogen production efficiency was demonstrated at an optimum Cu-loading. Xu et al. compared photocatalytic activities of various (La, Ce, Er, Pr, Gd, Nd and Sm) rare earth metal ion doped TiO_2 [199]. TiO_2 loaded with optimum dopant content demonstrated superior band-gap narrowing and visible-light photocatalytic activities. As a result of its ability to transfer both electrons and holes to the surface Gd-ions doped TiO_2 was found to be the most photoactive.

Another efficient method for improving the visible-light response is metal ion implantation [167,210,211]. This process involves bombarding a semiconductor with high-energy transition metal ions. During the collision, metal ions penetrate into the semiconductor crystal structure and improve the visible-light absorption by creating additional energy levels. A visible-light response up to 600 nm has been reported for metal ions implanted TiO_2. Takeuchi et al. employed this method to implant Cr ions in TiO_2 thin films for the visible-light induced degradation of nitric oxide (NO) [210]. For this implantation, they used an ionized cluster beam (ICB). The UV–Vis absorption studies revealed the band gap narrowing in these TiO_2 samples and the extent of band gap narrowing was found to be directly proportional to the Cr-ion loading. Visible-light photocatalytic activities of these Cr-doped TiO_2 were highly promising for NO degradation. This high activity compared to the chemically Cr-doped TiO_2 point towards the fact that the metal ion implantation did not create recombination centres. A wide range of metal ions (V, Cr, Mn, Ni, Mg, Ti and Fe) has been implanted for visible-light activation of TiO_2 [167,211]. Visible-light absorption was observed for all ions except Mg and Ti ions. The effectiveness of dopant ions in the band gap narrowing was found to be in the following order: V > Cr > Mn > Fe > Ni. In the case of ion implanted TiO_2 no sacrificial agents and electron mediators are necessary to maintain the reaction cycles. For improved carrier transferring and photocatalytic activity, metal ions should be doped close to the TiO_2 surface. In the case of deep doping, carrier (electrons and holes) transfer to the interface is more difficult and metal ions act as recombination centres. Similarly, photocatalytic activity decreases above an optimum metal ion doping due to increased carrier recombination.

Metal doping of TiO_2 has been investigated theoretically in order to establish how the doping element effectively modifies the semiconducting oxide electronic structure for the absorption in the visible and the molecular adsorption properties at the surface [212–215]. In most of the cases the dopant is a transition

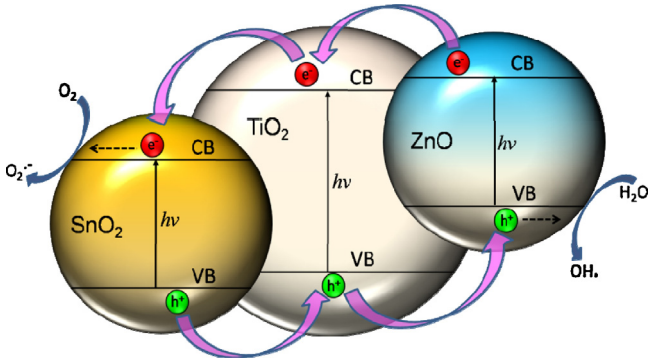

Fig. 12. Electron transfer mechanism in composite semiconductor.

metal in a substitutional lattice cationic site. The correct description of the metal *d* states, especially when these are partially occupied, requires the use of methods, which reduce the electron self-interaction problem. For the case of Cr-doped TiO_2, GGA calculations indicate a spurious half-metallic character of the system (no splitting of the partially occupied Cr t_{2g} *d* states), contrarily to the semiconducting properties (splitting of the occupied-unoccupied Cr t_{2g} 3*d* states) by more accurate hybrid functional methods [216]. The presence of transition metal *d* states in the TiO_2 band gap is clearly the origin of the experimentally observed red-shift in the absorption properties of metal doped TiO_2 [217].

4.4. Heterojunction semiconductors

Coupling of semiconductors having different band gap values is another method to efficiently utilize visible-light and enhancing the photocatalytic activity. The necessary condition for coupling is that the conduction band level of at least one of the semiconductors must have a more negative value compared to the other. The electron injection mechanism in composite semiconductors can occur through the following mechanism (Fig. 12). In the case of semiconductor heterojunctions, photogenerated electrons can be effectively transferred from the conduction band of one semiconductor to that of the other. The electron injection always occurs from the more negative conduction band to the less negative one. This electron transfer is identical to the dye sensitization of TiO_2, except the difference being the electron injection happens between two semiconductors. Coupling of TiO_2 with CdS (band gap 2.4 eV) and SnO_2 (band gap 3.5 eV) for visible-light induced water splitting and purification were previously investigated [145,218,219].

In this case, the small band gap CdS (CB = −0.76 eV) cause visible-light sensitization, and inject electrons to the conduction band of SnO_2 (CB = −0.34 eV), which results in an efficient electron–hole separation and an increase of photocatalytic activity. EDTA was used as a hole scavenger to prevent the photo-corrosion of CdS. Doong et al. reported very high photocatalytic activity of CdS coupled TiO_2 towards the photocatalytic decomposition of 2-chlorophenol [220]. The better photocatalytic activity resulted from the electron injection from CdS to TiO_2 and hole injection from TiO_2 to CdS, which results in better charge separation. Kang et al. demonstrated the photodegradation of 4-chlorophenol using CdS–TiO_2 composite semiconductor [221]. The photocatalytic activities of the composite were found to be very high in comparison to that of CdS and TiO_2 used separately.

TiO_2 coupled with CdS can also be utilized for photocatalytic water splitting due to the more negative conduction band of TiO_2 compared to E_{H_2/H_2O}. So et al. prevented the photo-corrosion of CdS with the help of Na_2S during photocatalytic hydrogen generation from water [222]. Since the optical absorption of CdS–TiO_2 extends up to 520 nm, this can be utilized for the visible-light

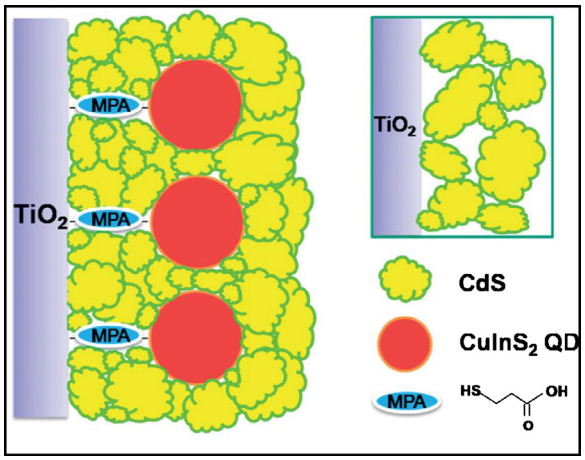

Fig. 13. A conceptual schematic of the $CuInS_2$-QDs/CdS heterostructure on the TiO_2 surface.

Reproduced with permission from Ref. [235]. Copyright 2012 The Royal Society of Chemistry.

induced photocatalytic reactions. Compared to pure CdS and TiO_2, a higher rate of hydrogen production was observed for CdS–TiO_2 under visible-light illumination. De et al. proved the improved visible-light activity of CdS–ZnS composite semiconductor for the photocatalytic water splitting [223]. Similar enhancements in the photocatalytic water splitting reactions using CdS–ZnS were also reported by Koca et al. [224]. TiO_2 coupled with wide band gap semiconductors were found to be highly photocatalytic under UV light. Superior photocatalytic activities of TiO_2–WO_3 and TiO_2–SiC composite semiconductors were observed by Keller and Garin [225]. In the case of TiO_2–SiC composite, the efficient electron injection occurs from the more negative conduction band of SiC to the less negative conduction band of TiO_2. On the other hand, excited electrons transfer from the conduction band of TiO_2 to the less negative conduction band of WO_3 in TiO_2–WO_3 composite. As a result of an improved electron–hole separation, these composite semiconductors were more efficient for the photochemical decomposition of methyl ethyl ketone (MEK). Recently, Li et al. synthesized a series of highly visible-light efficient semiconductors by combining N-doped ZnO with WO_3, V_2O_5 and Fe_2O_3 [226]. In these composite semiconductors, visible-light activation was achieved through nitrogen doping and the small band gap semiconductors such as WO_3, V_2O_5 and Fe_2O_3 were responsible for effective electron–hole separation. Coupling of TiO_2 with WO_3 and V_2O_5 were found to be more effective compared to Fe_2O_3 due to carrier recombination on Fe_2O_3. However, these composites were not suitable for hydrogen production due to the less negative position of WO_3 and V_2O_5 conduction bands.

Besides dyes and metal nanoparticles, semiconductor quantum dots (QDs) could also be used for sensitizing TiO_2 photocatalysts, where the QDs absorb light energy and transfer electrons to the conduction band [227]. Recently, extending the visible-light harvesting with various QDs such as of PbS, InP, CdS, CdTe, $CuInS_2$, Bi_2S_3 and CdSe attracted a great attention for solar energy conversion [228–235]. A high performance quantum dot sensitized solar cell composed of TiO_2/$CuInS_2$-QDs/CdS/ZnS photoanode (Fig. 13) was reported recently [235]. An efficient way to harvest the entire solar spectrum is by tuning the particle size of QDs [236]. For instance, CdSe quantum dots of particle sizes 2.3, 2.6, 3.0, and 3.7 nm correspond to visible-light absorptions of 557, 543, 520, and 505 nm respectively [237].

Additionally, the Shockley–Queisser limit of energy conversion efficiency can be overcome by the unique electronic structure of QDs [238]. Moreover, integration of various QDs with different

sizes allows energy absorption over a wide range. QDs are excellent sensitizers in solar cells due to their ability to harvest hot electrons and generate multiple carriers [239,240]. They were also used in combination with dye-sensitization and nitrogen doping to enhance the visible-light photocatalytic activity of TiO_2 photocatalysts [241,242].

An important chalcogenide compound Ag_2S (band gap = 1.0 eV) has been investigated as for the visible-light sensitization of TiO_2 nanoparticles for photocatalytic and photovoltaic applications [243,244]. In addition to semiconductor nanoparticles, carbon quantum dots (CQDs) with excellent broadband light absorption, strong photoluminescence, chemical stability, and nontoxity has been coupled with TiO_2 nanoparticles to improve the visible-light photocatalytic activities [245,246]. Recently, carrier recombination in QDs sensitized TiO_2 has been reduced by forming a ZnO layer between them [247].

From the computational point of view, the band level arrangement at the heterojunctions between TiO_2 and QDs is a challenging task, even for state-of-the-art methodologies. It has been proposed to use slab models based on the calculated value of the electrostatic energy at the interface as a reference for the band-edge positions [248]. This approach was shown to be successful in the case of the ZnO/TiO_2 interface if a proper exact exchange contribution is introduced in the hybrid functional used for performing the calculations.

4.5. Nonstoichiometric TiO_2

Imperfections within the crystal structure significantly affect the phase stability, electronic structure and photocatalytic activity of TiO_2 photocatalysts [8,115]. TiO_2 samples containing oxygen vacancies were found to exhibit enhanced visible-light absorption, and photocatalytic activities. In the case of TiO_2 containing oxygen vacancies, a partially occupied impurity energy level ~2.0–2.5 eV above the valence band was experimentally observed [249–252]. The additional energy level has also been attributed to the existence of partially occupied Ti^{3+} states, which create energy inter band gap energy levels just below the conduction band [253]. The theoretical modelling of Ti^{3+} centres in reduced TiO_2 is a very delicate issue since they have a strong polaronic character (i.e. the electron trapping causes a lattice reorganization around the Ti^{3+} centre). The proper position of Ti^{3+} associated states in the band gap of TiO_2 is not an easy task and must be addresses with electron self-interaction corrected methods (DFT + U or hybrid functionals), since LDA and GGA approaches, which underestimate the band gap value and overestimate the excess electron delocalization, provide the incorrect picture of fully delocalized Ti^{3+} states in resonance with the bottom of the conduction band [254–257]. Heat treatment of TiO_2 under oxygen deficient atmosphere and anionic doping were reported as the key synthesis methods for TiO_2 containing oxygen vacancies.

Oxygen vacancy formation is more pronounced in the case of N doped TiO_2 [142,258,259]. Formation of oxygen vacancies and Ti^{3+} ions were experimentally supported by EPR studies and DFT calculations [260]. Formation oxygen vacancies and Ti^{3+} in titanium dioxide calcined under hydrogen atmosphere were reported by previous researchers [115,261,262]. Recently, visible-light absorption of TiO_2 has been improved through hydrogenation of TiO_2 [263]. This is a very efficient method in which the mid-gap states above the valence band maximum (Fig. 14) due to the hydrogenated, engineered disorders cause band gap narrowing [263]. Though TiO_2 containing oxygen vacancies can absorb visible-light, their quantum efficiencies were low due to increased electron–hole recombination [8,11,17]. Identical to oxygen vacancies, oxygen excess defects can also result in new states in the band gap. Etacheri et al. recently synthesized oxygen rich TiO_2 through a peroxo-TiO_2 route, which demonstrated excellent visible-light photocatalytic

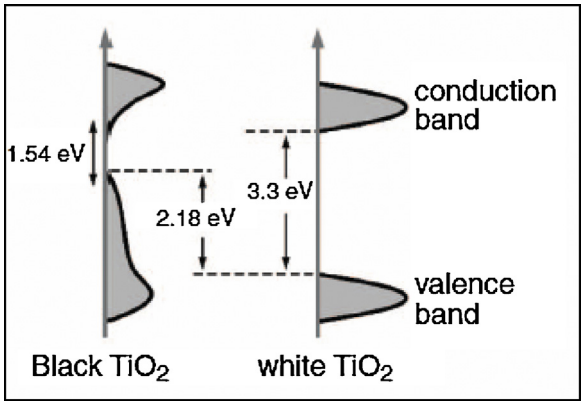

Fig. 14. Electronic structure of black hydrogenated TiO_2. Reproduced with permission from Ref. [263]. Copyright 2011 American Association for the Advancement of Science.

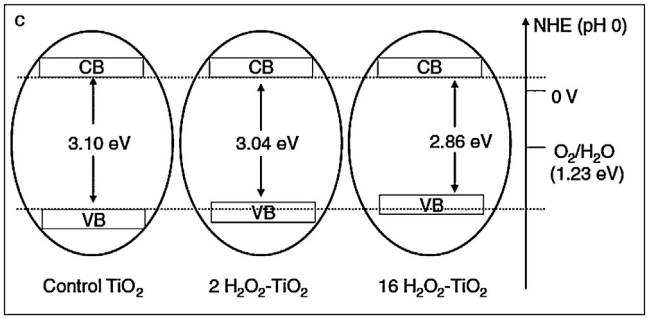

Fig. 15. Electronic structure of oxygen rich TiO_2. Reproduced with permission from Ref. [8]. Copyright 2011 Wiley VCH.

activity [8]. In this case, in situ formation of oxygen creates interstitial oxygen excess defects, which was confirmed from FTIR and XPS studies. These oxygen excess defects bind with lattice oxygen atoms and result in the formation of a substitutional O_2 molecule, causing a decrease in lattice parameters.

Oxygen excess defects also cause band-gap narrowing by valence band shifting (Fig. 15), which was confirmed using valence band XPS and photoluminescence (PL) studies. Oxygen rich TiO_2 samples exhibited reduced PL-intensities compared to phase pure anatase TiO_2 due to reduced electron–hole recombination. Oxygen excess defects also act as electron scavengers that increase the lifetime of photo-generated holes and decrease luminescence. Compared to pure anatase TiO_2 and Evonik Degussa P-25, oxygen rich TiO_2 exhibited six-fold and two-fold higher visible-light photocatalytic activities respectively. Only a few studies of interstitial oxygen species are available. These show that an additional neutral oxygen atom prefers to bind to a lattice oxygen atom forming an O—O bond, instead of being stabilized as a charged species in the middle of an interstice [264,265]. Interestingly, oxygen interstitials are predicted to be good electron traps by GGA + U calculations. The extra electron occupies a σ^* state, which leads to a consistent elongation of the O—O bond from 1.484 to 1.970 Å.

4.6. Non-metal doping

4.6.1. Nitrogen doping

Anion doping to enhance the visible-light photocatalytic activity in a semiconductor is a relatively a new method compared to other techniques. Improved visible-light absorption was observed for a variety of anions (N, F, C, S, etc.) doped TiO_2 [142,266–269]. Non-metal dopants were found to be more efficient compared to most of the metal ions due to the less formation of recombination

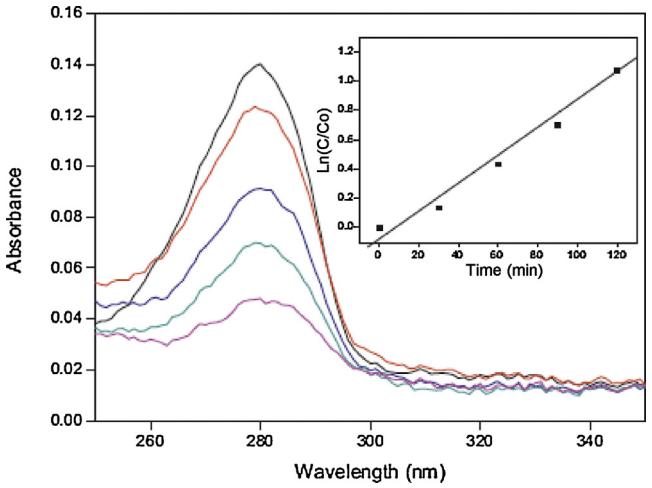

Fig. 16. Solar photocatalysis of 4-chlorophenol using "N doped TiO_2". Reproduced with permission from Ref. [278]. Copyright 2012 Elsevier Science.

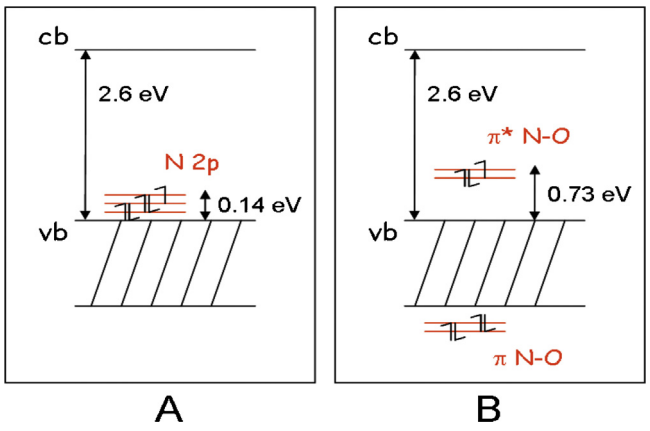

Fig. 17. Electronic band structure of (A) substitutional and (B) interstitial N-doped anatase TiO_2.

Reproduced with permission from Ref. [260]. Copyright 2005 American Chemical Society.

centres. Asahi et al. synthesized a series of anion-doped TiO_2 and also determined the substitutional doping contents of these ions [142]. In contrast to other anion doped TiO_2, the nitrogen-doped compositions have been found to be more effective and extensively investigated [207,270]. "N doped TiO_2" can be synthesized through various physical and chemical methods [258,271–275]. Fabrication of "N doped TiO_2" thin film involved sputtering under N_2/Ar gas atmosphere and annealing in an N_2 atmosphere [142,276,277]. Sol–gel synthesis of N-doped TiO_2 use 1,3-diaminopropane, and urea as precursor modifier to incorporate nitrogen [278,10,279]. "N-doped TiO_2" sample calcined at 500 °C was found to be highly effective in the degradation of 4-chlorophenol under solar irradiation (Fig. 16). No degradation was recorded for the undoped TiO_2 prepared under similar experimental conditions [278].

In another study, "N-doped TiO_2" powders, prepared by treating TiO_2 with NH_3 followed by calcinations, were reported to be highly active for the decomposition of methylene blue under visible-light irradiation [280]. A mechanochemical method using crystalline TiO_2 and hexamethylenetetramine (HMT) was also reported [281]. Hydrothermal and microwave assisted hydrothermal methods were also very effective for the synthesis of mesoporous TiO_2 containing nitrogen [282,283].

Electronic structure and type of dopant species of N-doped TiO_2 highly depends on the synthetic method. Several researchers proposed that lattice nitrogen causes the visible-light absorption, while other studies attributed NO_x and NH_x adsorbed on the surface to band gap narrowing [142,284]. Thus, a controversy still remains regarding the dopants nature and electronic structure of anion doped TiO_2. Asahi et al. illustrated the electronic structure and visible-light absorption of N-doped TiO_2 based on Ti—N bonding [142]. They performed density state calculations and concluded that N-atoms substitute O-atoms of anatase TiO_2, and a consequent mixing of O 2*p* and N 2*p* state results in the band gap narrowing. This finding was also supported by the observations of Irie et al. [285]. However, a negative contribution of Ti—N bonding towards to band gap narrowing was identified by Diwald et al. [286]. Further detailed investigations of electronic structure modification mechanism by of N–TiO_2 have subsequently been conducted by a number of researchers [258,285,287–290].

Di Valentin et al. performed a DFT study of N-doped TiO_2 with the hybrid functional B3LYP [260,269]. Their results showed that substitutional N-doping introduces localized impurity states just above the valence band level, and negligible mixing occurs between N 2*p* and O 2*p* states. In the same study it was also shown that N could enter the TiO_2 lattice also in an interstitial position (NO species). It is evident that both conduction and valence band edges are unaffected by the dopants, and visible-absorption is resulted by localized energy levels generated by the NO bond [285]. Two bonding energy-levels are positioned below the valence band level, and antibonding orbitals lie 0.73 eV above the valence band. It is also proposed that antibonding NO orbitals act as stepping stone between conduction band and valence band of TiO_2 (Fig. 17) [237] and facilitate visible-light absorption [291–293]. Sugihara and co-workers have indicated that nitrogen doping could stabilize oxygen vacancies, which induce visible-light absorption [258]. This has been fully corroborated by DFT calculations in combination with EPR experiments on N-doped polycrystalline powder samples, showing that the stabilization results from electron transfer between high energy Ti^{3+} states to the low lying N induce impurity states (Fig. 18) [294].

TiO_2 surface nitrogen doping was also investigated by DFT calculations. Both the rutile (1 1 0) and anatase (1 0 1) surfaces were considered [295,296]. Analogous substitutional and interstitial species were identified as in the bulk of TiO_2. The electronic interplay with oxygen vacancies is found to be synergistic; confirming that surface N-doping is expected to cause an enhanced defect concentration. Pillai and co-workers [278] observed an unexpected blue shift in the UV/Vis absorbance of N–TiO_2 samples heat treated at ≥600 °C. XRD analysis showed that these N doped

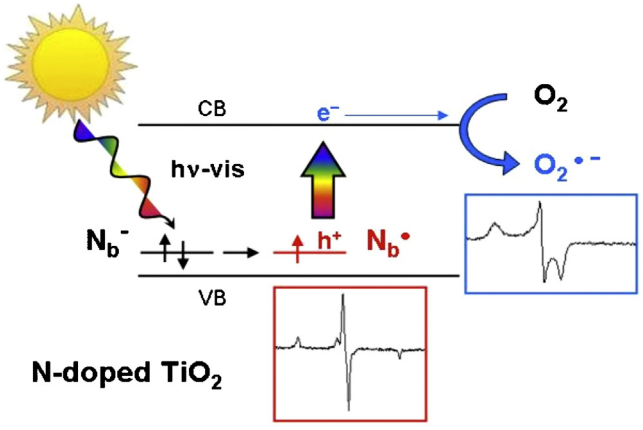

Fig. 18. Schematic representation showing electron transfer between high energy Ti^{3+} states to the low lying N induce impurity states.

Reproduced with permission from Ref. [294]. Copyright 2006 American Chemical Society.

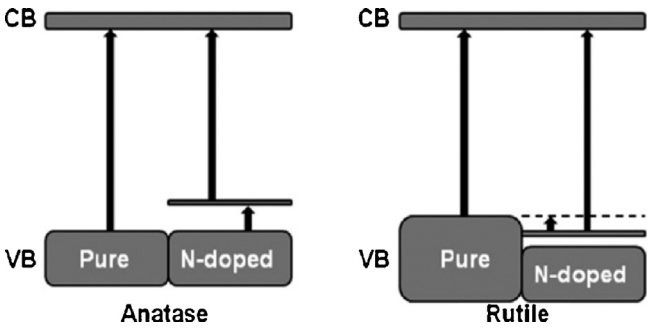

Fig. 19. Schematic diagram showing the energy states of pure and N-doped anatase and rutile TiO_2.
Reproduced with permission from Ref. [278]. Copyright 2012 Elsevier Science.

TiO_2, processed significant amounts of rutile phase. Di Valentin and co-workers [297] had previously explained using theoretical calculations that a blue shift was observed with N-doped (rutile) because not only the TiO_2 valence band lowered (by 0.4 eV) but the newly introduced N 2*p* states were also lower in energy than the valence band of pure rutile phase (0.05 eV). This resulted in an overall blue shift due to an effective band gap widening (Fig. 19).

4.6.2. Other non-metal doping

Kisch and co-workers for the first time reported daylight-induced photocatalysis using carbon-modified TiO_2 [298]. Many physical and chemical investigations were reported for the synthesis of carbon doped nanoparticles and thin films [19,299–302]. This narrow band gap TiO_2 showed significantly improved photocatalytic activities upon visible-light irradiation compared to pure anatase TiO_2 and the standard photocatalyst Evonik Degussa P-25. Control of porosity, morphology, and synthesizing hierarchical structures further improved the visible-light photocatalytic activities of C-doped TiO_2 [303–305]. Mechanism of visible-light absorption in C-doped TiO_2 was explained by the formation of Ti^{3+} and oxygen vacancies due to carbon doping [142,298,306,307]. On the basis of DFT calculations, it was concluded that substitution of O by C-atoms (Ti—C bond formation) resulted in the mixing of O 2p states with C 2p states, and band gap narrowing [306,308]. Later, further, DFT based calculations of C-doped rutile and anatase TiO_2 showed that C impurities can be both substitutional and interstitial, depending on the preparation conditions (i.e. oxygen partial pressure). Eventually, both types of species may even coexist since there is a synergistic effect associated to the electron transfer from the oxidized interstitial species to the reduced substitutional one [309].

Another interesting class of visible-light active photocatalyst consists of sulfur-doped TiO_2. Sulfur was detected as hexavalent (S^{6+}), tetravalent (S^{4+}), or sulfide (S^{2-}), depending on the synthetic method of S-doped TiO_2 [100,105,310]. Umebayashi et al. thermally oxidized TiS_2 to synthesize anionic S-doped TiO_2, and Ohno et al. fabricated cationic S-doped TiO_2 powder through chemical modification of titanium tetraisopropoxide using thiourea [266,310]. These S-doped materials were found to have notably improved photocatalytic decomposition of 2-propanol and methylene blue under visible-light irradiation. Absorption of visible-light by these photocatalyst is explained by the mixing of O 2p and S 3p states [266,310]. On the other hand, recent studies explained the band gap narrowing by the formation of S 3p impurity states above the valance band [311,312]. Formation of S 3p level 0.38 eV above the valence band was identified in the case of cationic S-doped TiO_2 [312]. Though S-doped TiO_2 is a promising visible-light active photocatalyst, incorporation of S in the TiO_2 crystal structure is difficult due to its large ionic radius [313].

It was demonstrated that F-doping is useful for improving the visible-light photocatalytic activity of TiO_2 [314–316]. F-doping was also effective for stabilizing the most reactive (0 0 1) facets of anatase TiO_2 [317]. The photocatalytic activity of such F-doped TiO_2 with dominant exposed (0 0 1) facets was remarkably higher than other F-doped TiO_2 nanoparticles [318]. F-doped thin films also showed improved visible-light photocatalytic activities towards the photodegradation of X-3B dye [319]. Iodine doping was also successful for significantly reducing the band gap of anatase TiO_2 photocatalysts [320–323]. Yu et al. explained that F-doping cause the reduction of Ti^{4+} to Ti^{3+}, which resulted in the band-gap narrowing [324]. Li et al. confirmed the formation of additional energy levels below the conduction band of F-doped TiO_2 due to oxygen vacancy formation [314].

Iodine is another potential dopant that can induce visible-light absorption by altering the electronic structure of TiO_2 photocatalyst. Cheng et al. synthesized mesoporous bicrystalline network of mesoporous TiO_2 with improved photodegradation of methylene blue under visible-light irradiation [321]. Synthesis, characterization, and electronic structure of multivalent iodine (I^{7+}/I^{-}) doped TiO_2 was reported by Fu et al. [323]. It was suggested that the recombination of photogenerated electron–hole pairs is inhibited due to the electron trapping action of the I sites [320]. A maximum absorption edge of 550 nm was experimentally determined for the lattice I-doped TiO_2. Whereas, an extended absorption up to 800 nm was observed for the surface iodine doped TiO_2 [325]. Photocatalytic activities of narrow band gap I-doped bronze phase TiO_2 was nanosheets were also investigated recently [326]. Iodine doped TiO_2 was highly effective for the degradation of dyes, 4-chlorophenol and CO_2 reduction under visible-light irradiation [320,325,327]. In the case of I-doped TiO_2, electronic excitation from the I–O–Ti states positioned just above the valence band to the I–O–I levels below the conduction band [325].

Moussab Harb has recently reported the optoelectronic properties of Se-doped TiO_2 using DFT and perturbation theory approach DFPT. A range of selenium doping at various substitutional sites for oxygen or titanium, interstitial sites or at mixed substitutional and interstitial sites were investigated. Various structures such as $Ti_{(1-2x)}O_2Se_{2x}$ (Se^{4+} species), $TiO_{(2-x)}Se_x$ (Se^{2-} species), and $TiO_{(2-x)}Se_{2x}$ (Se_2^{2-} species) with visible-light optical absorption spectra were identified (Fig. 20) [328]. Theoretical predictions were found to be in good agreement with the experimental results. The study of Grey et al. that boron doping of TiO_2 lead to partial reduction of Ti^{4+} to Ti^{3+}, which could improve the photocatalytic activity [329]. Compared to other non-metals, boron doping was not investigated in detail. Recently Chen et al. reported band gap widening for B-doped TiO_2, whereas Zhao et al. showed a band gap narrowing [330,331].

It was later demonstrated that proper doping of an optimum B-doping results in significantly higher visible-light absorption and visible-light photocatalytic activities [332]. These B-doped TiO_2 were successfully utilized for the decomposition of methyl orange, methyl tertiary butyl ether, orange II, 4-cholorophenol and nicotinamide adenine dinucleotide (NADH) under visible-light irradiation [330,332–334]. Based on LDA calculations, the band gap narrowing of boron doped TiO_2 was illustrated by the formation of isolated B 2p impurity levels in the band gap [291]. More refined hybrid density functional results indicate that B enters the TiO_2 lattice in the interstitial sites, forming oxidized borate species and, consequently, reduced Ti^{3+} centres [335].

Several attempts have been reported for the spectroscopic band gap investigation of the anion doped TiO_2. For instance, Etacheri et al. [17,19] performed valence band (VB) XPS to illustrate the consequence of S, N and C doping on the electronic structure of TiO_2 (Fig. 21). They identified similar valence band maximum (1.95 eV) for both pure and anion doped TiO_2, which was also identical to

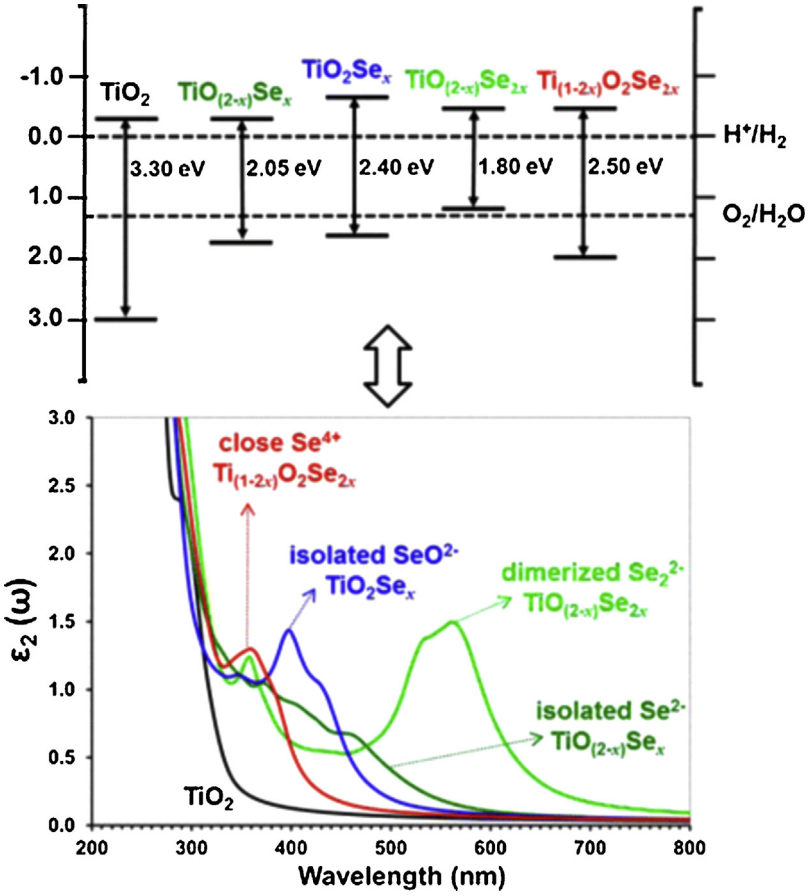

Fig. 20. Effect of selenium doping in the visible light activation of anatase TiO_2.
Reproduced with permission from Ref. [328]. Copyright 2013 American Chemical Society.

the previously reported valence band levels of pure anatase TiO_2 [8,336,337]. Additionally, equal width (9.5 eV) of the valence band explained identical mobilities of the photogenerated holes.

These spectroscopic results clearly ruled out the band gap narrowing due to the mixing of O 2*p* bands with C 2*p*, N 2*p* and S 3*p* states. Electronic structure of the anion doped TiO_2 highly depends on the electronegativity of dopant atoms. Only poor mixing of C 2*p*, S 3*p* and N 2*p* bands with O 2*p* bands can be expected due to the low electronegativity of C, S and N atoms (2.55, 2.58 and 3.04 respectively) compared to oxygen (3.44) [291,292]. Consequently, visible-light absorption of TiO_2 doped with anions such as C, S, and N doped TiO_2 can be illustrated by the electronic excitation from isolated C 2*p*, S 3*p*, N 2*p*, and Π^* N—O states in the band gap. Their findings demonstrated the fact that anion-doping does not actually causing band gap narrowing, and the visible-light absorption resulted from the isolated impurity levels in the band gap (Fig. 22).

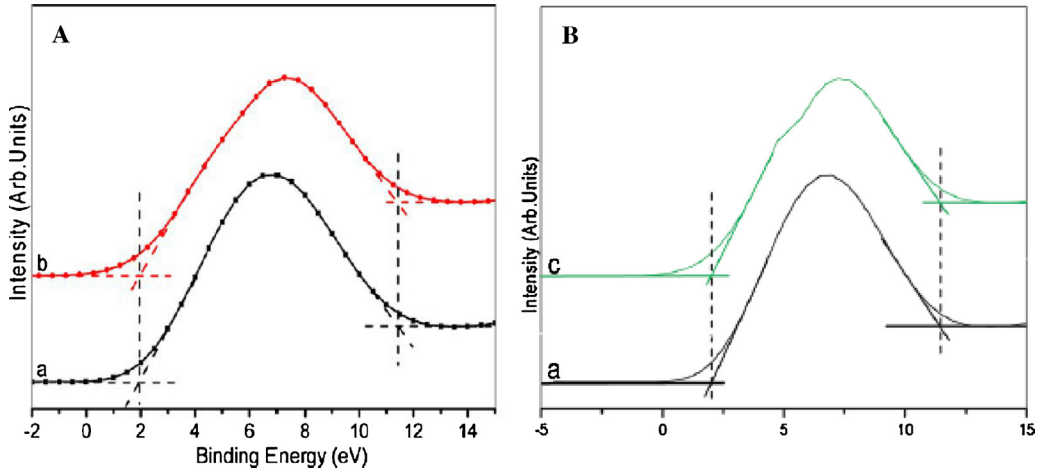

Fig. 21. Valence band XPS study of (A) C-doped anatase–brookite heterojunctions (a) pure TiO_2, (b) C-doped TiO_2. Reproduced with permission from Ref. [19]. Copyright 2013 American Chemical Society. and (B) S, N-codoped anatase–rutile heterojunctions (a) Pure TiO_2 (b) S, N-codoped TiO_2. Reproduced with permission from Ref. [17]. Copyright 2012 American Chemical Society.

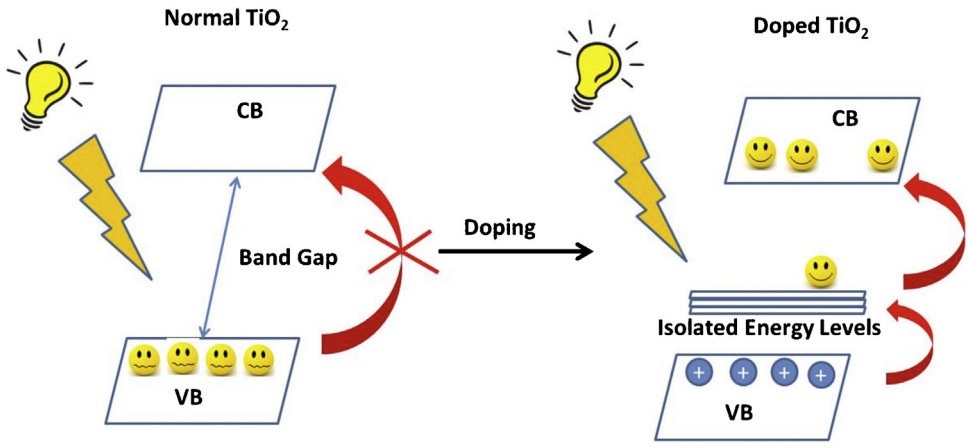

Fig. 22. Schematic mechanism of band gap narrowing in anion doped TiO_2.

The computational community has also made an effort to investigate and compare various non-metal dopants [309,338–343]. Recently, a systematic comparative hybrid DFT study was reported where N, C, B, F dopants are treated at an equal footing (Fig. 23) [344]. Clear trends emerged from this study. In particular, B and C are found to be preferentially oxidized by the TiO_2 lattice forming borate or carbonate species and reducing Ti^{4+} lattice sites to Ti^{3+} species. Nitrogen is not inclined to oxidation; even in the interstitial NO form [252]. Fluorine prefers the substitutional (to O) doping mode, which also causes the reduction of lattice Ti^{4+} ions, given the larger atomic number (F > O). All these non-metal dopants are prone to interact with intrinsic defects such as oxygen vacancies and Ti interstitials through long-range internal charge transfer process.

4.6.3. Non-metal codoping

Another efficient strategy for increasing the visible-light utilization of non-metal doped TiO_2 was the incorporation of multiple dopants (codoping). For example, (S, N)-codoped anatase TiO_2 exhibited enhanced visible-light photocatalytic performance compared to both S and N-doped TiO_2 [94,345,346]. XPS is identified as an effective tool to identify N and S incorporation in TiO_2 photocatalysts [10,11,17,19,113,347]. Pillai and co-workers explained that the peak at 402 eV is due to the presence of both NO and chemisorbed nitrogen (Fig. 24). Sulfur presents in the TiO_2 show a peak around 169 eV, which was assigned to S^{6+} cation [347].

Modification of TiO_2 precursor by ammonium sulphate and thiourea was found to be the most promising methods for the cationic S and anionic N-codoping of TiO_2 nanoparticles [17,347]. Additionally, Xiang et al. recently reported synthesis and improved activity of S, N-codoped (0 0 1) facet exposed anatase nanosheets [348]. Superior photocatalytic performance was endorsed to effective band gap narrowing by (S, N)-codoping and exposure of highly reactive (0 0 1) facets. Hydrothermal synthesis of B, N-codoped TiO_2 was reported to be highly effective for extending the visible-light absorption and improving visible-light photocatalytic activity. Xu et al. developed an organic-free sol–gel method for the fabrication of (C, N)-codoped TiO_2 films, which showed high visible-light photocatalytic activities towards the photodegradation of stearic acid [349]. (C, N)-codoped TiO_2 with special morphologies such as nanotubes and nanorods have been also reported previously. These visible-light active photocatalysts were superior to Evonik Degussa P-25 for the photodegradation of Rhodamine-B [350]. Macroporous TiO_2 microspheres codoped with C and F were highly efficient for the visible-light photocatalytic degradation of styrene [351].

Notably improved photocatalytic performance of mesoporous hierarchical TiO_2 containing C and S dopants was also reported

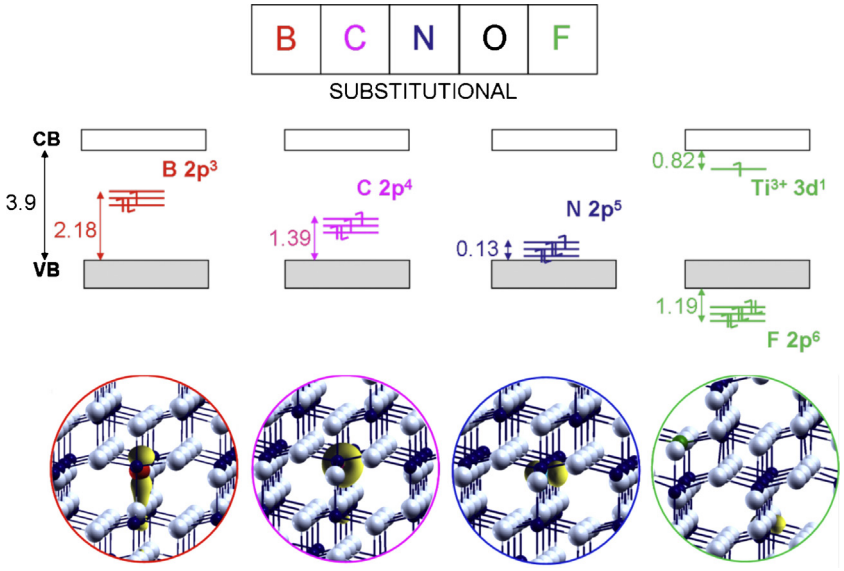

Fig. 23. Schematic representations of B, C, N and F doping in TiO_2.
Reproduced with permission from Ref. [344]. Copyright 2013 Elsevier Science.

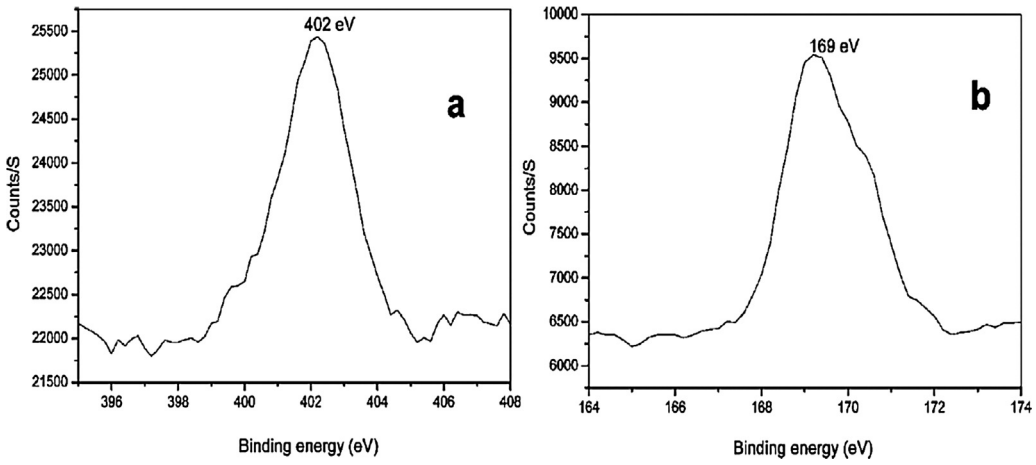

Fig. 24. XPS spectra of (a) nitrogen and (b) sulfur in TiO_2 photocatalysis.
Reproduced with permission from Ref. [347]. Copyright 2009 American Chemical Society.

recently [352]. First principle electronic structure calculation and XPS studies of (B, N), (B, I), (B, F) and (C, N)-codoped TiO_2 identified a synergetic effect between individual anions are accountable for the improved visible-light absorption [353,354]. Visible-light absorption up to 700 nm was observed in the case of (C, N)-codoped TiO_2. Highly visible-light active B, N codoped red anatase TiO_2 microspheres with a band gap of 1.94 eV on the surface and 3.22 eV in the core has been reported recently [355]. The synthesis method involved pre-doping of TiO_2 with boron to weaken the Ti—O bonding, and thereby improving the solubility of the second dopant nitrogen. In this case, visible-light absorption has been extended up to 700 nm (Fig. 25), and colour changed from white to red, which is completely different from the yellow colour and small visible-light absorption of N-doped TiO_2. Substitutional nitrogen doping in this case was also demonstrated using Raman spectroscopy.

The principles at the basis of the synergistic effect of non-metal codoping for visible-light photocatalysis were unravelled again by means of DFT calculations [356–360]. The most efficient pairs, such as N—F codopants, essentially present and electron donor (F) and an electron acceptor (N) which interact through internal long-range charge transfers, in analogy with what observed for non-metal impurities with oxygen vacancies. A donor species is an excellent substituent of the oxygen vacancy; therefore it has the beneficial effect of largely reducing the sample defectivity, commonly associated for example with N-doping. Thus, the role of one dopant (e.g. N) is to induce the visible-light absorption properties, whereas the role of the second dopant (e.g. F) is to compensate the overall electron counting, which is an efficient way to avoid the undesired formation of lattice defects. The photocatalytic activity can largely benefit from these effects since the electron/hole recombination rate is found to be directly proportional with the presence of lattice defects. Hamilton et al. [361] employed photo electrochemical measurements to examine the mechanism of visible light photocatalysis. The N,F doped TiO_2 did not provide any

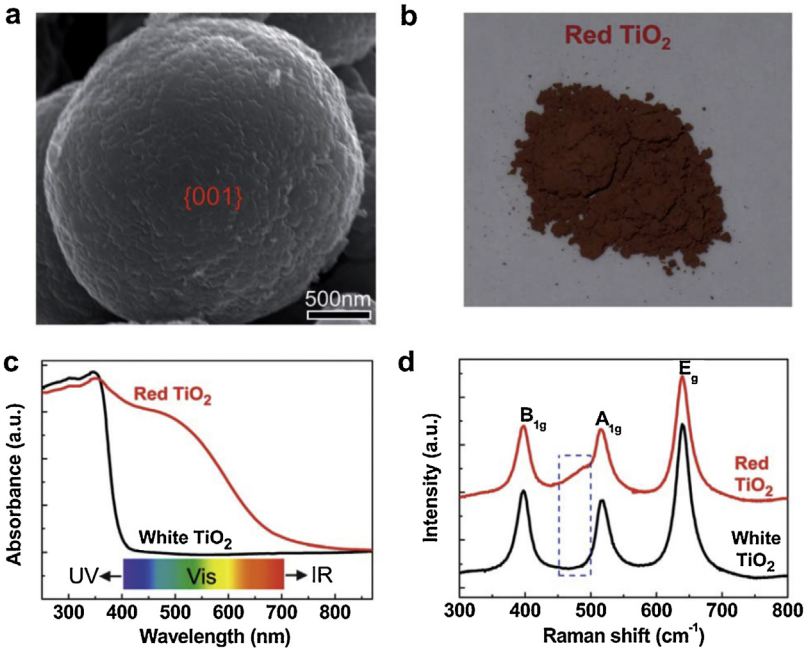

Fig. 25. (a) SEM image of a red TiO_2 microspheres; (b) optical photograph of the prepared red TiO_2 sample; (c) and (d) UV–visible absorption and Raman spectra of the white and red TiO_2.
Reproduced with permission from Ref. [355]. Copyright 2012 The Royal Society of Chemistry.

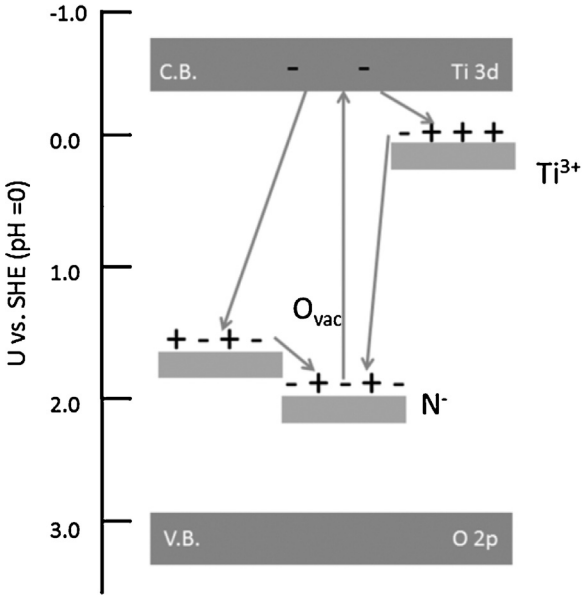

Fig. 26. Mechanism of electron transfer from either Ti^{3+} or oxygen vacancies in N–F doped TiO_2 explained using photo-electrochemical studies.

Reproduced with permission from Ref. [361]. Copyright 2014 American Chemical Society.

significant photocurrent response in presence of visible light at fixed potential under monochromatic irradiation, as compared to band gap irradiation (Fig. 26). Addition of KI and hydroquinone as 'hole acceptors' showed slight increases in the photocurrent. KO_2 (superoxide source) produced enhancement of photocurrent under visible light. This improvement in the photocurrent is explained as the oxidation of superoxide radical to singlet oxygen by the mid-gap level formed by N doping.

The F-doping induces the creation of shallow Ti^{3+} donor levels slightly below the conduction band. Oxygen vacancies transfer electrons to re-populate N states. The conduction band electrons can then move to the oxygen vacancies. Therefore a cycle of excited electrons occurred starting at the N mid-gap state, to conduction band and then to Ti^{3+} or oxygen vacancies with subsequent re-population of the empty nitrogen states (Fig. 27). The occurrence of visible light activity in this example is explained as mainly due to the reduction reaction involving conduction band electrons with molecular oxygen.

Zhao et al. [362] conducted TiO_2 photocatalysis of 6-hydroxymethyl uracil (a model Cyanobacteria toxin or cynotoxin)

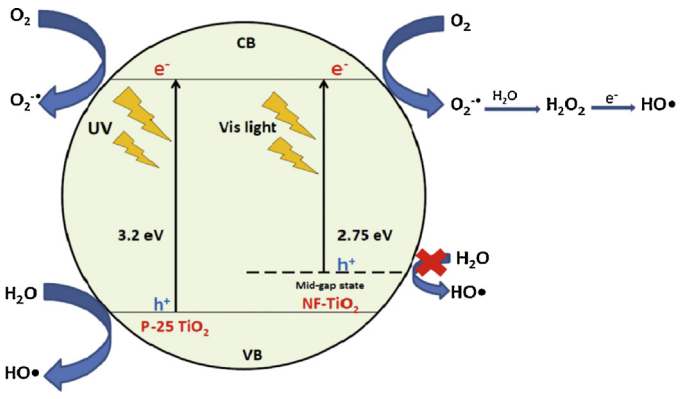

Fig. 27. Role of various reactive oxidation species during the photocatalysis process of N–F doped TiO_2.

Reproduced with permission from Ref. [362]. Copyright 2014 Elsevier Science.

using various non-metal doped TiO_2 materials. It was found that N-F-TiO_2 was the most active photocatalyst, while P-F-TiO_2 showed marginal activity and S-TiO_2 was fully inactive. In order to understand the mechanism of action, they also have conducted the photocatalysis in presence of a number of scavengers for $O_2^{\bullet -}$, $^1O_2$, HO• and h_{vb}^+. These investigations showed that $O_2^{\bullet -}$, is the leading ROS (reactive oxidation species) employed for the photocatalytic destruction of 6-hydroxymethyl uracil (Fig. 21).

4.6.4. Metal non-metal codoping

Co-alloying of anion doped TiO_2 with metal ions is another effective method for improving the visible-light photocatalytic activity of TiO_2 [363–366]. The benefits of co-alloying have been validated in numerous compositions including N/Fe^{3+}, N/V^{5+}, N/Sn^{2+}, N/Ta^{2+}, N/Ni^{3+}, N/Cr^{3+}, N/W^{5+}, N/Ce^{3+}, N/La^{3+}, N/Sm^{3+} and C/V^{5+} [367–377]. Performances of these co-doped TiO_2 were significantly higher than those containing single dopants. For instance, visible-light photocatalytic activity of Nb-coalloyed "N-doped" anatase TiO_2 was 7-fold higher in contrast to the undoped phase [363]. (Ga, N) codoped anatase TiO_2 was reported to be highly visible-light active for the water decomposition to hydrogen [378]. Increased oxygen vacancy formation and the band gap realignment leading by the synergetic effect of Ga and N-ions were responsible for the enhancement of photocatalytic activity. For increasing the visible-light photocatalytic activities, Li et al. successfully co-alloyed Mo with "C-doped" TiO_2 through a hydrothermal method [379]. This resulted in the formation of narrow band gap TiO_2 with lattice Mo^{6+} (Ti-site substitution) and surface adsorbed carbon impurities. In this case, synergetic effect of the individual ions resulted in the enhanced photocatalytic activity. In addition to the visible-light absorption, Mo and C dopants also improved the photogenerated electron–hole separation. A one step solution combustion method was developed by Thind et al. for the synthesis of mesoporous (N, W) codoped TiO_2, which exhibited superior decomposition of Rhodamine-B under visible and UV-light irradiation [380].

Several studies on the metal/non-metal codoping of TiO_2 are present in the literature [381–384]. The underlying mechanisms for the enhanced photocatalytic activity of the codoped systems are analogous to those described for non-metal codoping. The presence of one dopant is found to favour the introduction of the second in the TiO_2 lattice. Besides enhancing the visible-light absorption, due to the different chemical nature, the two codopants are found to facilitate the photogenerated electron–hole separation, with beneficial consequences on the measured photocurrent and observed photocatalytic activity.

4.6.5. Non-metal doped heterojunctions

Increased recombination of photogenerated electron–hole pairs due to inter band gap impurity energy levels is the main drawback of anion doped TiO_2. Theoretical studies of these narrow band gap TiO_2 using DFT calculations proved that anion doping cause a substantial lowering of energy required for oxygen vacancy formation. Photo-electrochemical studies of N doped anatase TiO_2 demonstrated the existence of supplementary energy levels located 1.3 eV below the conduction band level [385]. These additional energy levels act as recombination sites for the photogenerated electron–hole pairs. Increased dopant concentration also promotes carrier recombination through band gap narrowing. Thus visible-light photocatalytic activity of anion doped TiO_2 is limited due to the increased rate of electron–hole recombination. Consequently, coupling of anion doped TiO_2 with electron–hole separating agents (metal nanoparticles, quantum dots, semiconductor nanoparticles etc.) are necessary to attain high photocatalytic activity. Improved photocatalytic performance of biphasic TiO_2, for example Evonik Degussa P-25 (70% anatase + 30% rutile) under UV-light irradiation has been reported earlier. Efficient electron transfer from anatase

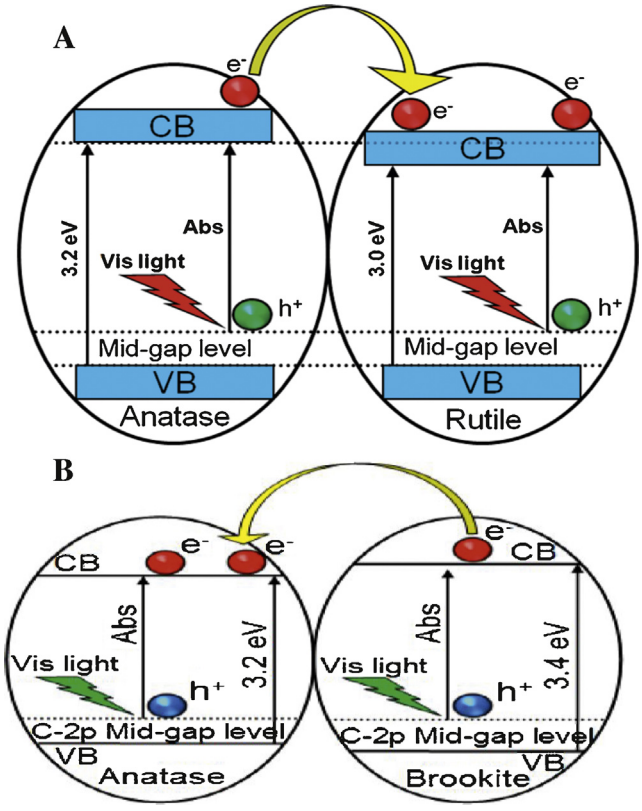

Fig. 28. Electron transfer mechanism in (A) S, N-codoped anatase–rutile heterojunctions. Reproduced with permission from Ref. [17]. Copyright 2012 American Chemical Society. (B) C-doped anatase–brookite heterojunctions. Reproduced with permission from Ref. [19]. Copyright 2013 American Chemical Society.

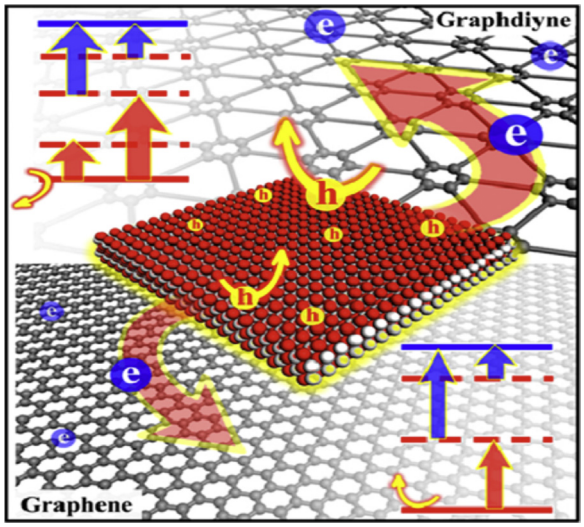

Fig. 29. Photoinduced electron transfer mechanism in graphene and graphdiyne modified TiO_2.

Reproduced with permission from Ref. [405]. Copyright 2013 American Chemical Society.

to rutile was found to be responsible for the enhanced activities of these mixed phase photocatalysts [67,386]. Similar approaches have also been implemented for improving the performance of several anion doped TiO_2 polymorphs. A microwave hydrothermal method for the synthesis of high surface area N-doped TiO_2 containing anatase and rutile nanoparticles has been reported by Zhang et al. [387] These biphasic narrow band gap TiO_2 outperformed the standard commercial photocatalyst Evonik Degussa P-25 towards the decomposition of NO_x gas.

In addition, Etacheri et al. recently reported novel synthetic methods and superior visible-light induced photocatalytic performances of N-doped/S, N-codoped anatase–rutile heterojunctions and C-doped anatase–brookite heterojunctions [11,17,19]. These visible-light active TiO_2 nanoheterojunctions exhibited notably higher photocatalytic activities compared to pure anatase phase, single-phase anion doped TiO_2, and the commercial biphasic standard photocatalyst Evonik Degussa P-25 [11,17]. Improved separation of electrons and holes at the anatase/rutile and anatase/brookite interface due to anatase to rutile and brookite to anatase electron transfer was demonstrated as the key reason for their very high photocatalytic activities (Fig. 28). Moreover, various anion doped anatase TiO_2 coupled with Ag and Au nanoparticles also exhibited superior visible-light photocatalytic activities compared to their single-phase counterparts [388–391]. These studies demonstrate the necessity of combining anion-doped TiO_2 with electron–hole separating agents for attaining the best visible-light photocatalytic activity. As mentioned in Section 4.4, the band alignment of different materials or of different phases of the same material, as in this case (rutile vs. anatase TiO_2), is a critical aspect and a challenging task, even for contemporary methodologies. Recently, a combined experimental and theoretical study has demonstrated that anatase possesses a higher electron affinity or work function with respect to rutile, resulting in a staggered band alignment of about 0.4 eV. The two polymorphs were modelled with QM/MM finite clusters for which the absolute values of ionization potentials and electron affinities can be obtained by computing charge states [392].

5. Graphene, carbon nanotube, *g*-C_3N_4 and perovskite modified TiO_2

Recently, coupling between TiO_2 and graphene have attracted much attention for considerable improvement in the photocatalytic performance [393–397]. Strong absorption of visible-light, unique 2-D morphology, and high electronic conductivity of graphene were found to be responsible for the photocatalytic activity enhancement. Graphene is an excellent electronic conductor that scavenge photo-excited electrons on TiO_2 surface [398,399]. In addition, large surface area and 2-D planar structure of graphene enable the anchoring of impurities and TiO_2 (Fig. 29) for increasing the photocatalytic activity. A number of methods have been presented for the synthesis of graphene-TiO_2 composites with improved visible-light photocatalytic performance. Most of these synthetic methods involve photocatalytic, chemical and hydrothermal reduction of a suspension or thin films of graphene oxide (GO) and TiO_2 [393,398,400–407]. These TiO_2–RGO hybrids exhibited excellent photocatalytic activities towards the degradation of methylene blue, benzene, *E. coli* bacteria, and water oxidation. In the case of photocatalytic water splitting, RGO also act as an excellent co-catalyst due to its high surface area and superior electron mobility.

Recently, Kamat et al. verified the electron scavenging activity in a TiO_2-graphene hybrid photocatalyst [408]. Composites consist of TiO_2 nanorods and (0 0 1) face exposed nanoparticles/nanosheets on large graphene sheets were reported to exhibit enhanced photocatalytic H_2-production activity [409–411]. Graphene-TiO_2 composite coupled with Ag nanoparticles, which combine the plasmon sensitization and excellent electrical properties of graphene has been reported as an excellent photocatalyst under visible-light irradiation [395].

In another recent investigation to understand the photocatalytic mechanism of visible light active ZnO-graphene composites,

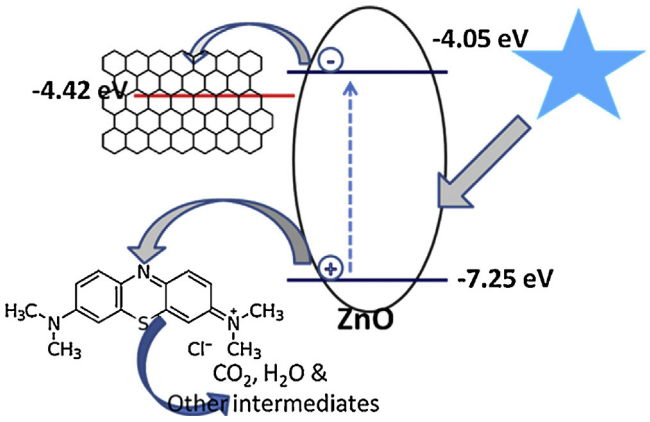

Fig. 30. Mechanism of photocatalytic degradation using ZnO-graphene hybrid.
Reproduced with permission from Ref. [412]. Copyright 2015 Elsevier Science.

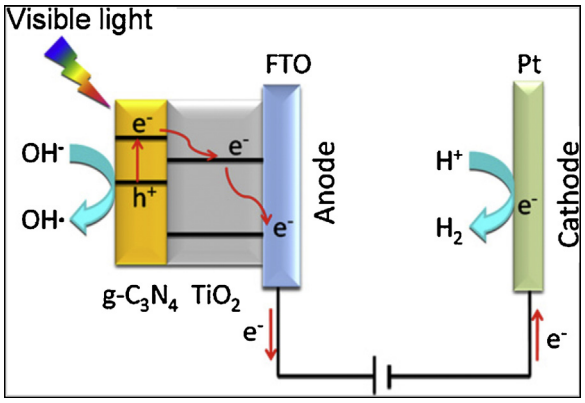

Fig. 31. Mechanism of charge separation and transfer between g-C_3N_4 and TiO_2 nanorod arrays under visible-light irradiation.
Reproduced with permission from Ref. [416]. Copyright 2012 Elsevier Science.

Kavitha et al. used reagents such as a radical scavenger t-BuOH and a hole scavenger EDTA-2Na [412]. The addition of the radical scavenger t-BuOH did not provide any significant changes in the photo-degradation properties, while the incorporation of EDTA-2Na significantly reduced the photo-degradation properties. This study has proved that the photo-generated holes are the major ROS responsible for the photo-degradation properties. Fluorescent quenching occurred in the zinc oxide–graphene composites showed photo-induced electron transfer (Fig. 30). These charge transfer processes could significantly improve the photocatalytic activity by reducing the recombination of electron–hole pairs. It has been concluded that the appropriate absorption range, effective electron–hole charge separation and high surface area make the ZnO–graphene hybrids a better photocatalyst under UV and visible light [412].

In this photocatalyst, Ag nanoparticles enhance the visible-light absorption, and graphene effectively separate photogenerated electron–hole pairs, which significantly improve the photocatalytic performance. Highly visible-light active hybrid semiconductor heterostructure of TiO_2/Bi_2O_3/graphene has been also reported previously [413]. Formation of Ti—C chemical bonds in TiO_2/graphene composites was identified to be enhancing the efficiency of photo-induced interfacial electron transfer [414]. Photocatalytic performances of these chemically bonded composites are exceptional compared to pure TiO_2 and the physically mixed samples with no chemical bonds. Multi-walled carbon nanotube (MWCNT) is a promising alternative to graphene for the visible-light activation of TiO_2 and for electron scavenging [415].

As a result of the narrow band gap (2.75 eV) graphitic carbon nitride (g-C_3N_4) has attracted a considerable interest in the field of visible-light induced photocatalysis [417–421]. Due to strong covalent bonds between nitrogen and carbon atoms, g-C_3N_4 is considered as the most stable carbon nitride under acidic and basic conditions [416]. It was noted that nitrogen doping using urea precursor result in the formation of some carbon nitride polymers on the TiO_2 surface [422,423]. Subsequently, Wang et al. reported the powerful visible-light water splitting activity of g-C_3N_4 with a conjugative polymeric structure [424]. Visible-light photocatalytic activity of TiO_2 was extensively improved after modification with g-C_3N_4 [416,420,425,426]. Yan et al. found that coupling of TiO_2 with g-C_3N_4 remarkably improved the visible-light water splitting performance by transferring photoexcited electrons from g-C_3N_4 to TiO_2 [427]. In the case of TiO_2-g-C_3N_4 hybrids, interfacial electron transfer is facilitated by the higher conduction band level of g-C_3N_4 [424]. It is proposed that in addition to sensitization, g-C_3N_4 is also capable of separating photogenerated charge carriers (Fig. 31) [416], which is analogous to other carbonaceous materials such as carbon nanotubes [428], and graphene [429–431].

Organo-lead halide perovskites possessing narrow band gap, improved stability in dry air, high carrier mobility, and great absorption coefficient were recently reported as efficient visible-light harvesters in heterojunction solar cells [432–437]. Use of $CH_3NH_3PbI_3$ as sensitizer in photo-electrochemical cells with liquid electrolyte has been reported previously [438–440]. However, dissolution of the sensitizer resulted in rapid performance decay, which was later solved by using a solid-state electrolyte [441]. A power conversion efficiency (PCE) of 8.5% has been demonstrated recently for a solid-state solar cell containing $CsSnI_3$ perovskite hole conductor and N719 as sensitizer [442]. Extremely high room temperature hole mobility ($\mu h = 5585\ cm^2\ V^{-1}\ S^{-1}$) and narrow band gap (1.3 eV) of $CsSnI_3$ makes it an ideal sensitizer. Further increase in the power conversion efficiency (η) and photocurrent density (J_{SC}) was achieved by F and SnF_2 doping of $CsSnI_3$ [442]. A heterojunction solar cell composed of $CH_3NH_3PbI_3$ perovskite (which act as absorber and hole-conductor) and (0 0 1) facet exposed TiO_2 nanosheets was also reported recently (Fig. 32) [443]. A remarkably high photovoltaic performance was observed for this heterojunction cell compared to the previous reports.

A number of computational studies, based on standard DFT but also on the more sophisticated GW approach (see Section 3), mostly by De Angelis et al., have investigated perovskite-based solar cells (Fig. 33), with particular attention to the oxide/perovskite interface [444–452]. These works have been able to reveal fundamental aspects of the device's operational mechanism.

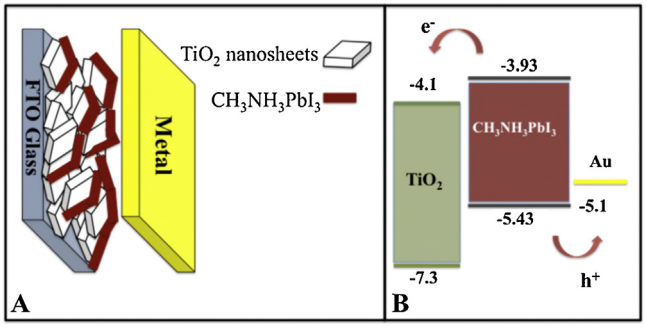

Fig. 32. (A) Device structure and (B) energy level diagram of the $CH_3NH_3PbI_3/TiO_2$ heterojunction solar cell.
Reproduced with permission from Ref. [443]. Copyright 2012 American Chemical Society.

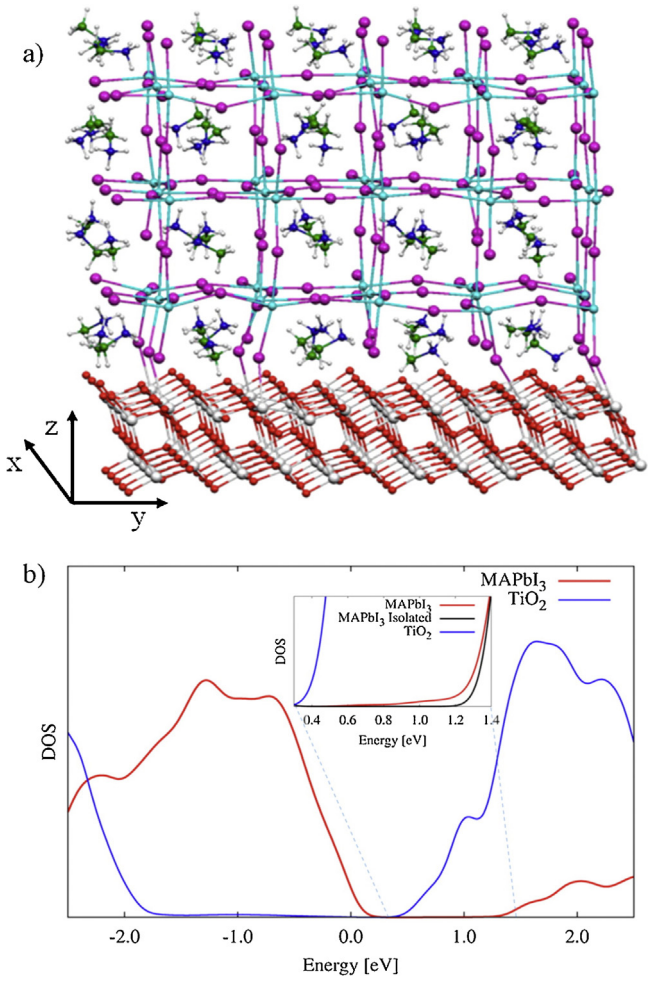

Fig. 33. (a) Optimized structure of the simulated TiO_2/$MAPbI_3$ interface along with reference axes. (b) Calculated DOS including spin–orbit coupling for the TiO_2/$MAPbI_3$ interface, decomposed into the contributions of $MAPbI_3$ (red) and TiO_2 (blue). The inset shows the bottom of the interacting perovskite DOS, compared with the noninteracting DOS at the same geometry.

Reproduced with permission from Ref. [444]. Copyright 2014 American Chemical Society.

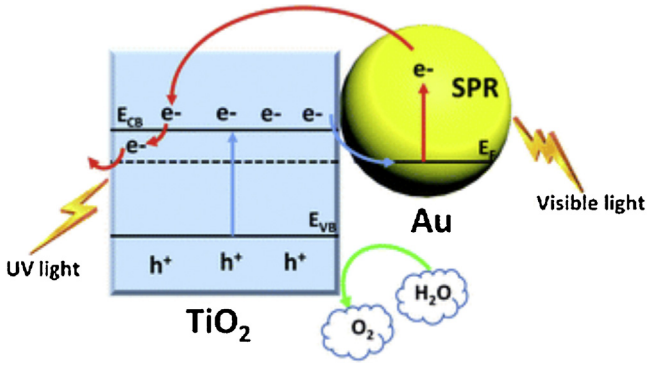

Fig. 34. Mechanism of visible-light driven photoelectrochemical water splitting on Au nanoparticles modified dendritic TiO_2 nanorod arrays.

Reproduced with permission from Ref. [468]. Copyright 2013 Royal Society of Chemistry.

6. Recent developments in visible light active TiO_2

Noteworthy advances have been recently made on the application of TiO_2 photocatalysts for visible-light induced water splitting, degradation of environmental pollutants, water/air purification and antibacterial applications. While visible-light activation of TiO_2 is developed through one of the modification or band-gap engineering discussed above, charge separation is another key factor need to be addressed for the efficient use of TiO_2 for these applications [453]. Recent developments in the area of visible-light induced water splitting involve the use of a variety of cocatalysts and electron–hole separating agents. Since the Fermi level of noble metal are lower than that of TiO_2 photocatalyst, photogenerated electrons are entrapped by the metal nanoparticles anchored on the semiconductor surface. Platinum has been widely used as the cocatalysts over many other metal oxides and up until now the highest H_2 generation performance are from Pt-loaded photocatalysts [454–457]. Recently, Iwase et al. reported excellent H_2 production using Au-modified TiO_2 [458]. This mainly resulted due to creation of active sites for water splitting and reduced charge recombination. Another major advantage of these Au cocatalysts is the negligible back reaction (recombination of H_2 and O_2 to form H_2O) compared to Pt cocatalysts. Wu et al. investigated the photocatalytic performance of Rh loaded TiO_2, and found enhanced rate of H_2 production [459]. They explained this unusual enhancement by the Schottky barrier formed at the TiO_2–Rh interface that acts as an efficient electron trap, preventing electron–hole recombination.

Type of electronic interactions between metals and semiconductors are used for explaining the effect of various noble metal cocatalysts [460]. It was suggested that smaller Schottky barrier height at the metal/semiconductor interface is beneficial for improved electron flow and photocatalytic activity for water splitting [461]. When Au/Pd bimetallic cocatalysts are loaded on the TiO_2 surface, significant H_2 production efficiency from aqueous ethanol solutions was observed due to selective donation of electrons to the protons [462]. Synergistic effect in the visible-light photocatalytic activity of TiO_2 was observed by Borgarello et al. when both RuO_2 and Pt nanoparticles are deposited on the surface [140]. They proposed that Schottky barrier is formed by RuO_2, while Pt provides ohmic contact acting as electron trap, while holes are trapped by RuO_2. Moreover, Teramura et al. reported that uniform dispersion of RuO_2 nanoparticles on TiO_2 is essential for obtaining improved H_2 and O_2 evolution [463]. Tada et al. developed a three component CdS–Au–TiO_2 photocatalyst, which exhibited water splitting photocatalytic activity exceeding most of the single and two component systems [464]. Further investigation of this composition was carried out by Park et al., and found that direct contact between CdS and TiO_2 are required for vectorial electron transfer and highest photocatalytic activity [465]. Similar performance increase was also observed in the case of MWCNT–TiO_2 and Bi_2S_3–TiO_2 systems [466,467].

Recently, branched TiO_2 nanorod arrays modified with plasmonic Au nanoparticles are demonstrated as highly efficient for photoelectrochemical water splitting under visible-light illumination [468]. The obtained photocurrent and efficiency was the highest value ever reported, indicating superior charge separation and transportation efficiencies. The high water splitting performance was attributed to the plasmonic effect of Au nanoparticles, which increases visible-light absorption and improve charge separation/carrier mobility (Fig. 34). Similar approach was also employed in the case of Au-nanoparticle modified TiO_2 aerogel [469]. The magnitudes of photocatalytic activity improvement in this case prove that a three-phase boundary is beneficial for excited surface plasmon to charge-carrier conversion (Fig. 35).

Biphasic TiO_2–Fe_2O_3 photocatalysts are also modified with plasmonic metal nanoparticles to induce visible-light activated photocatalytic water splitting [470]. In this case, a photocurrent 20 times higher than pure Fe_2O_3 was observed using an optimized ratio of plasmonic TiO_2–Fe_2O_3/Ag composition. Absorption

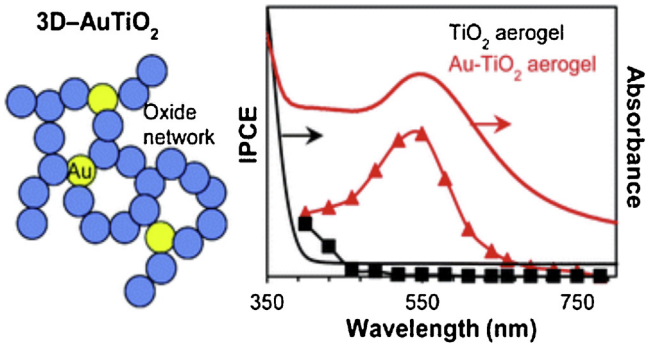

Fig. 35. Plasmonic enhancement of the visible light water splitting with Au–TiO_2 composite aerogel.

Reproduced with permission from Ref. [469]. Copyright 2013 Royal Society of Chemistry.

of incident photons and charge carrier separation was enhanced due to broadband absorption and strong electric field of the composite. Improved photoelectrochemical water splitting was also reported using Fe-doped TiO_2 nanorod arrays [471]. This work demonstrated Fe-doping as the most effective method to improve the photocatalytic activity of TiO_2. Efficiency measurements reveal that Fe-doping improve UV/Vis absorption by creating additional energy levels near conduction band and increase the carrier density, leading to effective carrier separation. S-doped TiO_2 nanotube arrays are recently reported as a highly active photocatalyst for photoelectrochemical water splitting [472]. Three component CdS–TiO_2/metallosilicates were also reported as effective for visible-light induced photocatalytic water splitting [473].

TiO_2 photocatalysts are recently proved as very effective towards visible-light induced decomposition of a number of organic and inorganic pollutants [474–482]. Recent developments in this area include the synthesis of novel TiO_2 compositions containing anions, cations, metal oxides and carbonaceous materials. Cavalcante et al. synthesized B-doped TiO_2 through a boric acid modified sol–gel method, and tested for the sunlight driven degradation of metoprolol [474]. They found a significant increase in the photocatalytic activity (48–70% by doping 5%) due to B-doping. 5% was identified as the optimum B-loading, which resulted in high surface area and mesoporous structure. Boron was introduced into the crystal structure as B–O–Ti, which causes Ti^{3+} formation due to charge compensation. Photocatalysis play an important role in water purification. Zhang et al. reported humic acid removal from water through photocatalytic decomposition using hybrid Fe_2O_3/TiO_2 nanowires [475]. These membranes also exhibited antifouling property up on sunlight irradiation. Fe_2O_3 played an important role in the biphasic catalyst by improving humic acid adsorption, increasing electron–hole separation by interfacial charge transfer, and by absorbing visible light. Under UV-light irradiation, electron–hole pairs are generated on both TiO_2 and Fe_2O_3 (Fig. 36a). Water oxidation by holes produces OH radicals, which in turn decompose humic acid molecules. Under visible-light irradiation, Fe_2O_3 absorbs visible light and transfer conduction band electrons formed to the electron trapping sites of anatase TiO_2 (Fig. 36b).

Nanocomposite formation between TiO_2 and clay is a recently reported method for the photocatalytic removal of phenol and methylene blue from water [476]. In this method, photoresponse of the final composite was shifted from UV to the visible light range. Their kinetic study proved that TiO_2-clay nanocomposites are efficient for phenol and methylene blue removal from water under UV and visible light.

An efficient sonophotocatalytic degradation of reactive blue 19 (RB 19) using sulfur-doped TiO_2 nanoparticles was reported

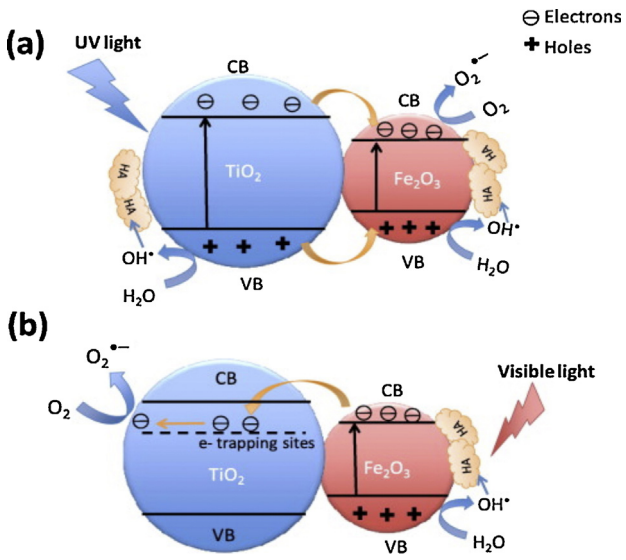

Fig. 36. Proposed mechanism for the photocatalytic degradation of humic acid on Fe_2O_3/TiO_2 hybrid nanowires under UV and visible light irradiation.

Reproduced with permission from Ref. [475]. Copyright 2015 Elsevier Science.

recently [477]. In this method, coupling of ultrasound and photocatalysis improved dye degradation through synergistic effect, which increased the amount of reactive radicals $OH^{\bullet}$ and H_2O_2. It is also proposed that ultrasound increases the mass transport between the solution phase and catalyst surface, and de-agglomeration of particles increase the surface area of the catalyst. Jiang et al. recently reported a novel ternary photocatalyst composed of TiO_2–In_2O_3 nanocrystals decorated with g-C_3N_4 for dye degradation and H_2 evolution [481]. These ternary composites exhibited the highest RhB degradation rate, which is 6.6 times higher than that of g-C_3N_4. H_2-generation rate was 48 times of the pure g-C_3N_4. They attributed the enhanced photocatalytic activity to efficient interfacial transfer of photogenerated electrons and holes among TiO_2, In_2O_3 and g-C_3N_4 (Fig. 37).

Other recent developments in the area of visible-light induced environmental cleaning involve the use of GO-TiO_2 composites for Microcystin-LA removal [479], N-doped TiO_2 on glass spheres for Eriochrome Black-T decomposition [480], and CdO/TiO_2 coupled semiconductor for Reactive Orange degradation [478]. Superior decomposition of air pollutants by visible-light active TiO_2 photocatalysts has been lately reported by several researchers [483–487].

Bacterial killing under visible-light irradiation is one of the most versatile applications of TiO_2 photocatalysis. Various strategies

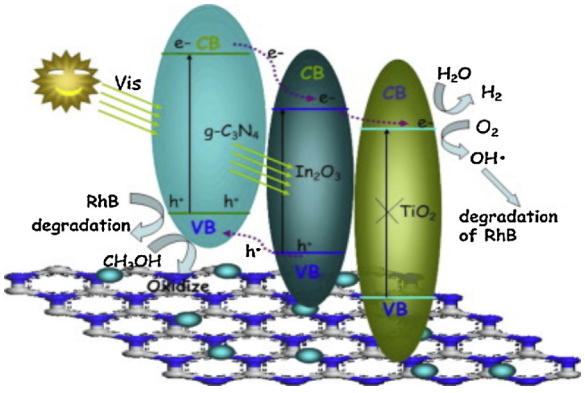

Fig. 37. Possible photocatalytic mechanism of the TiO_2-In_2O_3-g-C_3N_4 ternary hybrid composite.

Reproduced with permission from Ref. [481]. Copyright 2015 Elsevier Science.

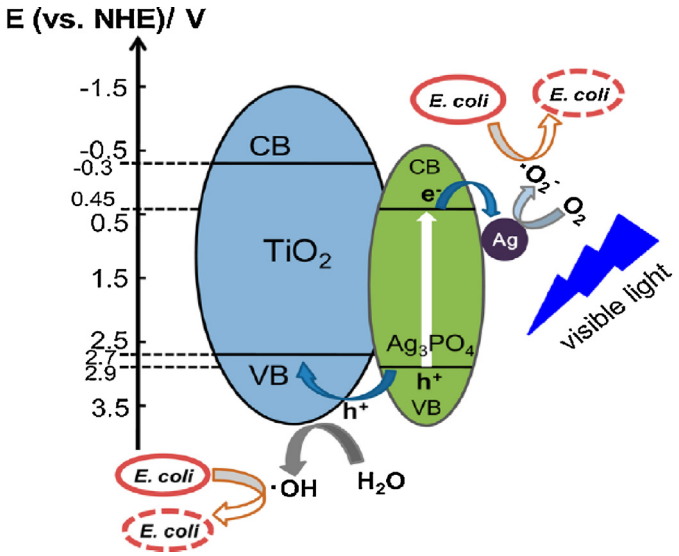

Fig. 38. Visible-light induced antibacterial activity $Ag_3PO_4/TiO_2/Fe_3O_4$ heterostructure towards *E. coli*.

Reproduced with permission from Ref. [491]. Copyright 2014 American Chemical Society.

are recently developed for the visible-light activation of TiO_2 for visible-light induced bacterial killing. Lin et al. reported the synthesis of Se/Te-TiO_2 nanorods with dominant (0 0 1) facets with high visible-light photocatalytic activity [488]. In this case, highly active (0 0 1) facets exhibited significantly higher antibacterial activity than Degussa P25 when activated under visible-light. A sol–gel method is recently demonstrated for the synthesis of Ni^{2+} doped TiO_2 with superior antibacterial activity towards *S. aureus*, *E. coli*, *Bacillus subtilis*, and *Salmonella abony* under visible-light irradiation [489,490]. Surprisingly, antibacterial performances of this Ni^{2+}-doped TiO_2 are superior to N-doped TiO_2 under similar experimental conditions.

Heterojunctions with carbonaceous materials, metal nanoparticles, metal oxides and phosphates are reported as effective for improving the visible-light induced antibacterial activity of TiO_2 [491–496]. Akhavan et al. incorporated CNTs with TiO_2 thin films for the visible light photoinactivation of *E. coli* bacteria [492]. Post annealing of this film resulted in the formation of Ti—C and Ti—O—C bonds. Bacterial inactivation in the dark was also observed for films containing higher CNT loading. Improved visible-light was assigned to the charge transfer between CNTs and TiO_2 through the carbonaceous bonds formed. Xu et al. recently reported the synthesis of magnetically separable $Ag_3PO_4/TiO_2/Fe_3O_4$ heterostructure for photoinactivation of bacteria [491]. This three component photocatalyst exhibited excellent photocatalytic activity, and photogenerated oxidants ($^{\bullet}OH$ and $^{\bullet}O_2^-$) formed caused a strong considerable morphological changes in the cells and bactericidal effects towards *E. coli*. Visible-light activation was caused by narrow band gap Ag_3PO_4, and effective transfer of photogenerated holes to the valence band of TiO_2 (Fig. 38). Moreover, Etacheri et al. reported outstanding antibacterial performance of C-doped TiO_2 heterojunctions composed of nanosized anatase and brookite nanoparticles. A microwave synthetic method was used for the rapid synthesis of these nanoheterojunctions, and 90% bacterial killing occurred within 3 h visible-light irradiation. High visible-light induced photocatalytic activity was attributed to the efficient transfer of photogenerated electrons from the conduction band of brookite to that of anatase (Fig. 39), which facilitate the formation of reactive oxygen species and bacterial killing.

7. Strategies to select dopants and future recommendations for an improved electron–hole separation

In the last decades great attention has been paid to the synthesis of transition-metal ion doped TiO_2 possessing high photocatalytic activities to satisfy the requirements for practical applications. However, until now many questions are still open considering both the mechanism by which metal doping improves the photocatalytic activity as well as the determination of the optimal doping ratio. It is assumed that at low doping concentration the doping ions traps electron–hole pairs thus reducing the recombination rate, while at a higher doping ratio the formation of recombination centres occurs [40]. Consequently, for every transition metal doped TiO_2 there should be an optimal dopant concentration. Consequently, Bloh et al. developed a theoretical model, which describes the dependency of the photonic efficiency on the doping ratio and which can thus be applied for the determination of the optimal transition metal–ion ratio [497]. The idea behind this model is that

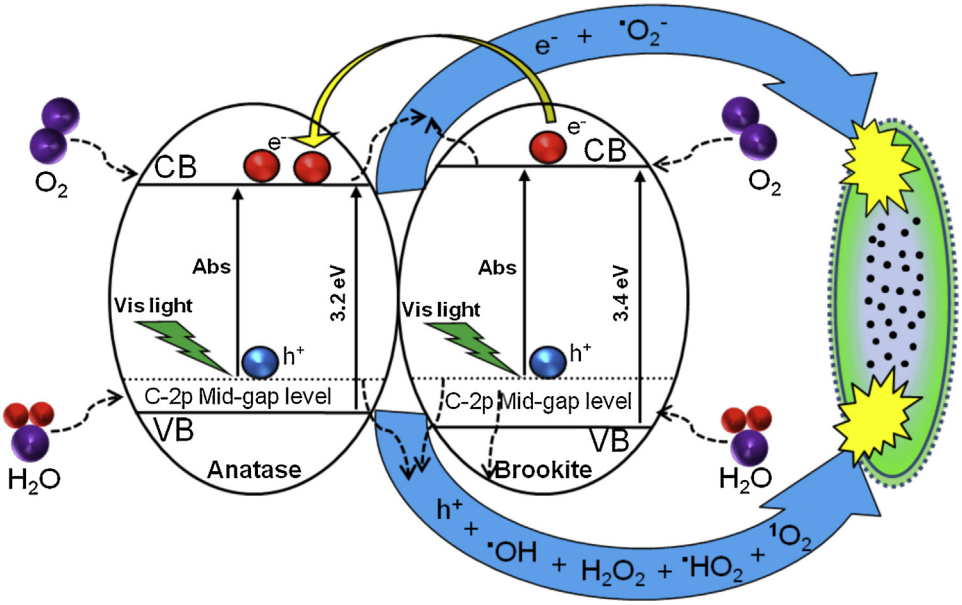

Fig. 39. Mechanism of visible-light induced photocatalytic bacterial killing using carbon doped anatase–brookite heterojunctions.

Reproduced with permission from Ref. [19]. Copyright 2013 American Chemical Society.

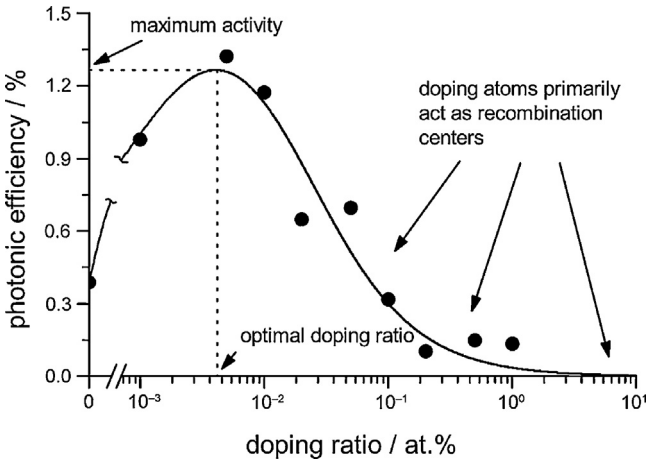

Fig. 40. The photocatalytic activity as a function of the doping ratio. Reproduced with permission from Ref. [497]. Copyright 2013 Wiley VCH.

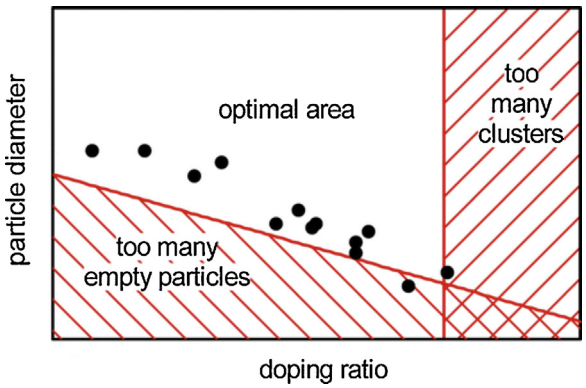

Fig. 41. Optimal combinations of particle size and doping ratio. Reproduced with permission from Ref. [499]. Copyright 2012 American Chemical Society.

the direct cationic neighbourhood of two dopant metal cations can be considered as a recombination centre, while more distant dopants can be ignored, since they induce a lower recombination probability. With increasing doping ratio, both the probability for the formation of the clusters and the amount of the doping atoms increases. The cluster ratio r_c, i.e., the product of the doping ratio and the cluster probability, depends quadratically on the doping ratio r_d and can be described by the following equation:

$$r_c = nr_d^2$$

where n corresponds to the number of the neighbouring cations ($n = 12$ for TiO_2 or ZnO (wurzite)). It is, on the one hand, assumed that the photonic efficiency increases linearly with the doping ratio due to the formation of the charge carrier trapping centres, while it concurrently decreases quadratically with the doping ratio due to the formation of recombination centres. The relation between doping ratio and photonic efficiency is shown in Fig. 40. Moreover, the experimentally determined data correlate very well with developed theoretical model. However, both the position and the height of the maximum can vary depending on the nature of dopants, ionic radius, number of the cationic neighbours, and the distance between the cations.

The drawback of the above-described model is that it does not consider the dependency between particle size, morphology, and optimum dopant ratio. Zhang et al. suggested a theory indicating a correlation between the optimal Fe^{3+}-doping ratio and the particle size of TiO_2, though, they have not developed a model to describe this phenomenon [498]. In a similar study, Bloh et al. presented another model that explains the relationship between dopant content, particle size and photocatalytic activity [499]. This model assumes a small dopant concentration, formation of recombination centres, and presence of at least one dopant atom per particle to achieve a doping action. This model (Fig. 41) includes the correlation between particle size and dopant content, defining regions with too many empty particles or too many cluster are present, respectively. For larger particles, the optimal loading of dopants is rather wide, and for smaller particles it gets smaller. No optimal solution can be obtained for particles below a critical size (2.8 nm for ZnO and 3.2 nm for TiO_2). The plotting of the experimentally determined data into the graph clearly shows a good agreement with the theory. There is no dependence between the material and the optimum dopant loading, which can be calculated using the following equation [499].

$$r_{d,opt} \approx \frac{6M}{N_A \rho \pi d^2}(2.40\,\mathrm{nm}^{-1})$$

where $r_{d,opt}$ is the optimum doping ratio, M is the molar mass, N_A is the Avogadro number, ρ is density of the material and d the particle diameter. This calculation is based on the assumption that individual semiconductor particles contain 2.4 dopant atoms for each nanometer of particle diameter. A good agreement of the calculated optimal doping ratio with the experimentally determined values was observed. Hence, this model allows, for the first time, to calculate the optimal doping concentration for a particular material and a given particle size.

As mentioned earlier, visible-light photocatalytic activity of cation doped TiO_2 was limited due to the formation of electron hole recombination centres. In addition, recent studies proved that non-metal or metalloids doped TiO_2 materials are much more promising than their metal-doped counterparts [1,2,17,500–505]. A number of recent reviews also address the use of modified TiO_2 for various environmental applications [506–511]. It is clear that the future development of visible-light active TiO_2 would mainly be based on anion doping. The main shortcoming of anion doped TiO_2 is the formation of oxygen vacancies that accelerate the recombination of photo-excited electron–hole pairs. The photocatalytic activity can be significantly improved by reducing the recombination rate of photoexcited electron–hole pairs. This can be pursued through different approaches. For instance, co-doping of TiO_2 is efficient in reducing the formation of compensating oxygen vacancies with a positive effect on the photocatalytic performance of the material. Alternatively, one may combine anion doped TiO_2 with small band gap semiconductors to improve the electron–hole separation. Coupling of anion-doped anatase TiO_2 with WO_3, Fe_2O_3 and V_2O_5 (which has less negative conduction band level compared to anatase) can effectively trap photo-excited electrons and thereby reducing electron–hole recombination. Metal nanoparticles (Au, Ag, Pt, Pd, etc.) can also be employed as photo-excited electron trap and thereby increasing the photocatalytic performance [63]. Due to the different conduction band energy levels of anatase, rutile and brookite phases, anion-doped multiphase TiO_2 is highly recommended over single phase photocatalyst. This should enable an efficient electron transfer from the conduction band of brookite to anatase, brookite to rutile and anatase to rutile, which can lead to a momentous enhancement in the photocatalytic activity [11,17,19].

Coupling of anionic doped TiO_2 with sensitizers such as graphene and carbon nanotubes, is highly recommended considering the fact that these visible-light absorbing carbonaceous dopants can sensitize TiO_2 and separate photogenerated electron–hole pairs. Modification of anion-doped TiO_2 with quantum dots could be very useful for significantly improving the visible-light photocatalytic activity. Semiconductor and noble metal quantum

dots can simultaneously sensitize TiO_2 through LSPR and act as electron–hole separating agents. In addition, coupling of anion doped TiO_2 with multiple sensitizers and electron–hole separating agents could be effective for the utilization of the whole visible spectrum. Since the photocatalytic activity of TiO_2 highly depends on the particle size, morphology and amount of exposed (0 0 1) crystal planes, it is highly recommended to optimize these parameters of anion doped TiO_2 to attain the best results.

Investigations of the electronic structure through DFT calculations can play a fundamental role in the study of these new generations of composite photocatalysts. Through these types of calculations it will be possible to determine how the band structure is modified when different materials are put into contact to create oxide/oxide, metal/oxide, QD/oxide or sensitizers/oxide heterojunctions for an efficient visible-light absorption and subsequent charge separation at the interface. Theoretical modelling provides a solid basis for identifying the key factors into play and for controlling the heterojunctions performance through band structure engineering. Such investigations can be used for predicting novel efficient photocatalytic systems and for improving the existing ones, in the continuous attempt to enhance the control of the structure–property relationship of materials for photocatalytic applications.

8. Conclusions

Titanium dioxide has been the focus of research efforts in the area of photocatalysis due to its improved chemical stability and the high oxidation potential of its valence band holes as compared with other semiconductor photocatalysts. Improving the visible-light spectral sensitivity of TiO_2 is one of the key challenges faced by the community involved in the research of photocatalysis. Recent developments in the area of TiO_2 photocatalysts are promising enough for the development of TiO_2 active in the visible-light region of the electromagnetic spectrum. A number of techniques have been employed by previous researchers to overcome the main shortcoming of TiO_2 photocatalyst, i.e., its poor visible-light induced photocatalytic activity. In this review, various strategies for the activation of TiO_2 photocatalysts under visible-light irradiation were discussed in detail. The effect of various visible-light activation techniques on the electronic structure and on the photocatalytic activities of TiO_2 was critically investigated. Recent theoretical developments explaining the electronic structure of visible-light active TiO_2 were discussed in detail. Previous studies demonstrated the fact that various non-metal doped TiO_2 materials are more promising than metal doped counterparts. Each anionic dopant was found to exhibit a distinctive consequence on the electronic structure and photocatalytic activities of TiO_2. The main drawback of the non-metal-doped TiO_2 is the increased carrier recombination, which makes these materials considerably less active under visible-light than the UV-light illumination. Since the synthesis methods, the dopant concentration and the phase purity crucially affect the photocatalytic activity of TiO_2, further optimization of these parameters is necessary for increasing the visible-light performance of anion-doped TiO_2. Another vital challenge is the fabrication of thermally stable TiO_2 with predictable performance under visible and UV-light illumination. Since the charge carrier recombination is the major drawback of the current generation of anion-doped TiO_2, future research should be devoted to enhance the lifetime of electron–hole pairs. The advancements made to date in the area of visible-light activated TiO_2 photocatalysts are encouraging and further widens its scope of applications in environmental protection. A number of recommendations for enhancing the photocatalytic performance of the current generation of visible-light active TiO_2 are also presented.

Acknowledgements

The authors would like to thank Enterprise Ireland for funding (CFTD/06/IT/326 and ARE/2008/0005). SP wish to acknowledge financial support under the U. S.–Ireland R&D Partnership programme from the Science Foundation Ireland (SFI-Grant Number 10/US/I1822(T)). One of the authors VE would also like to thank Dr. Michael Seery for providing valuable comments during his PhD. CDV thanks Gianfranco Pacchioni and Annabella Selloni for many helpful discussions and Cariplo foundation for an Advanced Materials Grant 2013-0615. JS gratefully acknowledges financial support from the German Ministry of Science and Technology (BMBF), Grant Number 03SF0482C (Duale Solarenergienutzung: Wasserstofferzeugung bei der Abwasserreinigung, DuaSol).

References

[1] S. Banerjee, S.C. Pillai, P. Falaras, K.E. O'Shea, J.A. Byrne, D.D. Dionysiou, J. Phys. Chem. Lett. 5 (2014) 2543.
[2] M. Pelaez, N.T. Nolan, S.C. Pillai, M.K. Seery, P. Falaras, A.G. Kontos, P.S.M. Dunlop, J.W.J. Hamilton, J.A. Byrne, K. O'Shea, M.H. Entezari, D.D. Dionysiou, Appl. Catal. B 125 (2012) 331.
[3] J. Schneider, M. Matsuoka, M. Takeuchi, J. Zhang, Y. Horiuchi, M. Anpo, D.W. Bahnemann, Chem. Rev. 114 (2014) 9919.
[4] S. Banerjee, D.D. Dionysiou, S.C. Pillai, Appl. Catal. B: Environ. 176–177 (2015) 396.
[5] A. Fujishima, K. Honda, Nature 238 (1972) 37.
[6] A. Mills, S.K. Lee, J. Photochem. Photobiol. A 152 (2002) 233.
[7] P.V. Kamat, J. Phys. Chem. C 111 (2007) 2834.
[8] V. Etacheri, M.K. Seery, S.J. Hinder, S.C. Pillai, Adv. Funct. Mater. 21 (2011) 3744.
[9] D.A. Keane, K.G. McGuigan, P.F. Ibáñez, M.I. Polo-López, J.A. Byrne, P.S.M. Dunlop, K. O'Shea, D.D. Dionysiou, S.C. Pillai, RSC Catal. Sci. Technol. 4 (2014) 1211.
[10] S.C. Pillai, P. Periyat, R. George, D.E. McCormack, M.K. Seery, H. Hayden, J. Colreavy, D. Corr, S.J. Hinder, J. Phys. Chem. C 111 (2007) 1605.
[11] V. Etacheri, M.K. Seery, S.J. Hinder, S.C. Pillai, Chem. Mater. 22 (2010) 3843.
[12] L. Vayssieres, Adv. Mater. 15 (2003) 464.
[13] V. Etacheri, R. Roshan, V. Kumar, ACS Appl. Mater. Interfaces 4 (2012) 2717.
[14] G.S. Li, D.Q. Zhang, J.C. Yu, Environ. Sci. Technol. 43 (2009) 7079.
[15] A. Kudo, M. Sekizawa, Chem. Commun. (2000) 1371.
[16] F.F. Kong, L.L. Huang, L.L. Luo, S.S. Chu, Y.Y. Wang, Z.Z. Zou, J. Nanosci. Nanotechnol. 12 (2012) 1931.
[17] V. Etacheri, M.K. Seery, S.J. Hinder, S.C. Pillai, Inorg. Chem. 51 (2012) 7164.
[18] M.R. Hoffmann, S.T. Martin, W. Choi, D.W. Bahnemann, Chem. Rev. 95 (1995) 69.
[19] V. Etacheri, G. Michlits, M.K. Seery, S.J. Hinder, S.C. Pillai, ACS Appl. Mater. Interfaces 5 (2013) 1663.
[20] N. Wetchakun, S. Chaiwichain, B. Inceesungvorn, K. Pingmuang, S. Phanichphant, A.I. Minett, J. Chen, ACS Appl. Mater. Interfaces 4 (2012) 3718.
[21] S. Polisetti, P.A. Deshpande, G. Madras, Ind. Eng. Chem. Res. 50 (2011) 12915.
[22] L. Li, M. Krissanasaeranee, S.W. Pattinson, M. Stefik, U. Wiesner, U. Steiner, D. Ede, Chem. Commun. 46 (2010) 7620.
[23] Y. Liu, L. Yu, Y. Hu, C. Guo, F. Zhanga, X.W.D. Lou, Nanoscale 4 (2012) 183.
[24] D. Chu, J. Mo, Q. Peng, Y. Zhang, Y. Wei, Z. Zhuang, Y. Li, ChemCatChem 3 (2011) 371.
[25] M. Grätzel, Heterogeneous Photochemical Electron Transfer, CRC Press, Boca Raton, FL, 1989.
[26] T. Daimon, T. Hirakawa, M. Kitazawa, J. Suetake, Y. Nosaka, Appl. Catal. A 340 (2008) 169.
[27] Y. Nosaka, T. Daimon, A.Y. Nosaka, Y. Murakami, Phys. Chem. Chem. Phys. 6 (2004) 2917.
[28] H. Sakai, R. Baba, K. Hashimoto, A. Fujishima, J. Phys. Chem. 99 (1995) 11896.
[29] K.T. Ranjit, I. Willner, S.H. Bossmann, A.M. Braun, Environ. Sci. Technol. 35 (2001) 1544.
[30] J.R. Harbour, M.L. Hair, J. Phys. Chem. 83 (1979) 652.
[31] P. Periyat, N. Leyland, D.E. McCormack, J. Colreavy, D. Corr, S.C. Pillai, J. Mater. Chem. 20 (2010) 3650.
[32] D.W. Synnott, M.K. Seery, S.J. Hinder, G. Michlits, S.C. Pillai, Appl. Catal. B: Environ. 106–111 (2013) 130.
[33] B. O'Regan, M. Grätzel, Nature 353 (1991) 737.
[34] B. Kraeutler, A.J. Bard, J. Am. Chem. Soc. 100 (1978) 2239.
[35] D.F. Ollis, H. Al-Ekabi, Photocatalytic Purification and Treatment of Water and Air, Elsevier, Amsterdam, 1993.
[36] R. Cai, Y. Kubota, T. Shuin, H. Sakai, K. Hashimoto, A. Fujishima, Cancer Res. 52 (1992) 2346.
[37] J. Yuan, S. Tsujikawa, J. Electrochem. Soc. 142 (1995) 3444.
[38] H. Honda, A. Ishizaki, R. Soma, K. Hashimoto, A. Fujishima, J. Illum. Eng. Soc. 27 (1998) 42.
[39] S.L. Pugh, J.T. Guthrie, Dyes Pigments 55 (2002) 109.
[40] W. Choi, A. Termin, M.R. Hoffmann, J. Phys. Chem. 98 (1994) 13669.

[41] H.A. Macleod, Thin Film Optical Filters, MacMillan, New York, 1986.
[42] P.T. Moseley, B.C. Tofield, Solid State Gas Sensors, Adam Hilger, Bristol, 1987.
[43] E.M. Logothetis, Ceram. Proc. Eng. Sci. 1 (1980) 281.
[44] L.D. Birkefeld, A.M. Azad, S.A. Akbar, J. Am. Ceram. Soc. 75 (1992) 2964.
[45] N. Savage, B. Chwieroth, A. Ginwalla, B.R. Patton, S.A. Akbar, P.K. Dutta, Sens. Actuators B 79 (2001) 17.
[46] Y. He, D. Langsdorf, L. Li, H. Over, J. Phys. Chem. C 119 (2015) 2692.
[47] H. Tong, S. Ouyang, Y. Bi, N. Umezawa, M. Oshikiri, J. Ye, Adv. Mater. 24 (2012) 229.
[48] M. Wang, J. Iocozzia, L. Sun, C. Lin, Z. Lin, Energy Environ. Sci. 7 (2014) 2182.
[49] A.E.R. Mohamed, S. Rohani, Energy Environ. Sci. 4 (2011) 1065.
[50] H. Li, Y. Zhou, W. Tu, J. Ye, Z. Zou, Adv. Funct. Mater. 25 (2015) 998.
[51] S. Chakrabarti, B.K. Dutta, J. Hazard. Mater. 112 (2004) 269.
[52] S.N. Frank, A.J. Bard, J. Am. Chem. Soc. 99 (1977) 303.
[53] S.N. Frank, A.J. Bard, J. Phys. Chem. 81 (1977) 1484.
[54] M.A. Fox, M.T. Dulay, Chem. Rev. 93 (1993) 341.
[55] J. Zhao, T. Wu, K. Wu, K. Oikawa, H. Hidaka, N. Serpone, Environ. Sci. Technol. 32 (1998) 2394.
[56] R. Wang, K. Hashimoto, A. Fujishima, M. Chikuni, E. Kojima, A. Kitamura, Nature 388 (1997) 431.
[57] Y. Wang, Y. Huang, W. Ho, L. Zhang, Z. Zou, S. Lee, J. Hazard. Mater. 169 (2009) 77.
[58] C. Su, C.M. Tseng, L.F. Chen, B.H. You, B.C. Hsu, S.S. Chen, Thin Solid Films 498 (2006) 259.
[59] R. Asahi, Y. Taga, W. Mannstadt, A.J. Freeman, Phys. Rev. B: Condens. Matter 61 (2000) 7459.
[60] A. Amtout, R. Leonelli, Phys. Rev. B: Condens. Matter 51 (1995) 6842.
[61] M. Koelsch, S. Cassaignon, C.T.T. Minh, J.F. Guillemoles, J.P. Jolivet, Thin Solid Films 451 (2004) 86.
[62] N.T. Nolan, M.K. Seery, S.C. Pillai, J. Phys. Chem. C 113 (2009) 16151.
[63] N.T. Nolan, L.F. Healy, M.K. Seery, S.J. Hinder, S.C. Pillai, J. Phys. Chem. C 114 (2010) 13026.
[64] A.L. Linsebigler, G. Lu, Y.T. Yates, Chem. Rev. 95 (1995) 735.
[65] M. Muruganandham, M. Swaminathan, Sol. Energy Mater. Sol. Cells 81 (2004) 439.
[66] T. Miyagi, M. Kamei, T. Mitsuhashi, T. Ishigaki, A. Yamazaki, Chem. Phys. Lett. 390 (2004) 399.
[67] L. Kavan, M. Grtzel, S.E. Gilbert, C. Klemenz, H.J. Scheel, J. Am. Chem. Soc. 118 (1996) 6716.
[68] M. Toyoda, Y. Nanbu, Y. Nakazawa, M. Hirano, M. Inagaki, Appl. Catal. B: Environ. 49 (2004) 227.
[69] E. Beyers, P. Cool, E.F. Vansant, J. Phys. Chem. B 109 (2005) 10081.
[70] A. Wisitsoraat, A. Tuantranont, E. Comini, G. Sberveglieri, W. Wlodarski, Thin Solid Films 517 (2009) 2775.
[71] G. Tomandl, F.D. Gnanam, Sol–Gel Processing of Advanced Ceramics, Oxford and IBH Publishing Co. Pvt. Ltd, New Delhi, 1996.
[72] A.C. Pierre, Introduction to Sol gel Processing, Kluwer Academic Press, Boston, 1990.
[73] G. Mills, M.R. Hoffmann, Environ. Sci. Technol. 27 (1993) 1681.
[74] D.F. Ollis, C.Y. Hsiao, L. Budiman, C.L. Lee, J. Catal. 88 (1984) 89.
[75] C.S. Turchi, D.F. Ollis, J. Catal. 119 (1989) 480.
[76] H. Noda, K. Oikawa, H. Kamada, Bull. Chem. Soc. Jpn. 66 (1993) 455.
[77] M. Anpo, T. Shima, Y. Kubokawa, Chem. Lett. 14 (1985) 1799.
[78] R.F. Howe, M. Gratzel, J. Phys. Chem. 89 (1985) 4495.
[79] R.F. Howe, M. Gratzel, J. Phys. Chem. 91 (1987) 3906.
[80] R.F. Howe, M. Gratzel, J. Phys. Chem. 94 (1990) 2566.
[81] Y. Mao, C. Schoneich, K.D. Asmus, J. Phys. Chem. 95 (1991) 80.
[82] C. Kormann, D.W. Bahnemann, M.R. Hoffmann, Environ. Sci. Technol. 25 (1991) 494.
[83] J. Moser, S. Punchihewa, P.P. Infelta, M. Gratzel, Langmuir 7 (1991) 3012.
[84] R.B. Draper, M.A. Fox, Langmuir 6 (1990) 1396.
[85] E.R. Carraway, A.J. Hoffman, M.R. Hoffmann, Environ. Sci. Technol. 28 (1994) 786.
[86] C.J. Richard, J. Photochem. Photobiol. A 72 (1993) 179.
[87] M. Mrowetz, E. Selli, J. Photochem. Photobiol. A: Chem. 180 (2006) 15.
[88] C.M. Wang, A. Heller, H. Gerischer, J. Am. Chem. Soc. 114 (1992) 5230.
[89] H. Gerischer, A. Heller, J. Phys. Chem. 95 (1991) 5261.
[90] A.J. Hoffmann, E.R. Carraway, M.R. Hoffmann, Environ. Sci. Technol. 28 (1994) 776.
[91] K. Sunada, T. Watanabe, K. Hashimoto, J. Photochem. Photobiol. A 156 (2003) 227.
[92] K. Sunada, Y. Kikuchi, K. Hashimoto, A. Fujishima, Environ. Sci. Technol. 32 (1998) 726.
[93] J. Podporska-Carroll, E. Panaitescu, B. Quilty, L. Wang, L. Menon, S.C. Pillai, Appl. Catal. B: Environ. 176 (2015) 70.
[94] J.A. Rengifo-Herrera, C. Pulgarin, Sol. Energy 84 (2010) 37.
[95] J.A. Byrne, P.A. Fernandez-Ibanez, P.S.M. Dunlop, D.M.A. Alrousan, J.W.J. Hamilton, Int. J. Photoenergy 2011 (2011) 1.
[96] M.B. Fisher, D.A. Keane, P. Fernández-Ibáñez, J. Colreavy, S.J. Hinder, K.G. McGuigan, S.C. Pillai, Appl. Catal. B: Environ. 130–131 (2013) 8.
[97] N. Daneshvar, A. Niaei, S. Akbari, S. Aber, N. Kazemian, Glob. Nest J. 9 (2007) 132.
[98] J. Zhang, Y. Nosaka, J. Phys. Chem. C 118 (2014) 10824.
[99] X. Chen, S.S. Mao, Chem. Rev. 107 (2007) 2891.
[100] A. Sclafani, J. Phys. Chem. 100 (1996) 13655.
[101] J. Liqiang, Q. Yichun, W. Baiqi, L. Shudan, J. Baojiang, Y. Libin, F. Wei, F. Honggang, S. Jiazhong, Sol. Energy Mater. Sol. Cells 90 (2006) 1773.
[102] N. Serpone, J. Photochem. Photobiol. A: Chem. 104 (1997) 1.
[103] J. Soria, J.C. Conesa, V. Augugliaro, L. Palmisano, M. Schiavello, A. Sclafani, J. Phys. Chem. 95 (1991) 274.
[104] J.C. Yu, L. Zhang, J.G. Yu, Chem. Mater. 14 (2002) 4647.
[105] Y.R. Do, K. Lee, K. Dwight, W. Wold, J. Solid State Chem. 108 (1994) 198.
[106] J. Engweiler, J. Harf, A. Baiker, J. Catal. 159 (1996) 259.
[107] K. Vinodgopal, P.V. Kamat, Environ. Sci. Technol. 29 (1995) 841.
[108] A.J. Maira, K.L. Yeung, C.Y. Lee, P.L. Yue, C.K. Chan, J. Catal. 192 (2000) 185.
[109] Z.L. Xu, J. Shang, C.M. Liu, C. Kang, H.C. Guo, Y.G. Du, Mater. Sci. Eng. B 63 (1999) 211.
[110] Y. Li, D.S. Hwang, N.H. Lee, S.J. Kim, Chem. Phys. Lett. 404 (2005) 25.
[111] R. Georgekutty, M.K. Seery, S.C. Pillai, J. Phys. Chem. C 112 (2008) 13563.
[112] G. Balasubramanian, D.D. Dionysiou, M.T. Suidan, I. Baudin, J.M. Laine, Appl. Catal. B 47 (2004) 73.
[113] P. Periyat, S.C. Pillai, D.E. McCormack, J. Colreavy, S.J. Hinder, J. Phys. Chem. C 112 (2008) 7644.
[114] J.A. Gamboa, D.M. Pasquevich, J. Am. Ceram. Soc. 75 (1992) 2934.
[115] R.D. Shannon, J.A. Pask, J. Am. Ceram. Soc. 48 (1965) 391.
[116] R.A. Eppler, J. Am. Ceram. Soc. 70 (1987) 64.
[117] H. Zhang, J.F. Banfield, J. Mater. Chem. 8 (1998) 2073.
[118] A.A. Gribb, J.F. Banfield, Am. Mineral. 82 (1997) 717.
[119] Y.Q. Wang, X.J. Yu, D.Z. Sun, J. Hazard. Mater. 144 (2007) 328.
[120] G. Mattioli, P. Alippi, F. Filippone, R. Caminiti, A.A. Bonapasta, J. Phys. Chem. C 114 (2010) 21694.
[121] C. Di Valentin, G. Pacchioni, Acc. Chem. Res. 47 (2014) 3233.
[122] C. Freysoldt, B. Grabowski, T. Hickel, J. Neugebauer, G. Kresse, A. Janotti, C.G.V.d. Walle, Rev. Mod. Phys. 86 (2014) 253.
[123] M. Choi, F. Oba, I. Tanaka, Phys. Rev. B 78 (2008) 014115.
[124] P. Reunchan, N. Umezawa, S. Ouyang, J. Ye, Phys. Chem. Chem. Phys. 14 (2012) 1876.
[125] A. Kafizas, N. Noor, P. Carmichael, D.O. Scanlon, C.J. Carmalt, I.P. Parkin, Adv. Funct. Mater. 24 (2014) 1758.
[126] J.B. Varley, A. Janotti, C.G.V.d. Walle, Adv. Mater. 23 (2011) 2343.
[127] B.A. Peter Deák, T. Frauenheim, Phys. Rev. B 83 (2011) 155207.
[128] C. Gionco, M.C. Paganini, E. Giamello, R. Burgess, C. Di Valentin, G. Pacchioni, J. Phys. Chem. Lett. 4 (2014) 447.
[129] K. Lai, Y. Zhu, Y. Dai, B. Huang, J. Appl. Phys. 112 (2012) 043706.
[130] H. Wan, L. Xu, W.Q. Huang, G.F. Huang, C.N. He, J.H. Zhou, P. Peng, Appl. Phys. A 116 (2014) 741.
[131] L.M. Tang, L.L. Wang, D. Wang, J.Z. Liu, K.Q. Chen, J. Appl. Phys. 107 (2010) 083704.
[132] M.V. Schilfgaarde, T. Kotani, S. Faleev, Phys. Rev. Lett. 96 (2006) 226401.
[133] W. Kang, M.S. Hybertsen, Phys. Rev. B 82 (2010) 085203.
[134] L. Chiodo, J.M. García-Lastra, A. Iacomino, S. Ossicini, J. Zhao, H. Petek, A. Rubio, Phys. Rev. B 82 (2011) 045207.
[135] C. Di Valentin, A. Selloni, J. Phys. Chem. Lett. 2 (2011) 2223.
[136] M. Watanabe, T. Hayashi, J. Lumin. 112 (2005) 88.
[137] Y.F. Li, A. Selloni, J. Am. Chem. Soc. 135 (2013) 9195.
[138] C. Di Valentin, D. Fittipaldi, J. Phys. Chem. Lett. 4 (2013) 1901.
[139] H.H. Kristoffersen, U. Martinez, B. Hammer, Top. Catal. 57 (2014) 171.
[140] E. Borgarello, J. Kiwi, M. Gratzel, E. Pelizzetti, M. Visca, J. Am. Chem. Soc. 104 (1982) 2996.
[141] S. Sato, Chem. Phys. Lett. 123 (1986) 126.
[142] R. Asahi, T. Morikawa, T. Ohwaki, K. Aoki, Y. Taga, Science 293 (2001) 269.
[143] C. Dette, M.A. Pérez-Osorio, C.S. Kley, P. Punke, C.E. Patrick, P. Jacobson, F. Giustino, S.J. Jung, K. Kern, Nano Lett. 14 (2014) 6533.
[144] W. Li, Phys. Status Solidi RRL 9 (2015) 10.
[145] K. Gurunathan, P. Maruthamuthu, V. Sastri, Int. J. Hydrogen Energy 22 (1997) 57.
[146] K. Dhanalakshmi, S. Latha, S. Anandan, P. Maruthamuthu, Int. J. Hydrogen Energy 26 (2001) 669.
[147] A. Jana, J. Photochem. Photobiol. A 132 (2000) 1.
[148] A. Polo, M. Itokazu, N. Iha, Coord. Chem. Rev. 248 (2004) 1343.
[149] R. Abe, K. Sayama, H. Arakawa, Chem. Phys. Lett. 362 (2002) 441.
[150] S. Yan, J. Hupp, J. Phys. Chem. B 100 (1996) 6867.
[151] T. Hannappel, B. Burfeindt, W. Storck, J. Phys. Chem. B 101 (1997) 6799.
[152] I. Martini, J. Hodak, G. Hartland, J. Phys. Chem. B 102 (1998) 607.
[153] B. Burfeindt, T. Hannappel, W. Storck, F. Willig, J. Phys. Chem. 100 (1996) 16461.
[154] J. Rehm, G. Mclendon, Y. Nagasawa, K. Yoshihara, J. Moser, M. Gratzel, J. Phys. Chem. 100 (1996) 9577.
[155] W.J. Youngblood, S.H.A. Lee, K. Maeda, T.E. Mallouk, Acc. Chem. Res. 42 (2009) 1966.
[156] J.R. Swierka, T.E. Mallouk, Chem. Soc. Rev. 42 (2013) 2357.
[157] P. Chowdhury, J. Moreira, H. Gomaa, A.K. Ray, Ind. Eng. Chem. Res. 51 (2012) 4523.
[158] G. Qin, Z. Sun, Q. Wu, L. Lin, M. Liang, S. Xue, J. Hazard. Mater. 192 (2011) 599.
[159] M.R. John, A.J. Furgals, A.F. Sammells, J. Phys. Chem. 87 (1983) 801.
[160] G.R. Bamwenda, S. Tsubota, T. Nakamura, M. Haruta, J. Photochem. Photobiol. A 89 (1995) 177.
[161] S. Sakthivel, M.V. Shankar, M. Palanichamy, B. Arabindoo, D.W. Bahnemann, V. Murugesan, Water Res. 38 (2004) 3001.
[162] V. Subramanian, E. Wolf, P. Kamat, J. Phys. Chem. B 105 (2001) 11439.
[163] M. Jakob, H. Levanon, P.V. Kamat, Nano Lett. 3 (2003) 353.

[164] I.H. Tseng, J.C.S. Wu, H.Y. Chou, J. Catal. 221 (2004) 432.
[165] A. Takai, P.V. Kamat, ACS Nano 5 (2011) 7369.
[166] T.L. Phan, P. Zhang, H.D. Tran, S.C. Yu, J. Korean Phys. Soc. 57 (2010) 1270.
[167] M. Anpo, M. Takeuchi, J. Catal. 216 (2003) 505.
[168] M.K. Seery, R. George, P. Floris, S.C. Pillai, J. Photochem. Photobiol. A 189 (2007) 258.
[169] K.M. Rahulan, S. Ganesan, P. Aruna, Adv. Nat. Sci: Nanosci. Nanotechnol. 2 (2011) 25012.
[170] J. Taing, M.H. Cheng, J.C. Hemminger, ACS Nano 5 (2011) 6325.
[171] K. Awazu, M. Fujimaki, C. Rockstuhl, J. Tominaga, H. Murakami, Y. Ohki, N. Yoshida, T. Watanabe, J. Am. Chem. Soc. 130 (2008) 1676.
[172] H.A. Atwater, A. Polman, Nat. Mater. 9 (2010) 205.
[173] M. Murdoch, G.I.N. Waterhouse, M.A. Nadeem, J.B. Metson, M.A. Keane, R.F. Howe, J. Llorca, H. Idriss, Nat. Chem. 3 (2011) 489.
[174] S.D. Standridge, G.C. Schatz, J.T. Hupp, J. Am. Chem. Soc. 131 (2009) 8407.
[175] Y. Ide, M. Matsuoka, M. Ogawa, J. Am. Chem. Soc. 132 (2010) 16762.
[176] Y. Tian, T. Tatsuma, J. Am. Chem. Soc. 127 (2005) 7632.
[177] Y. Tian, T. Tatsuma, Chem. Commun. 16 (2004) 1810.
[178] A. Furube, L. Du, K. Hara, R. Katoh, M. Tachiya, J. Am. Chem. Soc. 129 (2007) 14852.
[179] Y. Nishijima, K. Ueno, Y. Yokota, K. Murakoshi, H. Misawa, J. Phys. Chem. Lett. 1 (2010) 2031.
[180] M.D. Brown, T. Suteewong, R.S.S. Kumar, V. D'Innocenzo, A. Petrozza, M.M. Lee, U. Wiesner, H.J. Snaith, Nano Lett. 11 (2011) 438.
[181] A.M. Glass, P.F. Lioa, J.G. Bergman, D.H. Olson, Opt. Lett. 5 (1980) 368.
[182] B. Rand, P. Peumans, S. Forrest, J. Appl. Phys. 96 (2004) 7519.
[183] S.K. Cushing, J. Li, F. Meng, T.R. Senty, S. Suri, M. Zhi, M. Li, A.D. Bristow, N. Wu, J. Am. Chem. Soc. 134 (2012) 15033.
[184] Z. Bian, T. Tachikawa, W. Kim, W. Choi, T. Majima, J. Phys. Chem. C 116 (2012) 25444.
[185] X. Shi, K. Ueno, N. Takabayashi, H. Misawa, J. Phys. Chem. C 117 (2013) 2494.
[186] C. Wen, K. Ishikawa, M. Kishima, K. Yamada, Sol. Energy Mater. Sol. Cells 61 (2000) 339.
[187] J. Okumu, C. Dahmen, A.N. Sprafke, M. Luysberg, v.P.G.M. Wuttig, J. Appl. Phys. 97 (2005) 94305.
[188] G. Sandmann, H. Dietz, W. Plieth, J. Electroanal. Chem. 491 (2000) 78.
[189] L. Miao, Y. Ina, S. Tanemura, T. Jiang, M. Taneura, K. Kaneko, S. Toh, Y. Mori, Surf. Sci. 601 (2007) 2792.
[190] C. He, Y. Xiong, J. Chen, C. Zha, X. Zhu, J. Photochem. Photobiol. A 157 (2003) 71.
[191] H. Hidaka, H. Honjo, S. Horikoshi, N. Serpone, Sens. Actuators B 123 (2007) 822.
[192] M. Ye, J. Gong, Y. Lai, C. Lin, Z. Lin, J. Am. Chem. Soc. 134 (2012) 15720.
[193] C. Hu, T. Peng, X. Hu, Y. Nie, X. Zhou, J. Qu, H. He, J. Am. Chem. Soc. 132 (2010) 857.
[194] P. Christopher, D.B. Ingram, S. Linic, J. Phys. Chem. C 114 (2010) 9173.
[195] L. Wang, C. Clavero, Z. Huba, K.J. Carroll, E.E. Carpenter, D. Gu, R.A. Lukaszew, Nano Lett. 11 (2011) 1237.
[196] W. Choi, A. Termin, M. Hoffmann, J. Phys. Chem. 84 (1994) 13669.
[197] M. Litter, Appl. Catal. B 23 (1999) 89.
[198] D. Dvoranova, V. Brezova, M. Mazur, M. Malati, Appl. Catal. B 37 (2002) 91.
[199] A. Xu, Y. Gao, H. Liu, J. Catal. 207 (2002) 151.
[200] A.D. Paola, G. Marci, L. Palmisano, M. Schiavello, K. Uosaki, S. Ikeda, J. Phys. Chem. B 106 (2002) 637.
[201] X. Wu, Z. Ma, Y. Qin, X. Qi, Z. Liang, Chin. J. Chem. Phys. 20 (2004) 138.
[202] K. Wilke, H.D. Breuer, J. Photochem. Photobiol. A: Chem. 121 (1999) 49.
[203] M. Ni, M.K.H. Leung, D.Y.C. Leung, K. Sumathy, Renew. Sustain. Energy Rev. 11 (2007) 401.
[204] H. Irie, S. Miura, K. Kamiya, K. Hashimoto, Chem. Phys. Lett. 457 (2008) 202.
[205] H. Yu, H. Irie, Y. Shimodaira, Y. Hosogi, Y. Kuroda, M. Miyauchi, K. Hashimoto, J. Phys. Chem. C 114 (2010) 16481.
[206] T. Morikawa, T. Ohwaki, K.I. Suzuki, S. Moribe, S. Tero-Kubota, Appl. Catal. B 83 (2008) 56.
[207] R. Asahi, T. Morikawa, H. Irie, T. Ohwaki, Chem. Rev. 114 (2014) 9824.
[208] S. Peng, Y. Li, F. Jiang, G. Lu, S. Li, Chem. Phys. Lett. 398 (2004) 235.
[209] N.L. Wu, M.S. Lee, Int. J. Hydrogen Energy 29 (2004) 1601.
[210] M. Takeuchi, H. Yamashita, M. Matsuoka, M. Anpo, T. Hirao, N. Itoh, Catal. Lett. 67 (2000) 135.
[211] H. Yamashita, M. Harada, J. Misaka, M.I.K. Takeuchi, M. Anpo, J. Photochem. Photobiol. A 148 (2002) 257.
[212] Y. Yalçin, M. Kiliç, Z. Çinar, Appl. Catal. B 99 (2010) 469.
[213] A. Mattsson, M. Leideborg, K. Larsson, G. Westin, L. Österlund, J. Phys. Chem. B 110 (2006) 1210.
[214] B.J. Morgan, D.O. Scanlona, G.W. Watson, J. Mater. Chem. 19 (2009) 5175.
[215] J. Yu, Q. Xiang, M. Zhou, Appl. Catal. B 90 (2009) 595.
[216] C. Di Valentin, G. Pacchioni, H. Onishi, A. Kudo, Chem. Phys. Lett. 469 (2009) 166.
[217] G. Shao, J. Phys. Chem. C 113 (2009) 6800.
[218] X. Li, X. Chen, H. Niu, X. Han, T. Zhang, J. Liu, H. Lin, F. Qu, J. Colloid Interface Sci. 452 (2015) 89.
[219] I. Tamiolakis, I.N. Lykakis, G.S. Armatas, Catal. Today 250 (2015) 180.
[220] R.A. Doong, C.H. Chen, R.A. Maithreepala, S.M. Chang, Water Res. 35 (2001) 2873.
[221] M.G. Kang, H.E. Han, K.J. Kim, J. Photochem. Photobiol. A 125 (1999) 119.
[222] W.W. So, K.J. Kim, S.J. Moon, Int. J. Hydrogen Energy 29 (2004) 229.
[223] G.C. De, A.M. Roy, S.S. Bhattacharya, Int. J. Hydrogen Energy 21 (1996) 19.
[224] A. Koca, M. Sahin, Int. J. Hydrogen Energy 27 (2002) 363.
[225] V. Keller, F. Garin, Catal. Commun. 4 (2003) 377.
[226] D. Li, H. Haneda, N. Ohashi, S. Hishita, Y. Yoshikawa, Catal. Today 93 (2004) 895.
[227] Y.L. Lee, Y.S. Lo, Adv. Funct. Mater. 19 (2009) 604.
[228] A. Braga, S. Gimenez, I. Concina, A. Vomiero, I. Mora-Sero, J. Phys. Chem. Lett. 2 (2011) 454.
[229] H.J. Lee, P. Chen, S.J. Moon, F. Sauvage, K. Sivula, T. Bessho, D.R. Gamelin, P. Comte, S.M. Zakeeruddin, S.I. Seok, M. Gratzel, M.K. Nazeeruddin, Langmuir 25 (2009) 7602.
[230] P. Sudhagar, J.H. Jung, S. Park, Y.G. Lee, R. Sathyamoorthy, Y.S. Kang, H. Ahn, Electrochem. Commun. 11 (2009) 2220.
[231] V. Gonzalez-Pedro, X.Q. Xu, I. Mora-Sero, J. Bisquert, ACS Nano 4 (2010) 5783.
[232] R. Vogel, P. Hoyer, H. Weller, J. Phys. Chem. B 98 (1994) 3183.
[233] A. Zaban, O.I. Micic, B.A. Gregg, A.J. Nozik, Langmuir 14 (1998) 3153.
[234] L.M. Peter, K.G.U. Wijayantha, D.J. Riley, J.P.J. Waggett, Phys. Chem. B 107 (2003) 8378.
[235] T.L. Li, Y.L. Lee, H. Teng, Energy Environ. Sci. 5 (2012) 5315.
[236] A.M. Smith, S.M. Nie, Acc. Chem. Res. 43 (2010) 190.
[237] A. Kongkanand, K. Tvrdy, K. Takechi, M. Kuno, P.V. Kamat, J. Am. Chem. Soc. 130 (2008) 4007.
[238] W.A. Tisdale, K.J. Williams, B.A. Timp, D.J. Norris, E.S. Aydil, X.Y. Zhu, Science 328 (2010) 1543.
[239] V.I. Klimov, J. Phys. Chem. B 110 (2006) 16827.
[240] J.B. Sambur, T. Novet, B.A. Parkinson, Science 330 (2010) 66.
[241] J. Fang, J. Wu, X. Lu, Y. Shen, Z. Lu, Chem. Phys. Lett. 270 (1997) 145.
[242] T. López-Luke, A. Wolcott, L.P. Xu, S. Chen, Z. Wen, J. Li, E.D.l. Rosa, J.Z. Zhang, J. Phys. Chem. C 112 (2008) 1282.
[243] H.M. Pathan, P.V. Salunkhe, B.R. Sankapal, C.D. Lokhande, Mater. Chem. Phys. 72 (2001) 105.
[244] Y. Xie, S.H. Heo, Y.N. Kim, S.H. Yoo, S.O. Cho, Nanotechnology 21 (2010) 15703.
[245] H.T. Li, X.D. He, Z.H. Kang, H. Huang, Y. Liu, J.L. Liu, S.Y. Lian, C.C.A. Tsang, X.B. Yang, S.T. Lee, Angew. Chem. Int. Ed. 49 (2010) 4430.
[246] H.C. Zhang, H. Huang, H. Ming, H.T. Li, L.L. Zhang, Y. Liu, Z.H. Kang, J. Mater. Chem. 22 (2012) 10501.
[247] W. Lee, S.H. Kang, J.Y. Kim, G.B. Kolekar, Y.E. Sung, S.H. Han, Nanotechnology 20 (2009) 335706.
[248] J.C. Conesa, J. Phys. Chem. C 116 (2012) 18884.
[249] A.A. Lisachenko, V.N. Kuznetsov, M.N. Zacharov, R.V. Michailov, Kinet. Catal. 45 (2004) 189.
[250] I. Nakamura, N. Negishi, S. Kutsuna, T. Ihara, S. Sugihara, K. Takeuchi, J. Mol. Catal. A: Chem. 161 (2000) 205.
[251] D. Zhang, M. Yang, S. Dong, RSC Adv. 5 (2015) 35661.
[252] X. Xin, T. Xu, J. Yin, L. Wang, C. Wang, Appl. Catal. B 176–177 (2015) 354.
[253] A.G. Thomas, W.R. Flavel, R. Stockbauer, S. Patel, M. Gratzel, R. Hengerer, Phys. Rev. B 67 (2003) 035110.
[254] C. Di Valentin, G. Pacchioni, A. Selloni, Phys. Rev. Lett. 97 (2006) 166803.
[255] B.J. Morgan, G.W. Watson, Surf. Sci. 601 (2007) 5034.
[256] C.J. Calzado, N.C. Hernández, J.F. Sanz, Phys. Rev. B 77 (2008) 045118.
[257] G. Mattioli, F. Filippone, P. Alippi, A.A. Bonapasta, Phys. Rev. B 78 (2008) 241201.
[258] T. Ihara, M. Miyoshi, Y. Iriyama, O. Matsumoto, S. Sugihara, Appl. Catal. B: Environ. 42 (2003) 403.
[259] J.L. Gole, J.D. Stout, C. Burda, Y. Lou, X. Chen, J. Phys. Chem. B 108 (2004) 1230.
[260] C.D. Valentin, G. Pacchioni, A. Selloni, S. Livraghi, E. Giamello, J. Phys. Chem. B 109 (2005) 11414.
[261] H. Liu, H.T. Ma, X.Z. Li, W.Z. Li, M. Wu, X.H. Bao, Chemosphere 50 (2003).
[262] H.Y. Yin, X.L. Wang, L. Wang, Q.L. N, H.T. Zhao, J. Alloys Compd. 640 (2015) 68.
[263] X. Chen, L. Liu, P.Y. Yu, S.S. Mao, Science 331 (2011) 746.
[264] S. Na-Phattalung, M.F. Smith, K. Kim, M.H. Du, S.H. Wei, S.B. Zhang, S. Limpijumnong, Phys. Rev. B: Condens. Matter 73 (2006) 125205.
[265] H. Kamisaka, K. Yamashita, J. Phys. Chem. C 115 (2011) 8265.
[266] T. Umebayashi, T. Yamaki, H. Itoh, K. Asai, Appl. Phys. Lett. 81 (2002) 454.
[267] S.U.M. Khan, M. Al-Shahry Jr., W.B. Ingler, Science 297 (2002) 2243.
[268] A. Hattori, M. Yamamoto, H. Tada, S. Ito, Chem. Lett. 216 (1998) 707.
[269] G. Torres, T. Lindgren, J. Lu, C. Granqvist, S. Lindquist, J. Phys. Chem. B 108 (2004) 5995.
[270] H. Li, Y. Hao, H. Lu, L. Liang, Y. Wang, J. Qiu, X. Shi, Y. Wang, J. Yao, Appl. Surf. Sci. 344 (2015) 112.
[271] Y. Cong, J. Zhang, F. Chen, M. Anpo, J. Phys. Chem. C 111 (2007) 6976.
[272] S. Shakthivel, H. Kisch, Chem. Phys. Chem. 13 (2003) 2996.
[273] T. Lindgren, J.M. Mwabora, E. Avenano, J. Jonsson, A. Hoel, C.G. Granqvist, S.E. Lindquist, J. Phys. Chem. B 107 (2003) 5709.
[274] Y. Aita, M. Komatsu, S. Yin, T. Sato, J. Solid State Chem. 177 (2004) 3235.
[275] S. Livraghi, M. Pelaez, J. Biedrzycki, I. Corazzari, E. Giamello, D.D. Dionysiou, Catal. Today 209 (2013) 54.
[276] K. Prabakar, T. Takahashi, T. Nezuka, K. Takahashi, T. Nakashima, Y. Kubota, A. Fujishima, Renew. Energy 33 (2008) 277.
[277] Y. Liu, K. Mu, J. Zhong, K. Chen, Y. Zhang, G. Yang, L. Wang, S.H. Deng, F. Shen, X. Zhang, RSC Adv. (2015), http://dx.doi.org/10.1039/C1035RA05367F.
[278] N.T. Nolan, D.W. Synnott, M.K. Seery, S.J. Hinder, A.V. Wassenhoven, S.C. Pillai, J. Hazard. Mater. 211–212 (2012) 88.
[279] T.C. Jagadale, S.P. Takale, R.S. Sonawane, H.M. Joshi, S.I. Patil, B.B. Kale, S.B. Ogale, J. Phys. Chem. C 112 (2008) 14595.
[280] H. Li, J. Li, Y. Huo, J. Phys. Chem. B 110 (2006) 1559.

[281] S. Yin, H. Yamaki, M. Komatsu, Q. Zhang, J. Wang, Q. Tang, F. Saito, T. Sato, J. Mater. Chem. 13 (2003) 2996.
[282] D. Wu, M. Long, W. Cai, C. Chen, Y. Wu, J. Alloys Compd. 502 (2010) 289.
[283] F. Peng, L. Cai, H. Yu, H. Wang, J. Yang, J. Solid State Chem. 181 (2008) 130.
[284] T. Morikawa, R. Asahi, T. Ohwaki, K. Aoki, Y. Taga, Jpn. J. Appl. Phys. 40 (2001) L561.
[285] H. Irie, Y. Watanabe, K. Hashimoto, J. Phys. Chem. B 107 (2003) 5483.
[286] O. Diwald, T.L. Thompson, E.G. Goralski, S.D. Walck, J.T. Yates, J. Phys. Chem. B 108 (2004) 52.
[287] R. Nakamura, T. Tanaka, Y. Nakoto, J. Phys. Chem. B 108 (2004) 10617.
[288] A.V. Emeline, V.N. Kuznetsov, V.K. Rybchuk, N. Serpone, Int. J. Photoenergy 258 (2008) 1.
[289] F. Spadavecchia, G. Cappelletti, S. Ardizzone, M. Ceotto, L. Falciola, J. Phys. Chem. C 115 (2011) 6381.
[290] I.N. Martyanov, S. Uma, S. Rodrigues, K.J. Klabunde, Chem. Commun. 7 (2004) 2476.
[291] X. Tian-hua, S. Chen-lu, L. Yong, H. Gao-rong, J. Zhejiang Univ. Sci. B 7 (2006) 299.
[292] M.D. Segall, P.J.D. Lindan, M.J. Probert, C.J. Pickard, P.J. Hasnip, S.J. Clark, M.C. Payne, J. Phys.: Condens. Matter 14 (2002) 2717.
[293] G. Barolo, S. Livraghi, M. Chiesa, M.C. Paganini, E. Giamello, J. Phys. Chem. C 116 (2012) 20887.
[294] S. Livraghi, M.C. Paganini, E. Giamello, A. Selloni, C.D. Valentin, G. Pacchioni, J. Am. Chem. Soc. 128 (2006) 15666.
[295] E. Finazzi, C.D. Valentin, J. Phys. Chem. C 111 (2007) 9275.
[296] J. Graciani, L.J. Álvarez, J.A. Rodriguez, J.F. Sanz, J. Phys. Chem. C 112 (2008) 2624.
[297] C. Di Valentin, E. Finazzi, G. Pacchioni, A. Selloni, S. Livraghi, M.C. Paganini, E. Giamello, Chem. Phys. Chem. 339 (2007) 44.
[298] S. Sakthivel, H. Kisch, Angew. Chem. Int. Ed. 42 (2003) 4908.
[299] G. Wu, T. Nishikawa, B. Ohtani, A. Chen, Chem. Mater. 19 (2007) 4530.
[300] J.W. Park, D.W. Kim, H.S. Seon, K.S. Kim, D.W. Park, Thin Solid Films 518 (2010) 4113.
[301] D. Chu, X. Yuan, G. Qin, M. Xu, P. Zheng, J. Lu, L. Zha, J. Nanopart. Res. 10 (2008) 357.
[302] P. Shao, J. Tian, Z. Zhao, W. Shi, S. Gao, F. Cui, Appl. Surf. Sci. 324 (2015) 35.
[303] J.H. Park, S. Kim, A.J. Bard, Nano Lett. 6 (2006) 24.
[304] Z. Wu, F. Dong, W. Zhao, H. Wang, Y. Liu, B. Guan, Nanotechnology 20 (2009) 235701.
[305] J.W. Shi, X. Zong, X. Wu, H.J. Cui, B. Xu, L. Wang, M.L. Fu, Chem. Cat. Chem. 4 (2012) 488.
[306] S.U.M. Khan, M. Al-Shahry, W.B. Ingler, Science 297 (2002) 2243.
[307] Y. Choi, T. Umebayashi, M. Yoshikawa, J. Mater. Sci. 39 (2004) 1837.
[308] H. Irie, Y. Watanabe, K. Hashimoto, Chem. Lett. 32 (2003) 772.
[309] C. Di Valentin, G. Pacchioni, A. Selloni, Chem. Mater. 17 (2005) 6656.
[310] T. Ohno, M. Akiyoshi, T. Umebayashi, K. Asai, T. Mitsui, M. Matsumura, Appl. Catal. A 265 (2004) 115.
[311] Y. Cui, H. Du, L. Wen, Solid State Commun. 149 (2009) 634.
[312] F. Tian, C. Liu, W. Zhao, X. Wang, Z. Wang, J.C. Yu, J. Comput. Sci. Eng. 1 (2011) 32.
[313] F. Dong, W. Zhao, Z. Wu, Nanotechnology 19 (2008) 365607.
[314] D. Li, H. Haneda, N.K. Labhsetwar, S. Hishita, N. Ohashi, Chem. Phys. Lett. 401 (2005) 579.
[315] W. Ho, J.C. Yu, S. Lee, Chem. Commun. 10 (2006) 1115.
[316] S.C. Padmanabhan, S.C. Pillai, J. Colreavy, S. Balakrishnan, D.E. McCormack, T.S. Perova, Y. Gun'ko, S.J. Hinder, J.M. Kelly, Chem. Mater. 19 (2007) 4474.
[317] J. Yu, J. Fan, K. Lv, Nanoscale 2 (2010) 2144.
[318] M.V. Dozzi, E. Selli, Catalysts 3 (2013) 455.
[319] J. Xu, Y. Ao, D. Fu, C. Yuan, Appl. Surf. Sci. 254 (2008) 3033.
[320] S. Tojo, T. Tachikawa, M. Fujitsuka, T. Majima, J. Phys. Chem. C 112 (2008) 14948.
[321] G. Liu, Z. Chen, C. Dong, Y. Zhao, F. Li, G.Q. Lu, H.M. Cheng, J. Phys. Chem. B 110 (2006) 20823.
[322] X. Hong, Z. Wang, W. Cai, F. Lu, J. Zhang, Y. Yang, N. Ma, Y. Liu, Chem. Mater. 17 (2005) 1548.
[323] W. Su, Y. Zhang, Z. Li, L. Wu, X. Wang, J. Li, X. Fu, Langmuir 24 (2008) 3422.
[324] J.C. Yu, J.G. Yu, W.K. Ho, Z.T. Jiang, L.Z. Zhang, Chem. Mater. 14 (2002) 3808.
[325] G. Liu, C. Sun, X. Yan, L. Cheng, Z. Chen, X. Wang, L. Wang, S.C. Smith, G.Q. Lu, H.M. Cheng, J. Mater. Chem. 19 (2009) 2822.
[326] G. Xiang, T. Li, J. Zhuang, X. Wang, Chem. Commun. 46 (2010) 6801.
[327] Q. Zhang, Y. Li, E.A. Ackerman, M.G. Josifovska, H. Li, Appl. Catal. A: Gen. 400 (2011) 195.
[328] M. Harb, J. Phys. Chem. C 117 (2013) 25229.
[329] I.E. Grey, C. Li, C. Macrae, J. Solid State Chem. 127 (1996) 240.
[330] D. Chen, D. Yang, Q. Wang, Z.Y. Jiang, Ind. Eng. Chem. Res. 45 (2006) 4110.
[331] W. Zhao, W.H. Ma, C.C. Chen, J.C. Zhao, Z.G. Shuai, J. Am. Chem. Soc. 126 (2004) 4782.
[332] S. In, A. Orlov, R. Berg, F. García, S.P. Jimenez, M.S. Tikhov, D.S. Wright, R.M. Lambert, J. Am. Chem. Soc. 129 (2007) 13790.
[333] J. Xu, Y. Ao, M. Chen, D. Fu, J. Alloys Compd. 484 (2009) 73.
[334] V. Stengl, V. Houskova, S. Bakardjieva, N. Murafa, ACS Appl. Mater. Interfaces 2 (2010) 575.
[335] E. Finazzi, C. Di Valentin, G. Pacchioni, J. Phys. Chem. C 113 (2009) 220.
[336] J. Pan, G. Liu, G.Q. Lu, H.M. Cheng, Angew. Chem. Int. Ed. 50 (2011) 2133.
[337] G. Zheng, J. Wang, X. Liu, A. Yang, H. Song, Y. Guo, H. Wei, C. Jiao, S. Yang, Q. Zhu, Z. Wang, Appl. Surf. Sci. 256 (2010) 7327.
[338] FengHui, ChengBu, J. Phys. Chem. B 110 (2006) 17866.
[339] K. Yang, Y. Dai, B. Huang, J. Phys. Chem. C 111 (2007) 12086.
[340] K. Yang, Y. Dai, B. Huang, J. Phys. Chem. C 111 (2007) 18985.
[341] K. Yang, Y. Dai, B. Huang, M.H. Whangbo, Chem. Mater. 20 (2008) 6528.
[342] J. Graciani, Y. Ortega, J.F. Sanz, Chem. Mater. 21 (2009) 1431.
[343] R. Long, Y. Dai, B. Huang, Comput. Mater. Sci. 45 (2009) 223.
[344] C. Di Valentin, G. Pacchioni, Catal. Today 206 (2013) 12.
[345] J.H. Xu, J. Li, W.L. Dai, Y. Cao, H. Li, K. Fan, Appl. Catal. B: Environ. 79 (2008) 72.
[346] J.A.R. Herrera, E. Mielczarski, J. Mielczarski, N.C. Castillo, J. Kiwi, Appl. Catal. B: Environ. 84 (2008) 448.
[347] P. Periyat, D.E. McCormack, S.J. Hinder, S.C. Pillai, J. Phys. Chem. C 113 (2009) 3246.
[348] Q. Xiang, J. Yu, M. Jaroniec, Phys. Chem. Chem. Phys. 13 (2011) 4853.
[349] Q.C. Xu, D.V. Wellia, S. Yan, D.W. Liao, T.M. Lim, T.T. Tan, J. Hazard. Mater. 188 (2011) 172.
[350] J. Wang, B. Huang, Z. Wang, X. Qin, X. Zhang, Rare Met. 30 (2011) 161.
[351] M. Lim, Y. Zhou, B. Wood, Y. Guo, L. Wang, V. Rudolph, G. Lu, J. Phys. Chem. C 112 (2008) 19655.
[352] P. Xu, T. Xu, J. Lu, S. Gao, N.S. Hosmane, B. Huang, Y. Daid, Y. Wang, Energy Environ. Sci. 3 (2010) 1128.
[353] R. Zhang, Q. Wang, Q. Li, J. Dai, D. Huang, Phys. B: Condens. Matter 406 (2011) 3417.
[354] M. Xing, Y. Wu, J. Zhang, F. Chen, Nanoscale 7 (2010) 1233.
[355] G. Liu, L.C. Yin, J. Wang, P. Niu, C. Zhen, Y. Xie, H.M. Cheng, Energy Environ. Sci. 5 (2012) 9603.
[356] Y. Lin, Z. Jiang, C. Zhu, X. Hu, X. Zhang, H. Zhu, J. Fan, S.H. Lin, J. Mater. Chem. A 1 (2013) 4516.
[357] C. Di Valentin, E. Finazzi, G. Pacchioni, A. Selloni, S. Livraghi, A.M. Czoska, M.C. Paganini, E. Giamello, Chem. Mater. 20 (2008) 3706.
[358] A.M. Czoska, S. Livraghi, M.C. Paganini, E. Giamello, C. Di Valentin, G. Pacchioni, Phys. Chem. Chem. Phys. 13 (2011) 136.
[359] P. Zhou, J. Yu, Y. Wang, Appl. Catal. B 142 (2013) 45.
[360] V. Gombac, L.D. Rogatis, A. Gasparotto, G. Vicario, T. Montini, D. Barreca, G. Balducci, P. Fornasiero, E. Tondello, M. Graziani, Chem. Phys. 339 (2007) 111.
[361] J.W.J. Hamilton, J.A. Byrne, P.S.M. Dunlop, D.D. Dionysiou, M. Pelaez, K. O'Shea, D. Synnott, S.C. Pillai, J. Phys. Chem. C 118 (2014) 12206.
[362] C. Zhao, M. Pelaez, D.D. Dionysiou, S.C. Pillai, J.A. Byrne, K.E. O'Shea, Catal. Today 224 (2014) 70.
[363] T.M. Breault, B.M. Bartlett, J. Phys. Chem. C 116 (2012) 5986.
[364] T.M. Breault, B.M. Bartlett, J. Phys. Chem. C 117 (2013) 8611.
[365] M. Nasir, Z. Xi, M. Xing, J. Zhang, F. Chen, B. Tian, S. Bagwasi, J. Phys. Chem. C 117 (2013) 9520.
[366] L. Sun, X. Zhao, X. Cheng, H. Sun, Y. Li, P. Li, W. Fan, Langmuir 28 (2012) 5882.
[367] M.J. Yang, C. Hume, S. Lee, Y.H. Son, J.K. Lee, J. Phys. Chem. C 114 (2010) 15292.
[368] J.W. Liu, R. Han, Y. Zhao, H.T. Wang, W.J. Lu, T.F. Yu, Y.X. Zhang, J. Phys. Chem. C 115 (2011) 4507.
[369] E.J. Wang, T. He, L.S. Zhao, Y.M. Chen, Y.A. Cao, J. Mater. Chem. 21 (2011) 144.
[370] H.B. Liu, Y.M. Wu, J.L. Zhang, ACS Appl. Mater. Interfaces 3 (2011) 1757.
[371] J. Zhang, Y. Wu, M. Xing, S.A.K. Leghari, S. Sajjad, Energy Environ. Sci. 3 (2010) 715.
[372] Y. Cong, J.L. Zhang, F. Chen, M. Anpo, J. Phys. Chem. C 111 (2007) 10618.
[373] M.Y. Xing, J.L. Zhang, F. Chen, J. Phys. Chem. C 113 (2009) 12848.
[374] K. Obata, H. Irie, K. Hashimoto, Chem. Phys. Chem. 339 (2007) 124.
[375] X. Zhang, Q. Liu, Appl. Surf. Sci. 254 (2008) 4780.
[376] D.E. Gu, B.C. Yang, Y.D. Hu, Catal. Commun. 9 (2008) 1472.
[377] L. Yu, X. Yang, J. He, Y. He, D. Wang, J. Alloys Compd. 637 (2015) 308.
[378] X. Li, Q. Liu, X. Jiang, J. Huang, Int. J. Electrochem. Sci. 7 (2012) 11519.
[379] Y.F. Li, D. Xu, J.I. Oh, W. Shen, X. Li, Y. Yu, ACS Catal. 2 (2012) 391.
[380] S.S. Thind, G. Wu, M. Tian, A. Chen, Nanotechnology 23 (2012) 475706.
[381] M.E. Kurtoglu, T. Longenbach, K. Sohlberg, Y. Gogotsi, J. Phys. Chem. C 115 (2011) 17392.
[382] N. Feng, Q. Wang, A. Zheng, Z. Zhang, J. Fan, S.B. Liu, J.P. Amoureux, F. Deng, J. Am. Chem. Soc. 135 (2013) 1607.
[383] Y. Su, Y. Xiao, Y. Li, Y. Du, Y. Zhang, Mater. Chem. Phys. 126 (2011) 761–768.
[384] S. Bouhadoun, C. Guillard, F. Dapozze, S. Singh, D. Amans, J. Bouclé, N. Herlin-Boime, Appl. Catal. B 174–175 (2015) 367.
[385] G.R. Torres, T. Lindgren, J. Lu, C.G. Granqvist, S.E. Lindquist, J. Phys. Chem. B 108 (2004) 5995.
[386] T. Kawahara, Y. Konishi, H. Tada, N. Tohge, J. Nishii, S. Ito, Angew. Chem. Int. Ed. 41 (2002) 2811.
[387] P. Zhang, B. Liu, S. Yin, YuhuaWang, V. Petrykin, M. Kakihana, T. Sato, Mater. Chem. Phys. 116 (2009) 269.
[388] Y. Yuan, J. Ding, J. Xu, J. Deng, J. Guo, J. Nanosci. Nanotechnol. 10 (2010) 4868.
[389] Y. Ortega, N.C. Hernández, E.M. Proupin, J. Graciani, J.F. Sanz, Phys. Chem. Chem. Phys. 13 (2011) 11340.
[390] D.B. Hamal, J.A. Haggstrom, G.L. Marchin, M.A. Ikenberry, K. Hohn, K.J. Klabunde, Langmuir 26 (2010) 2805.
[391] P. Wu, R. Xie, K. Imlay, J.K. Shang, Environ. Sci. Technol. 44 (2010) 6992.
[392] D.O. Scanlon, C.W. Dunnill, J. Buckeridge, S.A. Shevlin, A.J. Logsdail, S.M. Woodley, C.R.A. Catlow, M.J. Powell, R.G. Palgrave, I.P. Parkin, G.W. Watson, T.W. Keal, P. Sherwood, A. Walsh, A.A. Sokol, Nat. Mater. 12 (2013) 798.
[393] H. Zhang, X. Lv, Y. Li, Y. Wang, J. Li, ACS Nano 4 (2010) 380.
[394] K.K. Manga, S. Wang, M. Jaiswal, Q. Bao, K.P. Loh, Adv. Mater. 22 (2010) 5265.
[395] Y. Wen, H. Ding, Y. Shan, Nanoscale 3 (2011) 4411.

[396] N. Li, G. Liu, C. Zhen, F. Li, L. Zhang, H.M. Cheng, Adv. Funct. Mater. 21 (2011) 1717.
[397] Y.T. Liang, B.K. Vijayan, K.A. Gray, M.C. Hersam, Nano Lett. 11 (2011) 2865.
[398] G. Williams, B. Seger, P.V. Kamat, ACS Nano 2 (2008) 1487.
[399] N.J. Bell, Y.H. Ng, A. Du, H. Coster, S.C. Smith, R. Amal, J. Phys. Chem. C 115 (2011) 6004.
[400] C. Nethravathi, M. Rajamathi, Carbon 46 (2008) 1994.
[401] T.N. Lambert, C.A. Chavez, B.H. Sanchez, P. Lu, N.S. Bell, A. Ambrosini, T. Friedman, T.J. Boyle, D.R. Wheeler, D.L. Huber, J. Phys. Chem. C 113 (2009) 19812.
[402] O. Akhavan, E. Ghaderi, J. Phys. Chem. C 113 (2009) 20214.
[403] X.Y. Zhang, H.P. Li, X.L. Cui, Y. Lin, J. Mater. Chem. 20 (2010) 2801.
[404] Y. Zhang, Z.R. Tang, X. Fu, Y.J. Xu, ACS Nano 4 (2010) 7303.
[405] N. Yang, Y. Liu, HaoWen, Z. Tang, H. Zhao, Y. Li, DanWang, ACS Nano 7 (2013) 1504.
[406] W. Liu, J. Cai, Z. Ding, Z. Li, Appl. Catal. B 174–175 (2015) 421.
[407] L.L. Tan, W.J. Ong, S.P. Chai, A.R. Mohamed, Nanoscale Res. Lett. 8 (2013) 465.
[408] I.V. Lightcap, T.H. Kosel, P.V. Kamat, Nano Lett. 10 (2010) 577.
[409] J.C. Liu, H.W. Bai, Y.J. Wang, Z.Y. Liu, X.W. Zhang, D.D. Sun, Adv. Funct. Mater. 20 (2010) 4175.
[410] Q. Xiang, J. Yu, M. Jaroniec, Nanoscale 3 (2011) 3670.
[411] L. Sun, Z.L. Zhao, Y.C. Zhou, L. Liu, Nanoscale 4 (2012) 613.
[412] M.K. Kavitha, S.C. Pillai, P. Gopinath, H. John, J. Environ. Chem. Eng. 3 (2015) 1194.
[413] J. Hou, C. Yang, Z. Wang, S. Jiao, H. Zhu, Appl. Catal. B: Environ. 129 (2013) 333.
[414] Q. Huang, S. Tian, D. Zeng, X. Wang, W. Song, Y. Li, W. Xiao, C. Xie, ACS Catal. 3 (2013) 1477.
[415] K. Woan, G. Pyrgiotakis, W. Sigmund, Adv. Mater. 21 (2009) 2233.
[416] J. Wang, W.D. Zhang, Electrochim. Acta 71 (2012) 10.
[417] S.C. Yan, Z.S. Li, Z.G. Zou, Langmuir 26 (2010) 3894.
[418] L. Ge, C. Han, J. Liu, Appl. Catal. B 108–109 (2011) 100.
[419] L. Song, S. Zhang, X. Wu, Q. Wei, Chem. Eng. J. 184 (2012) 256.
[420] H. Ji, F. Chang, X. Hu, W. Qin, J. Shen, Chem. Eng. J. 218 (2013) 183.
[421] Y. Li, J. Wang, Y. Yang, Y. Zhang, D. He, Q. An, G. Cao, J. Hazard. Mater. 292 (2015) 79.
[422] D. Mitoraj, H. Kisch, Angew. Chem. Int. Ed. 47 (2008) 9975.
[423] G. Li, N. Yang, W. Wang, W. Zhang, J. Phys. Chem. C 113 (2009) 14829.
[424] X. Wang, K. Maeda, A. Thomas, K. Takanabe, G. Xin, J.M. Carlsson, K. Domen, M. Antonietti, Nat. Mater. 8 (2009) 76.
[425] X. Lu, Q. Wang, D. Cui, J. Mater. Sci. Technol. 26 (2010) 925.
[426] B. Chai, T. Peng, J. Mao, K. Li, L. Zan, Phys. Chem. Chem. Phys. 14 (2012) 16745.
[427] H.J. Yan, H.X. Yang, J. Alloys Compd. 509 (2011) L26.
[428] W.D. Zhang, L.C. Jiang, J.S. Ye, J. Phys. Chem. C 113 (2009) 16247.
[429] Q.J. Xiang, J.G. Yu, M. Jaroniec, J. Phys. Chem. C 115 (2011) 7355.
[430] W.D. Zhang, B. Xu, L.C. Jiang, J. Mater. Chem. 20 (2010) 6383.
[431] L.C. Jiang, W.D. Zhang, Electrochim. Acta 56 (2010) 406.
[432] C.I. Covaliu, L.C. Chioaru, L. Craciun, O. Oprea, I. Jitaru, Optoelectron. Adv. Mater. 5 (2011) 1097.
[433] C.R. Kagan, D.B. Mitzi, C.D. Dimitrakopoulos, Science 286 (1999) 945.
[434] D.B. Mitzi, C.A. Feild, Z. Schlesinger, R.B. Laibowitz, J. Solid State Chem. 114 (1995) 159.
[435] A. Kojima, M. Ikegami, K. Teshima, T. Miyasaka, Chem. Lett. 41 (2012) 397.
[436] J. Burschka, N. Pellet, S.J. Moon, R.H. Baker, P. Gao, M.K. Nazeeruddin, M. Grätzel, Nature 499 (2013) 316.
[437] M.M. Lee, J. Teuscher, T. Miyasaka, T.N. Murakami, H.J. Snaith, Science 338 (2012) 643.
[438] A. Kojima, K. Teshima, Y. Shirai, T. Miyasaka, J. Am. Chem. Soc. 131 (2009) 6050.
[439] J.H. Im, J. Chung, S.J. Kim, N.G. Park, Nanoscale Res. Lett. 7 (2012) 353.
[440] J.H. Im, C.R. Lee, J.W. Lee, S.W. Park, N.G. Park, Nanoscale 3 (2011) 4088.
[441] H.S. Kim, C.R. Lee, J.H. Im, K.B. Lee, T. Moehl, A. Marchioro, S.J. Moon, R.H. Baker, J.H. Yum, J.E. Moser, M. Grätzel, N.G. Park, Nat. Sci. Rep. 2 (2012) 591.
[442] I. Chung, B. Lee, J. He, R.P.H. Chang, M.G. Kanatzidis, Nature 485 (2012) 486.
[443] L. Etgar, P. Gao, Z. Xue, Q. Peng, A.K. Chandiran, B. Liu, M.K. Nazeeruddin, M. Grätzel, J. Am. Chem. Soc. 134 (2012) 17396.
[444] F.D. Angelis, Acc. Chem. Res. 47 (2014) 3349.
[445] P. Umari, E. Mosconi, F.D. Angelis, Sci. Rep. 4 (2014) 4467.
[446] S. Colella, E. Mosconi, P. Fedeli, A. Listorti, F. Gazza, F. Orlandi, P. Ferro, T. Besagni, A. Rizzo, G. Calestani, G. Gigli, F.D. Angelis, R. Mosca, Chem. Mater. 25 (2013) 4613.
[447] A. Amat, E. Mosconi, E. Ronca, C. Quarti, P. Umari, M.K. Nazeeruddin, M. Grätzel, F.D. Angelis, Nano Lett. 14 (2014) 3608.
[448] J. Even, L. Pedesseau, J.M. Jancu, C. Katan, J. Phys. Chem. Lett. 4 (2013) 2999.
[449] J.M. Azpiroz, E. Mosconi, J. Bisquert, F.D. Angelis, Energy Environ. Sci. 8 (2015) 2118.
[450] R. Gottesman, E. Haltzi, L. Gouda, S. Tirosh, Y. Bouhadana, A. Zaban, J. Phys. Chem. Lett. 5 (2014) 2662.
[451] V. Roiati, E. Mosconi, A. Listorti, S. Colella, G. Gigli, F.D. Angelis, Nano Lett. 14 (2014) 2168.
[452] E. Mosconi, A. Amat, M.K. Nazeeruddin, M. Grätzel, F.D. Angelis, J. Phys. Chem. C 117 (2013) 13902.
[453] X. Chen, S. Shen, L. Guo, S.S. Mao, Chem. Rev. 110 (2010) 6503.
[454] D. Jing, Y. Zhang, L. Guo, Chem. Phys. Lett. 415 (2005) 74.
[455] Y. Ebina, T. Sasaki, M. Harada, M. Watanabe, Chem. Mater. 14 (2002) 4390.
[456] Y. Ikuma, H. Bessho, Int. J. Hydrogen Energy 32 (2007) 2689.
[457] J. Kiwi, M. Gratzel, J. Phys. Chem. 88 (1984) 1302.
[458] A. Iwase, H. Kato, A. Kudo, Catal. Lett. 108 (2006) 7.
[459] G. Wu, T. Chen, G. Zhou, X. Zong, C. Li, Sci. China Ser. B 51 (2008) 97.
[460] A.V. Korzhak, N.I. Ermokhina, A.L. Stroyuk, V.K. Bukhtiyarov, A.E. Raevskaya, V.I. Litvin, S.Y. Kuchmiy, V.G. Ilyin, P.A. Manorik, J. Photochem. Photobiol. A 198 (2008) 126.
[461] K. Gurunathan, Int. J. Hydrogen Energy 29 (2004) 933.
[462] Y. Mizukoshi, K. Sato, T.J. Konno, N. Masahashi, Appl. Catal. B 94 (2010) 248.
[463] K. Teramura, K. Maeda, T. Saito, T. Takata, N. Saito, Y. Inoue, K. Domen, J. Phys. Chem. B 109 (2005) 21915.
[464] H. Tada, T. Mitsui, T. Kiyonaga, T. Akita, K. Tanaka, Nat. Mater. 5 (2006) 782.
[465] H. Park, W. Choi, M.R. Hoffmann, J. Mater. Chem. 18 (2008) 2379.
[466] Y. Ou, J. Lin, S. Fang, D. Liao, Chem. Phys. Lett. 429 (2006) 199.
[467] R. Brahimi, Y. Bessekhouad, A. Bouguelia, M. Trari, Catal. Today 122 (2007) 62.
[468] F. Su, T. Wang, R. Lv, J. Zhang, P. Zhang, J. Lu, J. Gong, Nanoscale 5 (2013) 9001.
[469] P.A. DeSario, J.J. Pietron, D.E. DeVantier, T.H. Brintlinger, R.M. Stroud, D.R. Rolison, Nanoscale 5 (2013) 8073.
[470] W.H. Hung, T.M. Chien, C.M. Tseng, J. Phys. Chem. C 118 (2014) 12676.
[471] C. Wang, Z. Chen, H. Jin, C. Cao, J. Lia, Z. Mi, J. Mater. Chem. A 2 (2014) 17820.
[472] S.W. Shin, J.Y. Lee, K.S. Ahn, S.H. Kang, J.H. Kim, J. Phys. Chem. C 119 (2015) 13375.
[473] M. Khatamian, M.S. Oskoui, M. Haghighi, M. Darbandi, Int. J. Energy Res. 38 (2014) 1712.
[474] R.P. Cavalcante, R.F. Dantas, B. Bayarri, O. González, J. Giménez, S. Esplugas, A.M. Junior, Catal. Today 252 (2015) 27.
[475] Q. Zhang, G. Rao, J. Rogers, C. Zhao, L. Liu, Y. Li, Chem. Eng. J. 271 (2015) 180.
[476] E.M. Seftel, M. Niarchos, C. Mitropoulos, M. Mertens, E.F. Vansant, P. Cool, Catal. Today 252 (2015) 120.
[477] M.A.N. Khan, M. Siddique, F. Wahid, R. Khan, Ultrason. Sonochem. 26 (2015) 370.
[478] P. Dhatshanamurthi, B. Subash, M. Shanthi, Mater. Sci. Semicond. Process. 35 (2015) 22.
[479] M.J. Sampaio, C.G. Silva, A.M.T. Silva, L.M. Pastrana-Martínez, C. Han, S. Morales-Torres, J.L. Figueiredo, D.D. Dionysiou, J.L. Faria, Appl. Catal. B 170–171 (2015) 74.
[480] V. Vaiano, O. Sacco, D. Sannino, P. Ciambelli, Appl. Catal. B 170–171 (2015) 153.
[481] Z. Jiang, D. Jiang, Z. Yan, D. Liu, K. Qian, J. Xie, Appl. Catal. B 170–171 (2015) 195.
[482] H.M. Ibrahim, World J. Microbiol. Biotechnol. 7 (2015) 1049.
[483] F. Dong, Z. Wang, Y. Li, W.K. Ho, S.C. Lee, Environ. Sci. Technol. 48 (2014) 10345.
[484] J. Ma, H. He, F. Liu, Appl. Catal. B 179 (2015) 21.
[485] C.C. Pei, W.W.F. Leung, Appl. Catal. B 174–175 (2015) 515.
[486] G. Li, B. Jiang, S. Xiao, Z. Lian, D. Zhang, J.C. Yu, H. Li, Environ. Sci.: Processes Impacts 16 (2014) 1975.
[487] S.O. Hay, T. Obee, Z. Luo, T. Jiang, Y. Meng, J. He, S.C. Murphy, S. Suib, Molecules 20 (2015) 1319.
[488] Z.H. Lin, P. Roy, Z.Y. Shih, C.M. Ou, H.T. Chang, ChemPlusChem 78 (2013) 302.
[489] H.M. Yadav, S.V. Otari, R.A. Bohara, S.S. Mali, S.H. Pawar, S.D. Delekar, J. Photochem. Photobiol. A: Chem. 294 (2014) 130.
[490] J. Ananpattarachai, Y. Boonto, P. Kajitvichyanukul, Environ. Sci. Pollut. Res. Int. (2015), http://dx.doi.org/10.1007/s11356-015-4775-1.
[491] J.W. Xu, Z.D. Gao, K. Han, Y. Liu, Y.Y. Song, ACS Appl. Mater. Interfaces 6 (2014) 15122.
[492] O. Akhavan, R. Azimirad, S. Safa, M.M. Larijani, J. Mater. Chem. 20 (2010) 7386.
[493] K. Gupta, R.P. Singh, A. Pandey, A. Pandey, Beilstein J. Nanotechnol. 4 (2013) 345.
[494] H. Li, Q. Cui, B. Feng, J. Wang, X. Lu, J. Weng, Appl. Surf. Sci. 284 (2013) 179.
[495] W.S. Lee, Y.S. Park, Y.K. Cho, Analyst 140 (2015) 616.
[496] M.Y. Lan, C.P. Liu, H.H. Huang, S.W. Lee, PLOS ONE 8 (2013) 75364.
[497] J.Z. Bloh, R. Dillert, D.W. Bahnemann, ChemCatChem 5 (2013) 774.
[498] Z.B. Zhang, C.C. Wang, R. Zakaria, J.Y. Ying, J. Phys. Chem. B 102 (1998) 10871.
[499] J.Z. Bloh, R. Dillert, D.W. Bahnemann, J. Phys. Chem. C 116 (2012) 25558.
[500] D. Zhao, Y. Yu, C. Cao, J. Wanga, E. Wang, Y. Caoa, Appl. Surf. Sci. 345 (2015) 67.
[501] Y. Su, S. Han, X. Zhang, X. Chen, L. Lei, Mater. Chem. Phys. 110 (2008) 239.
[502] J. Cheng, J. Chen, W. Lin, Y. Liu, Y. Kong, Appl. Surf. Sci. 332 (2015) 573.
[503] N. Lu, H. Zhao, J. Li, X. Quan, S. Chen, Sep. Purif. Technol. 62 (2008) 668.
[504] V. Likodimos, C. Han, M. Pelaez, A.G. Kontos, G. Liu, D. Zhu, S. Liao, A.A. de la Cruz, K. O'Shea, P.S.M. Dunlop, J.A. Byrne, D.D. Dionysiou, P. Falaras, Ind. Eng. Chem. Res. 52 (2013) 13957.
[505] B. Li, Z. Zhao, F. Gao, X. Wang, J. Qiu, Appl. Catal. B 147 (2014) 958.
[506] R. Daghrir, P. Drogui, D. Robert, Ind. Eng. Chem. Res. 52 (2013) 3581.
[507] S. Morales-Torres, L.M. Pastrana-Martínez, J.L. Figueiredo, J.L. Faria, A.M.T. Silva, Environ. Sci. Pollut. Res. 19 (2012) 3676.
[508] R. Fagan, D.E. McCormack, D.D. Dionysiou, S.C. Pillai, Mater. Semicond. Process. (2015), http://dx.doi.org/10.1016/j.mssp.2015.07.052.
[509] D. Spasiano, R. Marotta, S. Malato, P. Fernandez-Ibañez, I. Di Somma, Appl. Catal. B: Environ. 170–171 (2015) 90.
[510] O. Ola, M.M. Maroto-Valer, Photochem. Photobiol. R 24 (2015) 16.
[511] S.W. Verbruggen, Photochem. Photobiol. R 24 (2015) 64.